Dynamic Performance Improvement of Wind Energy Conversion System Through Power Quality Enhancement

(Case Study: Adama Windfarm I)

Tamrat Edossa Toli

A Thesis Submitted to the Department of Electrical Power and Control Engineering (Power Engineering)

School of Electrical Engineering and Computing

Presented in Partial Fulfillment of the Requirement for the Degree of Master's in Power system Engineering (Power system)

Office of Graduate Studies

Adama Science and Technology University

June, 2024

Adama, Ethiopia

Dynamic Performance Improvement of Wind Energy Conversion System Through Power Quality Enhancement

(Case Study: Adama Windfarm I)

Tamrat Edossa Toli

Advisor: Dr. Shimeles Demissie.

A Thesis Submitted to the Department of Electrical Power and Control Engineering (Power Engineering)

School of Electrical Engineering and Computing

Presented in Partial Fulfillment of the Requirement for the Degree of Masters in Power system Engineering (Power system)

Office of Graduate Studies
Adama Science and Technology University

June, 2024
Adama, Ethiopia

Declaration

I hereby confirm that the thesis titled *"Dynamic Performance Improvement of Wind Energy Conversion System through Power Quality Enhancement (Case study on Adama wind farm 1)"* is entirely original and has not been submitted to any other academic institution. This thesis work appropriately acknowledges all the references it uses with the proper citations.

Tamrat Edossa Toli	________________________	________________
student Name	Signature	Date

Recommendation

As the thesis advisor, I hereby attest that I have read the updated thesis, "*Dynamic Performance Improvement of Wind Energy Conversion System Through Power Quality Enhancement (Case study on Adama windfarm I)*," which Tamrat Edossa Toli prepared under my supervision and submitted as part of the requirements for a Mater's of Science in Power system Engineering (Power system). As a result, I advise that the thesis is amended and submitted to the department in accordance with the relevant protocols.

____________________	____________________	____________________
Advisor	Signature	Date

Approval Sheet

I, as the advisor of the thesis titled "Dynamic Performance Improvement of Wind Energy Conversion System through Power Quality Enhancement (Case study on Adama wind farm 1)" by Tamrat Edossa Toli, am pleased to confirm that the valuable recommendations and suggestions put forward by the board of examiners have been thoughtfully integrated into the final version of the thesis.

___________________________	________________________	________________
Advisor	Signature	Date

The thesis, "Dynamic Performance Improvement of Wind Energy Conversion System Through Power Quality Enhancement (Case study on Adama windfarm 1)," was read and evaluated by the undersigned members of the board of examiners for Tamrat Edossa Toli. The candidate was also examined during the open defense. Therefore, this certifies that the thesis has been approved for partial fulfillment of the requirements needed to get a Master of Science in Power System Engineering (power system).

___________________________	________________________	________________
Chairperson	Signature	Date
___________________________	________________________	________________
Internal Examiner	Signature	Date
___________________________	________________________	________________
External Examiner	Signature	Date

The thesis must be submitted in its final copy to the Office of Postgraduate Studies (OPGS) via the Department Graduate Council (DGC) and School Graduate Committee (SGC) in order for it to be approved and accepted in whole.

___________________________	________________________	________________
Department Head	Signature	Date
___________________________	________________________	________________
School Dean	Signature	Date
___________________________	________________________	________________
Office of Postgraduate Studies, Dean	Signature	Date

Acknowledgement

I would like to express my heartfelt gratitude to Almighty God for bestowing upon me the gifts of grace, wisdom, and strength.These attributes have been invaluable in helping me to navigate all of my endeavors and obstacles. I would like to express my sincere gratitude for the tremendous assistance provided by ***Prof. Ravikumar and Dr. Shimeles Demissie.*** Their constant supervision, helpful comments, perceptive criticism, and encouragement have been crucial to the accomplishment of this survey study. The caliber of this work has been much enhanced by their knowledge and assistance. Furthermore, the technical staff of Adama I Windfarm has my sincere gratitude for their commitment, consideration, and assistance, all of which have been invaluable to me during the writing of my thesis.

I am immensely grateful to my family, especially my Mom and Dad, for their unwavering support and encouragement

Finally, I would like to express my gratitude to all my friends, individuals, and organizations who have supported me in various ways.

Table of Contents

List of Tables

List of Figures

List of Acronyms and Abbreviations

AC	Alternating Current
ANN	Artificial Neural Network
ANFIS	Adaptive Neuro-Fuzzy Inference System
BESS	Battery Energy Storage system
CCM	Continuous Current Mode
DC	Direct Current
DFIG	Doubly Fed Induction Generator
EMF	Electromotive Force
ESS	Energy Storage System
FACTS	Flexible AC Transmission System Controller
FESS	Flywheel Energy Storage System
FOD	Frequency of Damping
IGBT	Insulated Gate Bipolar Transistor
MPPT	Maximum Power Point Tracking
PCC	Point of Common Coupling
PMSG	Permanent Magnet Synchronous Generator
PMSM	Permanent Magnet Synchronous Machine
SCIG	Squirrel Cage Induction Generator
SPWM	Sine Pulse Width Modulation
SSSC	Series Static Synchronous Compensator
STATCOM	Static Synchronous Compensator
SVC	Static Var Compensator
SWB	Static Synchronous Compensator with Battery Energy storage
SMES	Superconducting magnetic energy storage
THD	Total Harmonic Distortion
UPFC	Unified Power Flow Controller
WECS	Wind Energy Conversion System

ABSTRACT

As a worldwide the demand for electricity is growing and the future electric power generation will rely heavily on clean, renewable energy sources such as wind, solar, hydropower, and geothermal. Wind energy conversion systems often use squirrel cage induction, doubly fed induction, and permanent magnet synchronous generators. The main problems with these systems are, in fact, their sporadic power outputs and poor dynamic performances caused by stochastic wind speed. Consequently, devices employing advanced power electronic converters such as static synchronous compensator (STATCOM) are frequently utilized to increase the dynamic performance of a wind energy conversion system, and hence its power quality. In accordance with this, the primary goal of this thesis is to study the impact of combining a STATCOM with a battery energy storage system (BESS) on the dynamic performance of a PMSG-based wind farm as a case study of Adama wind farm-I. In addition, the BESS was built with consideration for energy storage options and to support the real power source in the event of variable wind power. The reactive element of the STATCOM is intended to maintain a constant grid voltage and reactive power. but the active part is controlled by BESS which is intended to compensate for wind power. The proposed system and comprehensive dynamic models of the PMSG-based wind farm were designed and simulated in MATLAB/Simulink. Finally, the simulation results showed that using the STATCOM with BESS considerably improved the overshoots, rising time, and settling time of the DC-link voltage, active power, and reactive power of the wind farm and it is clearly discussed numerically on the result part of this thesis . Furthermore, the findings demonstrated that the negative effects of stochastic wind disturbances on the dynamic performance of a PMSG-based wind farm is reduced. As a result, a STATCOM with BESS has been shown to be effective in improving the dynamic performance of a PMSG-based of Adama wind farm-1 as subjected to stochastic wind disturbances.

Keywords: *BESS,Dynamic performance,PMSG, STATCOM and Wind farm,*

1. INTRODUCTION

1.1. Background

Wind power penetration in grid systems has risen considerably in recent years. As a result, it has become vital to address issues connected with maintaining a stable electric power system that includes various energy sources such as hydro, thermal, coal, nuclear, wind, and solar (Sun et al, 2017). For many decades, traditional energy resources such as petroleum, coal, and gas were commonly employed. Clean and sustainable energy sources including solar, wind, geothermal, tidal, hydro, and biomass are now more important than ever due to global warming and the damaging effects of carbon emissions on the ecosystem as a whole.(Mekdes et al,2022).

Previously, total installed wind power capacity was a small part of the power system, and ongoing grid connection of the wind farm was not a key problem. With an increasing share derived from wind power sources, continuous connection of wind farms to the system has played an increasing role in ensuring uninterrupted power delivery to the load, even in the event of small interruptions.

Ethiopia can produce power with an installed capacity of about 4238 MW. The majority of the electricity, or 3807 MW, is produced by hydroelectric power, with wind energy contributing 324 MW or 7.65%. Even though a total of 10,000 MW of energy is predicted from wind, wind energy is incredibly low. (Electric Power Ethiopia, 2020). Adama-I Wind Farm has a total installed capacity of 51MW, with 34 units rated at 1500kW each. In order to power a three-bladed rotor directly, the 1.5 MW Gold Wind wind turbine uses a gearless permanent magnet (PM) synchronous generator. (Ethiopian Electric Power, Wind Farm Adama-I, 2020).

Improved grid connection capabilities are offered by the converter technology and the PMDD (Permanent Magnet Direct Drive) synchronous generator. On the other hand, power quality issues on the linked grid as well as within the wind farm itself may result from harmonic emissions from the converter-inverter technology used in wind farms.

The wind farm connected to the grid through the generation substation are:

132 kV transmission line is linked to the Adama-old grid.

The rest is connected to Load Dispatch Center (LDC) (Wind Farm Adama-I, 2024).

Ethiopians prefer variable speed wind energy conversion systems over fixed speed ones because the former can track maximum power (MPPT) at varying wind speeds, which improves power quality, efficiency, and reduces noise from aerodynamics and mechanical strain on the wind turbine generator. (Ackermann (2012), Abu-Rub et al. (2014), and Wu et al. (2017))

Wind farm capacity is always increasing due to the installation of more and larger wind turbines. Higher penetration necessitates voltage stability and an efficient fault ride through capability (Sun et al, 2017). One of the key concerns about connecting a wind farm to a power grid is its dynamic stability on the power system (Muljadi et al, 2020). Voltage instability issues arise when a power system is unable to meet reactive power demand during breakdowns and high loading conditions. Massive power systems are more difficult to investigate, assess, and regulate in simulation studies than isolated systems. A wind farm is usually a big area with several wind turbines that generate different quantities of power depending on the wind patterns they are exposed to.

If a wind farm's dynamic stability issue is left unchecked, load shedding or even a blackout could happen. Using a variety of models, wind power integration research has demonstrated that the level of wind power penetration affects a power system's dynamic performance.(Wang et al, 2018). The ability of the operator to give consumers consistent, dependable service is essential to the power system's smooth operation. Stated differently, the power system operator is required to uphold an extremely high standard of uninterrupted electrical supply.

One feature of synchronous machines that enables them to react to deviations from a normal operating condition is power system stability. The emergence of instabilities in a power system can take many different forms, depending on the operating mode and system configuration. Dynamics in wind power controllers, synchronous machines, dynamic loads, and controllers themselves all affect dynamic performance.

1.2. Statement of the problem

Because wind is a clean, renewable energy source that generates electricity with minimal pollution, it has attracted a lot of interest in the last 30 years. In the wind business, wind turbines with fixed and variable speeds are used. Under different operating conditions, a STATCOM can provide the necessary reactive power to effectively manage network voltage, thereby enhancing the network's steady state stability. Compared to the integration of Doubly-Fed Induction Generator (DFIG) based wind power, the impact on the dynamic stability of a power system with high penetration of Permanent Magnet Synchronous Generator (PMSG) based wind power is often less explored.(Ayele et al, 2018). They also provide improved power quality and greater efficiency. Currently, the most commonly used variable-speed wind turbines in large-scale wind farms are DFIG-based wind turbines. However, wind turbine direct-driven permanent magnet synchronous generators (PMSGs) have recently garnered increased interest from scholars, engineers, and turbine manufacturers due to their high efficiency, minimal power loss, and compact size. Transmission system operators (TSOs) face a variety of problems when this type of wind power becomes more prevalent in a power grid.

One issue is the impact of the stochastic nature of wind and power electronic converters on the dynamic stability of the power system. Reactive power compensation via generation and/or absorption is possible with a STATCOM, a shunt-connected device whose output can be adjusted to control specific system parameters. To control voltage and improve dynamic stability, the STATCOM, a static compensator, is employed. The power converters in a PMSG-based wind turbine-generator system are rated for full-scale power, meaning they generate losses and introduce current and voltage harmonics into the power system. This reduces the power factor and causes voltage distortion. Preliminary research on the application of STATCOMs in wind farms indicates that they can enhance the dynamic performance of PMSG-based wind turbines when they are exposed to a stochastic wind speed series.(Ayele et al, 2018). This thesis aims to solve the mentioned problem by integrating Battery Energy Storage System (BESS) with a reliable and responsive (STATCOM) controller. This integration seeks to address the problem of low voltage, frequently encountered at Adama Wind Farm-1. Furthermore, it seeks to improve the dynamic performance of a grid-connected wind turbine utilizing a Permanent Magnet Synchronous Generator (PMSG) in response to fluctuating wind speeds, thereby establishing a more dependable and efficient grid integration system.

1.3. Objectives

1.3.1. General Objective

The General objective of this study is to improve the dynamic performance of the wind energy conversion system at Adama Windfarm I through power Quality Enhancement.

1.3.2. Specific Objectives

- To model STATCOM and BESS as well as overall components of PMSG used in wind farm;
- To define the standard parameters for the system and construct a grid-connected PMSG-based wind farm;
- To design a controller for STATCOM and BESS which is appropriate for the select ed STATCOM and Battery types(Lithium ion);
- Utilizing the MATLAB/Simulink platform, to simulate the grid-connected PMSG-based wind farm with the STATCOM and BESS.
- To show that integrating STATCOM with BESS can enhance the overshoots, rise time, and settling time of DC-link voltage, active, and reactive power, of the Adama-I wind farm.

1.4. Scope of the Thesis

This thesis explains into the design and modeling of a grid-connected wind farm employing a Permanent Magnet Synchronous Generator (PMSG). It investigates the utilization of a Battery Energy Storage System (BESS) to uphold a consistent DC capacitor voltage, along with a Static Synchronous Compensator (STATCOM) controller for governing the power converter on both the transmission system and grid side. The primary emphasis of this thesis lies in the development of control systems for grid-integrated DC/AC converters and BESS, combined with the STATCOM controller.

1.5. Significance of the Thesis

A significant challenge when integrating a wind farm with a power grid is ensuring its dynamic stability within the power system. The objective of this thesis is to investigate and develop power converter control systems to enhance and ensure reliable grid integration. The designed STATCOM controller combined with BESS systems aims to maintain DC voltage and enhance the dynamic performance of a power grid-connected wind farm utilizing PMSG technology.

2. LITERATURE REVIEW

2.1. Background of the Literature

This section offers a comprehensive examination of the existing literature concerning wind turbine systems employing permanent magnet synchronous generators (PMSGs). It specifically reviews prior research on converter configurations, modeling techniques, and control methodologies applied in PMSG-based wind turbine-generator systems. Additionally, it discusses the utilization of a STATCOM controller in conjunction with BESS.

2.2. FACTS Devices

Flexible AC Transmission System (FACTS) devices have recently been implemented to regulate power flow and mitigate power system oscillations. Additionally, they can enhance transmission line capacity, provide steady-state voltage control, prevent system collapse, and dampen power oscillations.FACTS devices can be employed in wind power systems to improve the overall power system's transient and dynamic stability. The STATCOM belongs to the FACTS device family, which can be utilized efficiently in wind farms to provide transient voltage support and prevent system collapse.

Thyristor-controlled series compensation (TCSC) devices have a considerable impact on system stability but *little or no* impact on voltage quality. The SVC and STATCOM have a substantial influence on voltage quality enhancement and perform moderately in terms of overall system stability. In terms of load flow support, stability, and voltage quality, unified power flow controllers (UPFC) have demonstrated efficient performance. In order to control specific parameters in an electric power system, a STATCOM is a shunt-connected reactive power compensation device that has the ability to produce, absorb, and/or gives reactive power. A static compensator, the STATCOM, is utilized to manage voltage and increase dynamic stability (Hingorani et al, 2017). Under different operating conditions, a STATCOM can provide the necessary reactive power to effectively manage network voltage, thereby enhancing the network's steady state stability. Compared to the integration of Doubly-Fed Induction Generator (DFIG) based wind power, the impact on the dynamic stability of a power system with high penetration of Permanent Magnet Synchronous Generator (PMSG) based wind power is often less explored.In addition, this thesis studies the use of a STATCOM in conjunction with BESS devices to improve the dynamic performance of a grid-connected PMSG-based wind farm as a Case study of Adama-I Wind farm. In transmission lines, UPFC can regulate the flow of both reactive and active electricity. Statcom and SVC improve the stability of the system voltage. Both active and reactive power can be independently controlled by UPFC. According to simulations, SVC and STATCOM are more capable than UPFC at regulating voltage, power factor, and active power.(Paramvir Sheoran, 2016). This is why i choose STATCOM than other FACTS device to control *under voltage* for this thesis work for the case study of Adama wind farm-1.

2.3. Wind turbine systems

Wind power conversion technology has evolved since the 1970s, with notable advancements beginning in the 1990s. The global market for electricity generated by wind turbine systems has steadily grown, leading to increased competitiveness in wind technology. Wind Energy Conversion (WECS) systems employ a generator to produce electricity by absorbing wind kinetic energy through a wind turbine's aerodynamically designed blades. Wind turbines can have a constant speed or a variable speed, depending on whether they are oriented vertically or horizontally.

2.3.1. Fixed speed wind turbine

The set-speed function of Wind Energy Conversion Systems (WECS) maintains a consistent pace. Essentially, regardless of wind speed, the grid frequency dictates the fixed rotor speed of the wind turbine. Squirrel-cage induction generators (SCIGs) are commonly employed in tandem with fixed-speed wind energy conversion systems (WECS). Once the wind speed exceeds the cut-in speed, typically ranging from 3 to 4 m/s, the fixed-speed WECS begins power generation (Chinchilla et al., 2020). The turbine's ability to generate energy at speeds exceeding the rated wind speed (13 to 15 m/s) is limited by either active or passive stall mechanisms or by adjusting the pitch of the rotor blades. When the turbine exceeds the cut-out speed (approximately 25 m/s), it is halted using either full blade stall or full pitch adjustment to safeguard the turbine and generator from damage (Chinchilla et al., 2020). Large fixed-speed turbines typically rotate at speeds ranging from 6 to 15 rpm, whereas induction generators have considerably faster rotational speeds, ranging from 750 to 1800 rpm. Fixed-speed wind turbines provide the following advantages (Whei-Min et al., 2019): inexpensive, highly reliable, and simple electrical systems.

The main drawbacks are as follows: the generated power from this wind turbine type cannot be adjusted; the extracted power is not optimized; When an induction generator is directly connected to the grid, capacitor banks need to be installed to mitigate the reactive power demanded by the grid. Induction generators do not regulate reactive power (Akhmatov et al., 2021).

2.3.2. Wind turbine with variable speed

Currently, variable-speed operation is achievable thanks to the integration of power electronic converters, allowing for full (or partial) disconnection from the grid. These turbines feature a DC voltage bus that links two converters an inverter and a rectifier (Akhmatov et al., 2021). Variable-speed wind turbines offer several advantages, including the capability to independently control both active and reactive power, maintain power supply at a constant frequency and voltage despite variations in rotor speed, and maximize wind energy capture when wind speeds are below the rated level. However, they also come with certain drawbacks, such as the need for sophisticated power electronic converters to manage variable frequency generation.

2.4. Operating regions of a wind turbine system

- The wind turbine operates with varying dynamics, ranging from minimum to maximum wind speeds, and its power curve, as depicted in Figure 2.1 which outlines the operational zones of the turbine. This power curve delineates three wind speeds and two operational modes, defined as follows (Lov et al., 2018):
- **cut-in speed**: The wind turbine will produce usable electricity at the lowest wind speed known as the cut-in speed. The majority of turbines run at wind speeds of 3.55 to 4.47 meters per second.
- **Rated Speed**: The optimal wind speed at which the wind turbine will generate its rated power is known as the rated speed. When a wind turbine operates in "maximum power point tracking (MPPT) mode," which occurs when wind velocities fall between the cut-in speed and the rated speed, the wind turbine's output power increases as a result.
- **Cut-Out Speed:** Most wind turbines stop producing power and shut down for safety at very high wind speeds, usually between 22 and 45 m/sec. We refer to the wind speed at which the shutdown occurs as the "cut-out speed." Maintaining a cut-out speed is a safety measure because excessive wind speeds might cause damage to the wind turbine's mechanical component.

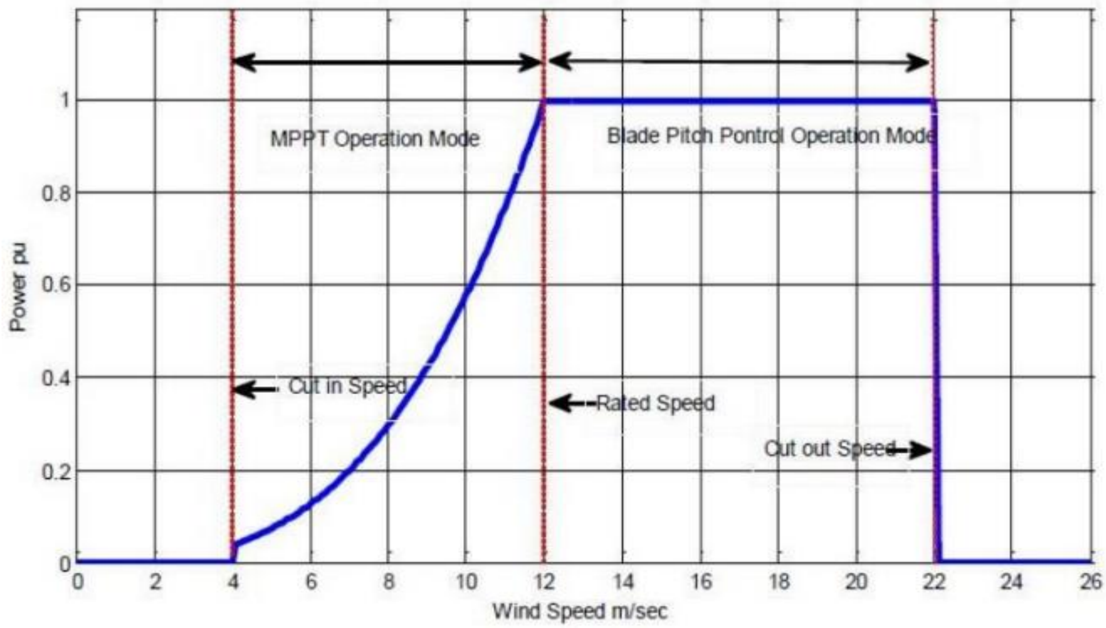

Figure 2.1: Power versus wind speed curve (Morimoto et al, 2018).

2.5. Wind Energy Generator System

The following are the most prevalent types of AC generators used in current wind turbine systems (Chinchilla et al, 2020):

- Squirrel-Cage rotor Induction Generator (SCIG),
- Doubly-Fed Induction Generator (DFIG),
- Permanent Magnet Synchronous Generator (PMSG)

Out of this Generator types this thesis work mainly focuses on the permanent Magnet synchronous generator (PMSG) as a case study of Adama-I wind farm.

2.5.1. Permanent magnet synchronous Generator (PMSG)

A wind turbine setup with a permanent magnet synchronous generator is depicted in Figure 2.2 below. Variable-speed wind turbines are incredibly versatile since they can have synchronous or asynchronous generators installed. Boldea (2020). There are two types of synchronous generators: permanent magnet synchronous generators (PMSG), which are most often used in the wind turbine sector, and wound rotor synchronous generators (WRSG). This arrangement is ideal for full power management because it is connected to the grid via a power converter. Permanent magnet synchronous generators (PMSGs) are low speed generators that have the appropriate number of poles to generate increased torque at low speed. This design uses PMSGs.

The Permanent Magnet Synchronous Generator can adapt to the grid with ease over its entire speed range. (Eduard Ned Mohan et al, 2021). There is no gearbox, and as Figure 2.2 illustrates, full-scale AC-DC-AC power converters are used to link the generator with the grid and load. The excitation energy of PMSG is derived from the permanent magnets, hence it doesn't require external energy. A PMSG's rotor is powered by a permanent magnet pole system, and the stator is wrapped. The gearbox is not required because of the PMSG main pole's low working speeds. A large diameter direct driven multi-pole PMSG can be utilized for the same reason(Taylor ,2016). The PMSG will require minimal maintenance because it doesn't need brushes or sliding rings. A wind turbine built using PMSG will therefore be more stable than one built using DFIG. Both reactive and active power may be managed by the PMSG. The control strategies are easy to understand and put into practice. (A. Raouf , 2023).

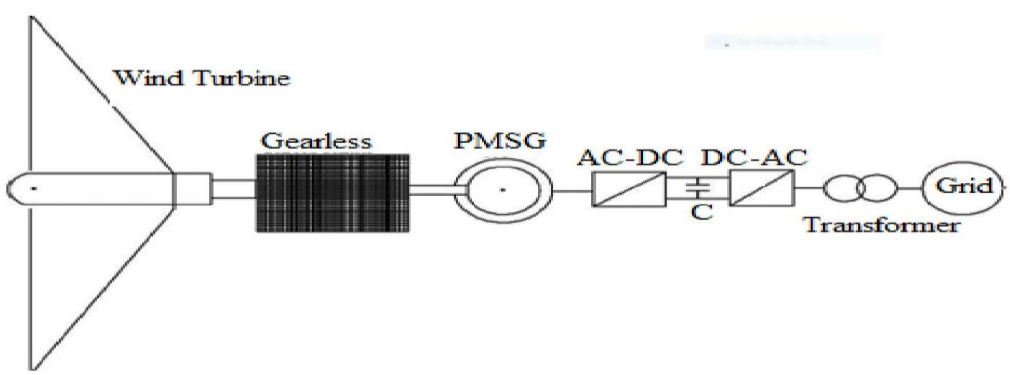

Figure 2.2: PMSG with grid connection (Taylor, 2016).

According to Wang et al. (2018), the PMSG-based producing system has the following drawbacks: A wind turbine-generator system based on PMSG is expected to generate losses and significant harmonic components due to the power converters' full-scale power rating. Additionally, the permanent magnets may demagnetize at high temperatures.

2.6. AC/DC/AC Converter

2.6.1. Diode rectifier

By using a diode rectifier, the three-phase output AC voltage at the PMSG terminals is converted to a DC voltage.

Figure 2.3 displays a three-phase diode rectifier circuit schematic. Despite being unregulated, the rectified output of the diode rectifier has no extra losses as a result of any power electronic component switching. It may be assumed that all of the power extracted from PMSG is converted from AC to DC if the diode losses are negligible.

Figure 2.3: Three-phase diode Rectifier(Chinchilla et al, 2020).

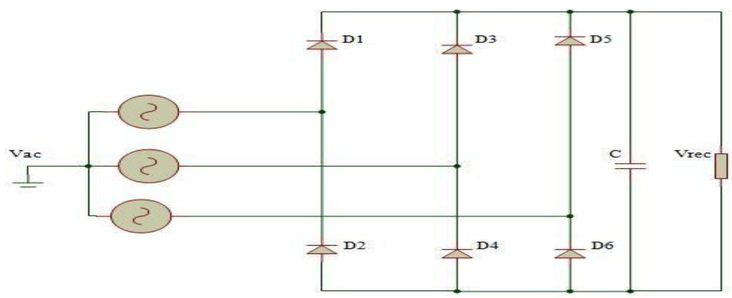

2.7. DC to DC converters

Depending on the output voltage level, the three most popular topologies for converters are buck, boost, and buck-boost. All three converters have identical components; the differences in the input-output connection arise only from the arrangement of those components inside the circuit. This section provides a detailed analysis of all three topologies.

2.7.1. Buck converter

The voltage at the buck converter's output (Vo) is lower than the voltage at its input terminals (Vin) when it is utilized with a continuous inductor current. (Chinchilla et al, 2020).

$$V_o = dV_{in} \qquad (2.1)$$

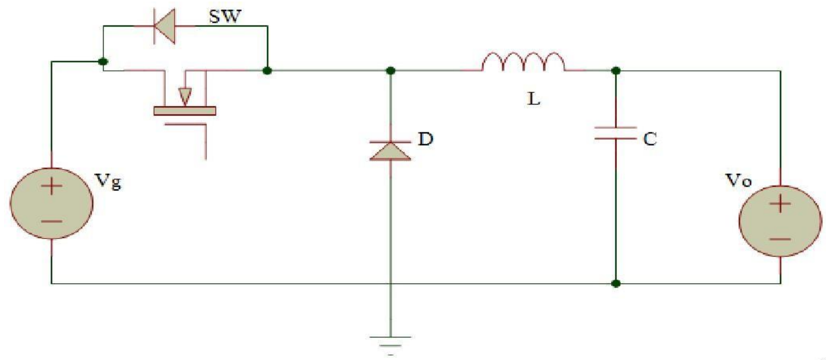

Figure 2.4: Buck converter (Chinchilla et al, 2020).

where D is the switch's duty cycle. Figure 2.4 displays a buck converter's circuit schematic.The input current becomes discontinuous because the switch is connected to the input terminal directly.

2.7.2. Boost converter

Figure 2.5 depicts a boost converter circuit diagram. The voltage obtained at the output (Vo) of a buck converter is greater than the voltage obtained at its input terminals (Vin) and is given by (Chinchilla et al, 2020).

$$Vo=\frac{Vg}{1-\mathrm{d}} \qquad (2.2)$$

Where, D is the switch's duty cycle, V_g is generated voltage.

Although the boost converter needs a larger output filter capacitor (C) and inductor (L) than the buck converter, the input current may be maintained constant by carefully choosing the inductor and capacitor.

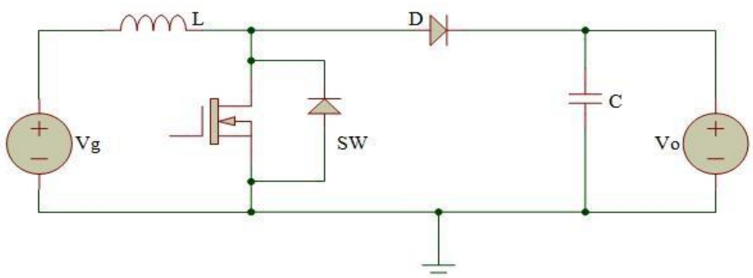

Figure 2.5: Boost converter (Chinchilla et al, 2020).

2.7.3. Buck to boost converter

Depending on the duty cycle (d), the output voltage (Vo) of a buck-boost converter can either exceed or be lower than its input voltage (Vin). The schematic of a buck-boost converter is depicted in Figure 2.6. The steady-state output voltage when operating in continuous current mode (CCM) can be determined. (Chinchilla et al., 2020).

$$Vo=\frac{-\mathrm{d}V in}{1-\mathrm{d}} \qquad (2.3)$$

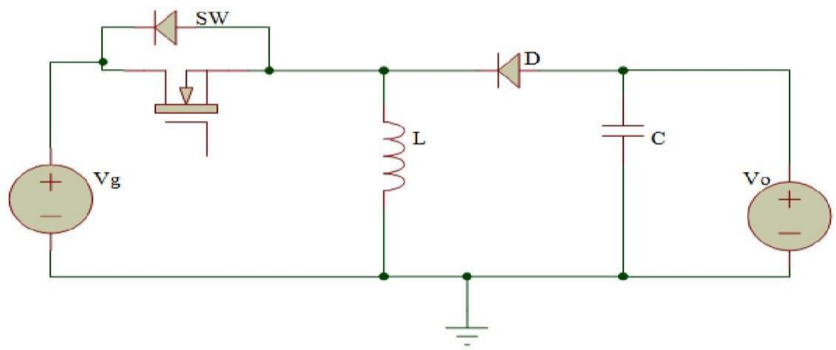

Figure 2.6: Buck-boost converter (Chinchilla et al, 2020).

The input voltage's polarity and the output voltage's are inversely correlated. There is a discontinuity in the input current since the switch is connected directly to the input terminal.

2.8. The AC voltage sourced inverter or DC-AC converter

The inverter, also known as a DC-AC converter, converts direct current (DC) power into alternating current (AC) power at a specified output voltage and frequency by manipulating semiconductor power switching devices.The DC power input is given to the inverter. To create a steady DC link voltage, the capacitor placed across the input terminals of the inverter serves as a filter. There are two types of inverters: voltage source inverters, which regulate the output voltage waveform, and current source inverters, which regulate the current waveform. Three primary types of configurable inverter typologies exist. Three different types of voltage source inverter constructions are available: half-bridge, full-bridge, and three-phase inverters.

2.8.1. Half bridge voltage source inverter

A half bridge rectifier that operates on one phase is used in low voltage applications. It is constructed from an assortment of controlled switches, or semiconductor devices. Power switch devices' switching mechanisms are intended to change a DC voltage source into an AC output voltage.

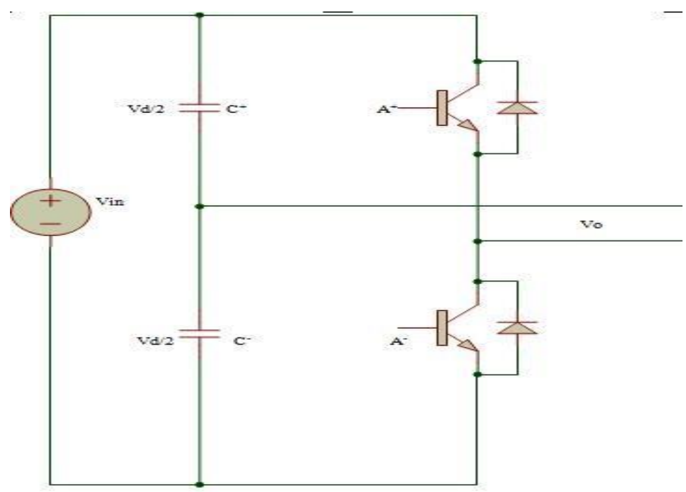

Figure 2.7: Single half-bridge VSI(Chinchilla et al, 2020).

An opposite-polarity current-conducting diode safeguards each IGBT switch. This gives an inductive load, as seen in Figure 2.7, a freewheeling path during the switching phase. Two large, identically sized capacitors are connected in series on the DC voltage source side. The N link between the two capacitors represents the allocation at the mid-potential point. The upper and lower switches on one leg, or both, cannot be activated simultaneously, according to the rule. Switches can be damaged when two are turned on at the same time on the same leg, resulting in a short circuit. There's still current flow and voltage loss between the switches even when they flip from ON to OFF.

2.8.2. Single-phase bridge voltage source inverter

The voltage is influenced by the pulse width, which is produced by the half-bridge just once every half-cycle. In contrast, a single-phase inverter architecture has two legs, each with two switching devices, as shown in Figure 2.8.

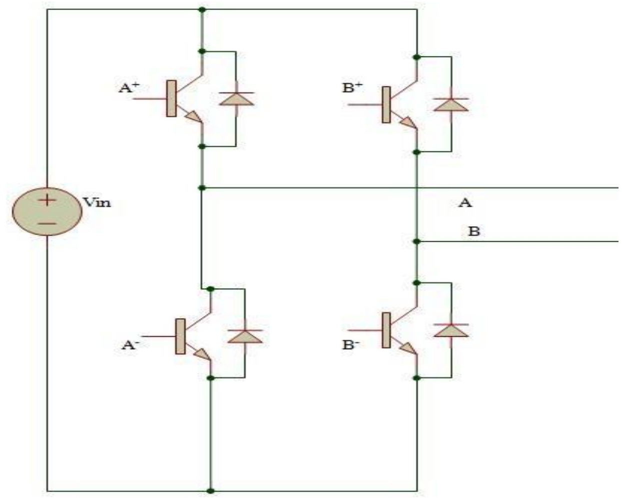

Figure 2.8: Single-bridge VSI(Chinchilla et al, 2020).

With the same input voltage, a half-bridge inverter generates half the output power as a full-bridge inverter. Nevertheless, alternative PWM switching schemes are being investigated to enhance the distinct inverter performance. The major goal of the transition phase is to insert a zero-voltage sequence in between the negative and positive voltage sequences. By doing this, the inverter's output voltage is improved, the load factor rises, and THD falls. The power circuit of a single-phase bridge inverter, which generates sinusoidal waves at the output, consists of four semiconductor switches.

2.8.3. Three phase voltage source inverter

Figure 2.9 below illustrates a three-phase voltage source inverter. The model is composed of three parallel connections, one for each phase, between two switches connected in series.

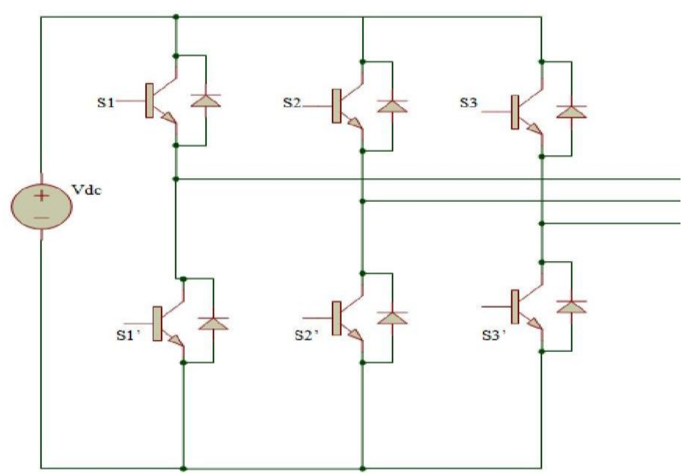

Figure 2.9: Three-Phase Voltage Source(Chinchilla et al, 2020).

2.9. Overview of BESS and FACTS Controller

2.9.1. Battery energy storage system

Because of their electrochemical energy storage characteristics, battery energy storage systems (BESS) are among the most affordable energy storage technologies available today. To offer a specific electrical characteristic in a battery system, power battery modules are connected both in series and parallel. Advanced battery technology allows for increased reliability, better cycle capabilities, lower costs, and larger energy storage densities. Battery energy storage systems, abbreviated as BESSs, have emerged as highly promising storage technologies for power applications in the near term. They find numerous applications in power systems, including area regulation, area protection, spinning reserve, and power factor correction. Power generation variations, such as those seen in wind energy conversion systems, can throw off the grid, particularly in weak infrastructure situations. Usually, the energy storage component is a battery. It can be used to store extra active power generated by the wind farm during times of high output or to provide active power during times of low production. A DC/AC power converter is required since the energy storage device has a DC output voltage, which makes it impossible to incorporate it into the grid. A FACTS power flow controller in conjunction with battery energy storage can also enhance power system performance and control.(Rolan et al, 2020). It consists of many voltaic cells, each of which is composed of a half-cell joined in series with anions and cations in a conductive electrolyte. Redox reactions that oxidize anions at the anode and decrease cations at the cathode power the battery. Primary batteries and secondary batteries are the two different types of batteries. They may also be categorized according to the kind of electrolytes they contain, which include alkaline and acid-based batteries. The principal batteries are disposable and cannot be recharged due to the irreversible nature of the chemical process. The first generation of voltaic heaps, Daniel cells, and grove cells are used as primary batteries.

For instance, atomic batteries may provide power for almost a decade before they require replacement. Fuel cells, which run as long as the fuel (often hydrogen) is refilled, are the most advanced primary batteries available today. Rechargeable batteries, also referred to as secondary batteries, consist of one or more cells that have electrochemical processes that are electrically reversible. By applying reverse polarity current to undo the chemical reaction that occurred during use, they can be recharged. Lead acid, nickel cadmium (NiCd), nickel metal hydride (Ni

MH), flow batteries, and lithium-ion (Li-ion) are a few examples. The following formulas are utilized by the model for several types of nickel metal hydride batteries:-

• Discharge Model (i*> 0)

$$f\ \ it, i*i, \exp\ = E_o - k.\frac{Q}{Q-it}.i + Laplace^{-1}(\frac{\exp(s).0}{sel(s)}) \tag{2.4}$$

• Charge Model (i*< 0)

$$f\ \ it, i*i, \exp\ = E - k\frac{Q}{|it|+0.1}.i* - k.\frac{Q}{Q-it}.it + Laplace^{-1}(\frac{\exp(s)}{sel(s)})\frac{1}{s} \tag{2.5}$$

In the equations, E0 is the constant voltage, Vo is the battery's open circuit voltage, Rb is the battery's internal resistance, ibis is the battery charging current, K is the polarization constant, i* is the low frequency current dynamics, i is the battery current, i is the extracted capacity, Q is the maximum battery capacity, A is the exponential in V, and B is the exponential Capacity in Ah-1.

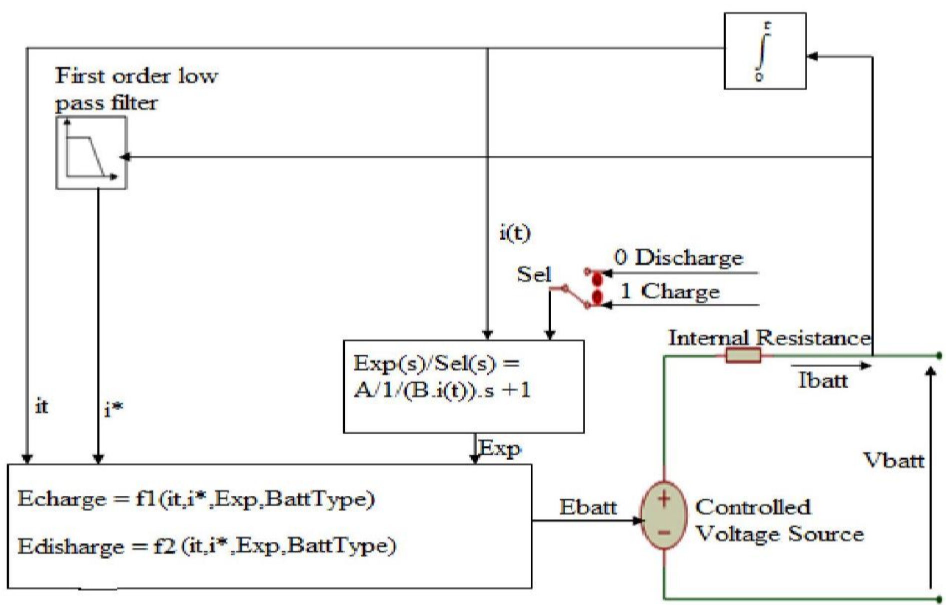

Figure 2.10: Battery equivalent circuit (Rolan et al, 2020)

From the figure 2.10 above we can say that, During the *charging process*, the switch S is closed, which connects the battery to an external power supply. Battery current (I_charge) enters the battery through the internal resistance (R) and the capacitor (C), The power source voltage

(V_charge) is greater than the open circuit voltage. Batteries provide electricity to an external load as they are being discharged. Connecting the battery to an external load involves closing the switch (S). Through the external load and internal resistance (R), current flows due to the open circuit voltage of the battery. Current (I_discharge) flowing from the battery to the load lowers the battery's state of charge.

2.10. FACTS (Flexible AC transmission system Controller)

The name "Flexible AC Transmission System" (FACTS) refers to alternating current transmission systems that enhance controllability and power transfer capabilities by utilizing static controllers, including those based on power electronics (Haque.M et al, 2019). A STATCOM, belonging to the FACTS family, is a shunt device that utilizes power electronics to manage power flow and improve transient stability within power grids. (Rolan et al., 2020). In ac systems, STATCOM's primary goal is to boost controllability and power transmission capacity. To follow grid regulations, a zigzag transformer is required. Grid filter, DC/AC power converter, and shunt capacitor make up the STATCOM system. The central component of STATCOM's integration into the grid is its DC/AC power converter, featuring a converter topology akin to that utilized in grid-integrated renewable energy systems. The STATCOM governs the amount of reactive power injected into or withdrawn from the power source to modulate the voltage at its terminal. When the system voltage is high, the reactive power generated by the STATCOM (STATCOM capacitive) is absorbed by the STATCOM (STATCOM inductive). Adjacent to the secondary side of the coupling transformer is a voltage source converter (VSC) responsible for reactive power adjustment.The control system block diagram of the STATCOM is shown in a single line in figure 2.11 below.

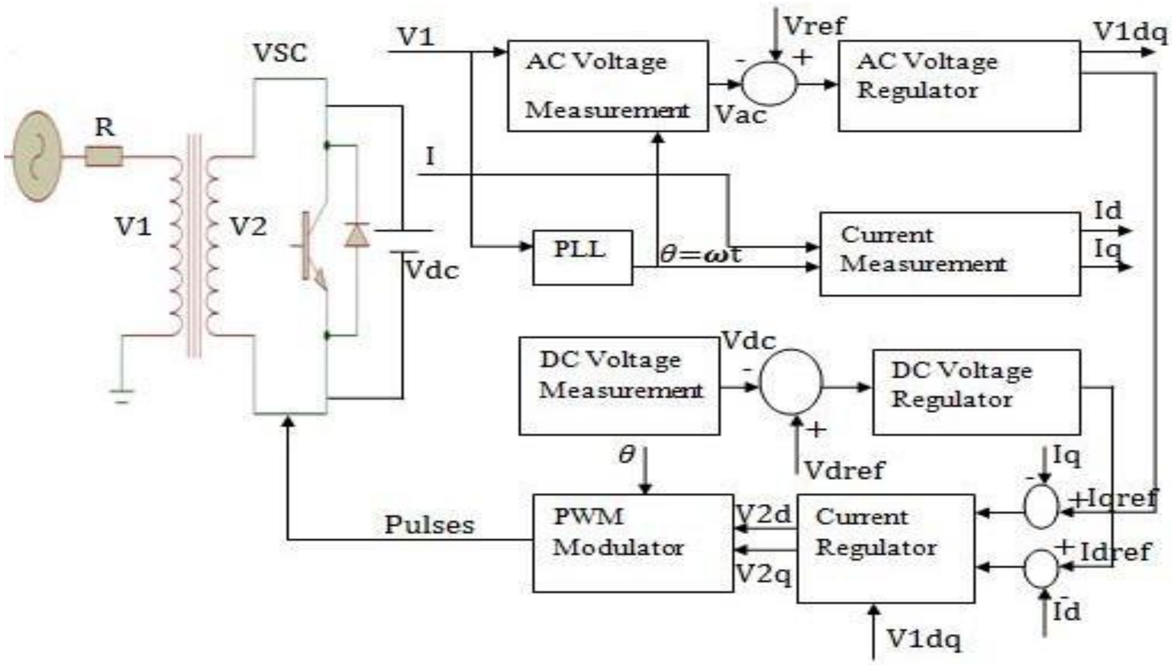

Figure 2.11: STATCOM and its control system block diagram (Rolan et al, 2020).

Based on the figure (2.11), The reference voltage generator calculates the target voltage level and the voltage regulator generates an error signal after comparing the observed voltage to the reference voltage. The reactive power need is converted into a suitable current reference by the current reference generator. The PWM controller uses this current reference to supply the proper gate drive signals to the VSC. The VSC adjusts its output to inject or absorb reactive power and regulate the AC bus voltage.

2.10.1. Operating principle of STATCOM

Phase shifting the voltage V2 slightly behind V1 is necessary to maintain the capacitor charged in a constant state and offset losses from the transformer and VSC. Two VSC technologies are available for usage by the VSC:

• Square wave inverters based on GTOs and certain connecting transformers are used by VSC. 4 three-level inverters are often used to create a 48-step voltage waveform. Connecting transformers designed for this purpose are used to decrease the harmonics in the square waves that each individual inverter produces. Proportionate to the voltage is the basic building block of this type of VSC. One way to regulate reactive power is to modify it.

• IGBT-based PMW inverters are used by VSC. This type of inverter creates a sinusoidal wave from a direct current voltage source using the pulse width modulation (PMW) approach, typically with a chopping frequency of a few kHz. Filters can be installed on the VSC's AC side to reduce harmonic voltages. The constant Dc voltage Vdc is used by this kind of VSC to operate. The voltage V2 is altered using the PWM modulator's modulation index.

The Control System is made up of:

• A phase-locked loop (PLL) locks onto the positive sequence components of a primary voltage V1, which comprises three phases. By utilizing the output of the PLL (angle = mt), the direct and quadrature axis components of the AC three-phase voltage and currents denoted on the graph as Vd, Vq, or Id, Iq, can be computed.

• An external regulation loop comprises a voltage regulator responsible for regulating both AC and DC voltages. The output of the AC voltage regulator, which adjusts the flow of reactive power by aligning current quadrature with voltage, acts as the reference current (Iq ref) for the current regulator. Meanwhile, the output of the DC voltage regulator (Id = current in phase with voltage regulating the active power flow) serves as the reference current (Id ref) for the current regulator.

• The grid-side converter's function is to manage reactive power exchange between the grid and itself, and to sustain a stable voltage across the DC-link capacitor.

• If the device generates active power, the grid-side converter should transfer this power to the grid.

• If the machine consumes active power, the grid-side converter should transfer power from the grid to the machine-side converter. Conversion of the three-phase grid voltages and currents into the dq reference frame is conducted for control purposes. PWM signals generated by the controller's output voltage signals are utilized to provide gate commands to the IGBT modules in the grid-side converter. A STATCOM presents several technological advantages over an SVC, including faster response time, compatibility with battery, fuel cell, or SMES (superconducting magnetic energy storage) interfaces, and reduced space requirements due to the elimination of large passive components like reactors (Rolan et al., 2020). A STATCOM performs better under voltage conditions because it can maintain a consistent level of reactive current.

2.11. Review of Related Works

Here, a brief discussion of the various methodologies used by various literatures to investigate the subject of dynamic performance enhancement of a grid-connected wind farm is provided. Numerous studies demonstrate how STATCOM combined with BESS can improve electricity quality and grid stability. El-Khattam et al. (2019), for example, showed how STATCOM and BESS work well together to reduce voltage sags and flickers and improve power quality in distribution networks. The power system becomes more dependable and efficient when STATCOM and BESS are combined. Research has demonstrated that this combination can greatly lower transmission losses and increase overall system efficiency, as demonstrated by studies like those conducted by Gao et al. (2021). An IEEE 30-bus system link to the main distribution system was used to evaluate the efficacy of STATCOM with micro grid integration. This technique was used to manage the voltage profile and lower power losses in a micro grid system that was connected to the grid and included a fuzzy-based STATCOM controller. Ultimately, it was found that STATCOM lowers power loss, improves voltage profiles, and expands distribution line capacity.(Mezigebu and associates, 2020).A comparison is made between the three scenarios' simulation results and the effectiveness of the suggested method. By using this method, grid-connected wind power producing facilities' LVRT capabilities were increased by modifying STATCOM controllers. When the system fails, a wind farm with a STACOM cooperative compensation control technique maximizes economic value and increases dynamic performance. The function of STATCOM is important, but how energy storage might be interfaced with STATCOM to increase active power was not investigated. Doubly Fed Induction Generators are the exclusive subject of this research. An Grid-Connected Direct Drive Wind Power System was designed for the development of the STATCOM with super capacitor energy storage to improve the wind energy system's dynamic performance. Nevertheless, super-capacitors have a lower energy density (storing less energy per unit mass) and a higher power density (storing and releasing more power in a short amount of time). This method can increase the LVRT capability of wind farms and keep grid voltage at PCC well above the wind farm trip voltage during grid faults with reactive power assistance from STATCOM (2019 saw Chowdhury et al). When coupled with dynamic performance analysis, mitigation techniques, and PMSG-Based Wind Power Integration modeling, it was discovered that stochastic wind speed disruptions had less detrimental effects.(2018 Ayele et al).

2.12. Review of Research Gap

despite notable progress in this area, a number of research gaps persist in the integration of Battery Energy Storage Systems (BESS) with Static Synchronous Compensators (STATCOM). These gaps point to areas that require more research and development in order to fully fulfill this technology's potential for improving energy management, power quality, and grid stability. The primary research gaps in the body of current literature are as follows:

Although a number of different control algorithms have been investigated for STATCOM with BESS, complete systems that can successfully handle the complex and dynamic character of contemporary power grids are still lacking. This thesis closes the gap between the effects of BESS and STATCOM on the dynamic performance of a grid-connected PMSG-based wind farm under stochastic wind speed disturbances, according to the reviewed literature. The electricity system may become dynamically unstable due to the detrimental effects of stochastic wind disturbances on a PMSG-based wind farm's dynamic performance. The goal of this thesis is to create a control system for three-phase DC/AC power converters that integrates with the grid. Therefore, a static synchronous compensator with a battery energy storage system was created in order to accomplish compensated reactive power, active power, and improve the dynamic performance of a grid-connected permanent magnet synchronous generator-based wind farm. It accomplishes this by controlling current, DC link voltage, AC voltage, and synchronizing the frequency and phase of a system's output signal with a specified input signal (PLL).

3. MATERIALS AND METHODS

3.1. Methodology

This thesis explores the design and deployment of a grid-connected wind farm utilizing a PMSG (Permanent Magnet Synchronous Generator). The main focus of this thesis is the development of control systems for grid-integrated DC/AC converters and BESS interfaced with the STATCOM controller. Subsequently, a comprehensive mathematical modeling of grid-connected PMSG, STATCOM, and BESS is presented, along with simulation experiments. In order to accomplish the overall and specific goals of the thesis, Figure 3.1 below displays the flow chart that outlines the process.

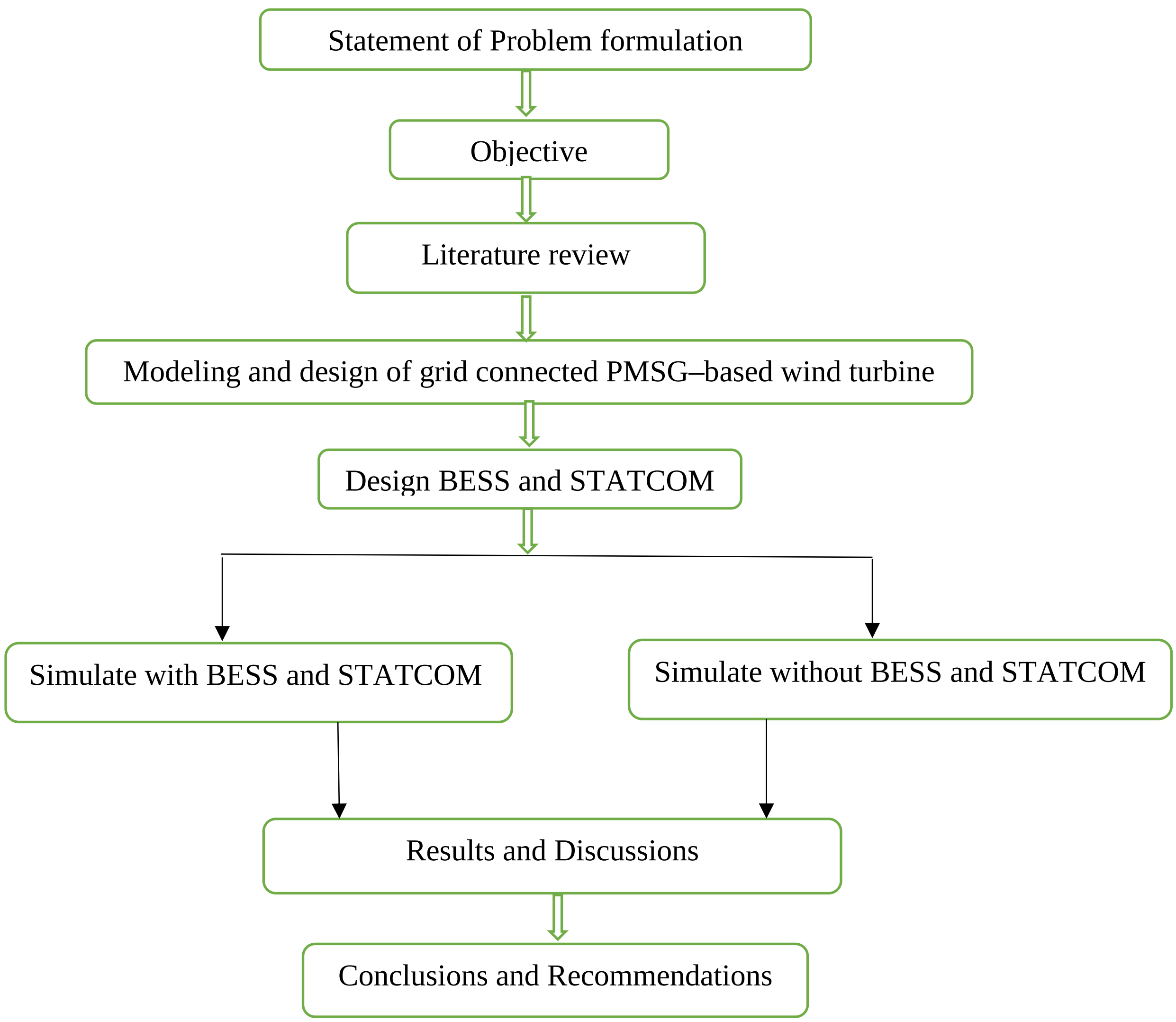

Figure 3.1 The research process flow chart

3.2. Dynamic modeling of a PMSG wind turbine

This section develops the power electronics converter circuits as well as the dynamic model of the Permanent Magnet Synchronous Generator (PMSG) that is connected to the wind turbine. This part uses WTG data from Adama Wind Farm-I (appendices 1 and 2) to construct controllers and create a system dynamic model.

Figure 3.1 shows a schematic representation of the grid-connected wind turbine-PMSG system. The converters are installed in between the generator and the grid. The wind speed, wind turbine, PMSG, power converter circuits, STATCOM, BESS, and transmission line connected to the grid are all shown in the system model that is seen in the graphic below. A direct current (DC) connection connects each voltage source converter (VSC) that makes up the power electronics converter. The generator side-converter (rectifier) system is powered by the generator's stator circuit. The active power exchanged with the grid is integrated in the grid side converter (inverter) system to maximize the power supplied into the back-to-back converter's DC link.

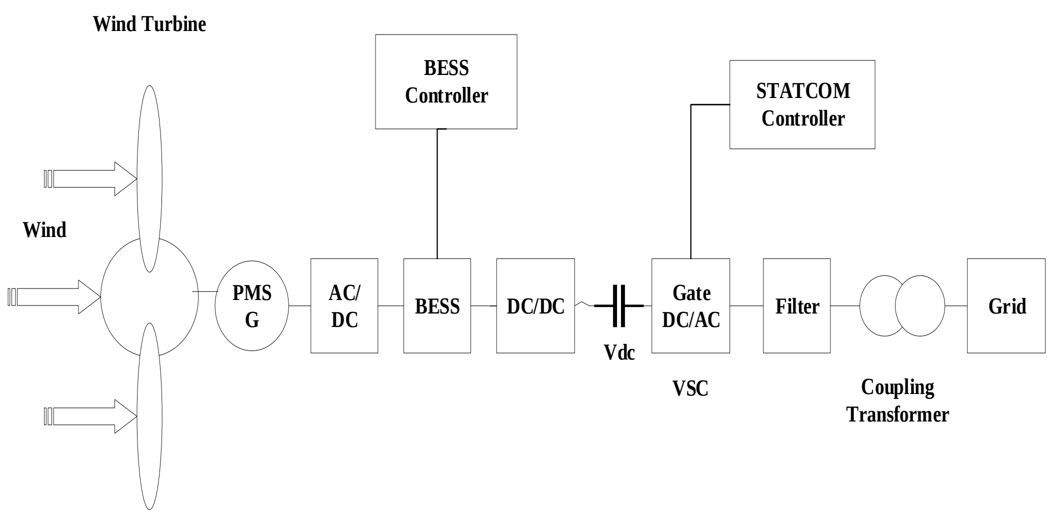

Figure 3.1: Schematic diagram of variable speed WT-PMSG connected to grid

3.3. Wind speed model

The Wind Speed Model is affected by the wind farm's location and climate. Wind speed components including noise, gusts, ramp fluctuations, and the spatial influence of wind behavior all affect a wind turbine's dynamic performance.(Ayele et al, 2018). As a result, the model is as follows:

$$V_w = V_{wb} + V_{wr} + V_{wg} + V_{wn} \tag{3.1}$$

Where Vwb, Vwr, Vwg, and Vwn are the base, ramp, gust, and noise components respectively.

3.3.1. Gust of wind

A sudden shift in wind direction is called a gust. Rezaiet al. (2017) demonstrate how it may be used to apply dynamic performance modeling of a wind turbine to an analysis of the system's behavior during considerable variations in wind speed.

$$Vwg = \begin{cases} 0 & (t - t_{1g}) \\ \frac{Vwg\max}{2}[1 - \cos(\frac{t - t_{1g}}{t_g}] & (t_{1g} < t \leq t_{1g} + t_g) \\ 0 & (t > t_1 + t_g) \end{cases} \tag{3.2}$$

Where t_{1g}, t_g, t_{gmax} represents the starting time, cycle and the maximum value of the gust

3.3.2. Ramp wind

The ramp component depicts the progressive shift in wind speed nature and is given by:

$$V_{wr} = \begin{cases} 0 & t \leq T_{1r} \leq t > T_{2r} + T_r \\ V_{\max}\frac{t - T_{1l}}{T_{2r} - T_{lr}} & t \leq T_{1r} \leq t \\ V_{\max} & t \leq T_{1r} \leq t > T_{2r} + T_r \end{cases} \tag{3.3}$$

V_{max}, is the maximum of value of wind speed; T_{1r} is the starting time; T_{2r} is the over time; T_r is the keep time for wind speed.

3.3.3. Noise wind speed

While it is possible to suppose that the noise component of wind speed is Gaussian noise with a changing wind probability density function (3.4), the mean and standard deviations in the noise scenario match the noise components of the average and standard deviation of wind speed. For fluctuating wind, the probability density function resembles the Gaussian distribution rather well. The probability density function of changeable wind can therefore be expressed as follows:

$$p(V_{wn}) = \frac{1}{\sigma\sqrt{2\pi}}\exp[-\frac{V_{wn^2}}{2\sigma^2}] \tag{3.4}$$

From minimal wind speed (cut in) to maximum wind speed (cut out), the wind turbine's dynamics are constantly changing. For the Adama-I wind farm, the variable wind speed can be calculated to be between 3 and 22 m/s.

Table 3.1 Fluctuating (Noise) wind speed in (m/s)

3.1	3.3	4.1	4.3	5.1	5.3	6.1	6.3	7.1	7.3
8.1	8.3	9.1	9.3	10.1	10.3	11.1	11.3	12.1	12.3
13.1	13.3	14.1	14.3	15.1	15.3	16.1	16.3	17.1	17.3
18.1	18.3	19.1	19.3	20.1	20.3	21.1	21.3	22.1	

Standard deviation	2.56
Mean	10.208

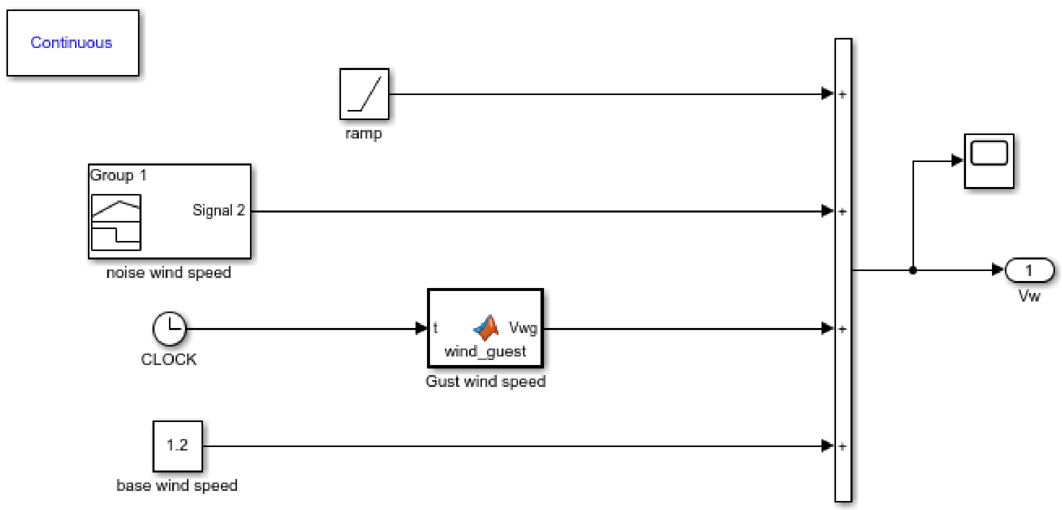

Figure 3.2: Simulink model of stochastic wind speed

As we can see from figure 3.2,Creating a Simulink model for stochastic wind speed entails simulating wind speed as a random process that changes over time. Gust wind speed is a crucial element of wind speed models because it shows transient changes in wind direction, which can have detrimental effects on systems and structures that are exposed to the wind. *Noise wind* speed in wind speed models refers to the random variations or turbulence in wind speed on short time scales.

3.3.4. Wind turbine (aerodynamic) modelling

The available wind energy must be calculated before the energy conversion efficiency of wind energy conversion systems can be examined. Actually, a large number of air particles with a total mass of m and a wind velocity of Vw are traveling with kinetic energy, which is known as wind energy. When calculating the potential accessible kinetic energy contained in the wind, use formulas (3.5) assuming that all air particles are moving in the same direction and at the same speed before hitting the wind turbine's rotor blades:

$$KE = \frac{1}{2} m V_w^{\ 2} \tag{3.5}$$

$$KE = \frac{1}{2} \rho A V_W^{\ 3} t \tag{3.6}$$

Given a constant wind velocity Vw, the total mass,(m) of the particles during a given time interval t, may be computed as follows:

$$m = \rho A V_w t \tag{3.7}$$

where, air density is expressed as ρ.

The following formula may be used to determine the power in the air as it passes through region A, like the area the rotor blades sweep:

$$P_{wind} = \frac{dK_E}{dt} = \frac{1}{2} \rho A V_W^{\ 3} = \frac{1}{2} \rho \pi r^2 V_W^{\ 3} \tag{3.8}$$

where Pwind is the potential wind power and Vw is the wind speed. Expression (3.8) leads us to the conclusion that wind power is exactly proportional to the cube of wind speed, i.e., a small increase in wind speed yields a large increase in wind power. Moreover, a wind turbine's output can be increased by increasing its rotor radius because power is correlated with the square of the rotor radius. Thus, for modeling purposes, the extractable electricity produced by the wind turbine is provided by:

$$P_m = \frac{1}{2} \rho A V^3 Cp(\lambda, \beta) \tag{3.9}$$

Where, tip speed ratio is represented by λ, blade pitch angle is represented by β, mechanical power collected from the wind is shown by Pm, and power coefficient by Cp. The highest power that a wind turbine can produce is limited by the power coefficient Cp. sometimes referred to as Betz's limit, which never rises over 59.3%, which is the theoretical efficiency of a wind energy converter (Wu et al, 2017). CP For the sake of simulation, the following can be defined as a function of the blade pitch angle and the tip speed ratio:

$$C_p(\lambda,\beta) = C1(\frac{C2}{\lambda i} - C3\beta - C4)e^{\frac{-C5}{\lambda i}+C6\lambda} \tag{3.10}$$

$$\frac{1}{\lambda i} = \frac{1}{\lambda - 0.08\beta} - \frac{0.035}{\beta^3+1} \tag{3.11}$$

Where; The generator's maximum electrical rating or Nominal power is 1.5 MW, and the settings or datas are gathered from Adama-I wind farm, and it is placed on appendix. Coefficients are C_1, C_2, C_3, C_4, C_5, and C_6 0.5174, 116, 0.4.1,5,21, and 0.00679 respectively. The tip speed ratio, denoted as follows:

$$\lambda = \frac{\text{Blade Tip Speed}}{\text{Wind Speed}} = \frac{r\omega_r}{V_w} \tag{3.12}$$

Where, r is rotor radius, V_W is wind speed and The wind turbine generator's angular speed is denoted by ωr, while its tip speed ratio is represented by λ.

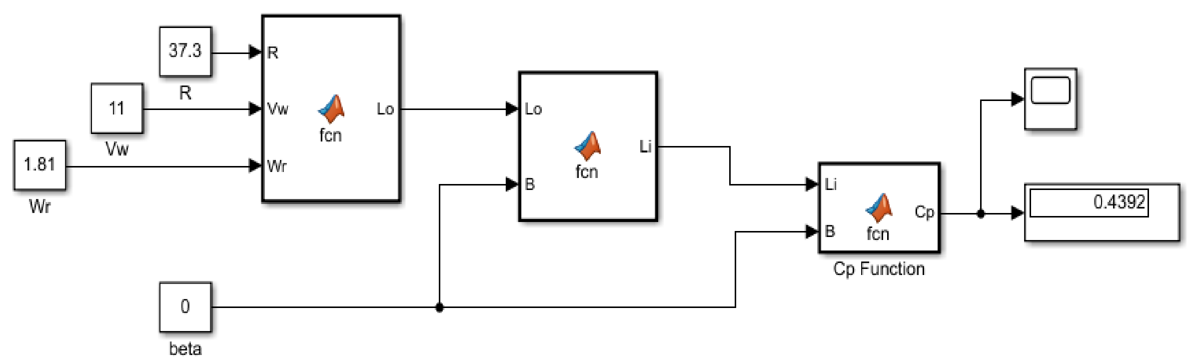

Figure.3.3 Power coefficients of the rotor

An essential component of wind energy analysis and turbine design is modeling a wind turbine's rotor's power coefficient (Cp). The rotor's ability to convert wind energy from kinetic to mechanical form is measured by its power coefficient. It is dependent upon the pitch angle (β) and tip speed ratio (λ) of the blade. So, based on the given data our Cp (power coefficient) was designed and is 43.9% or 0.439.

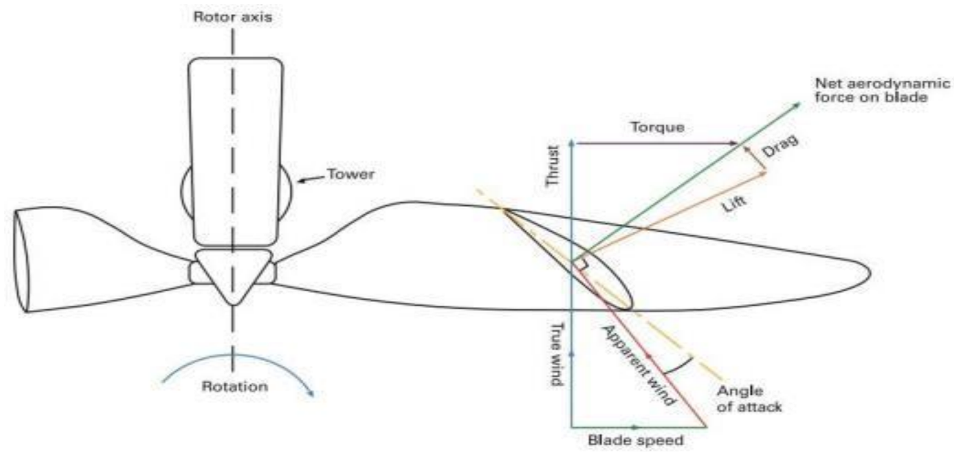

a. Blade angle diagram

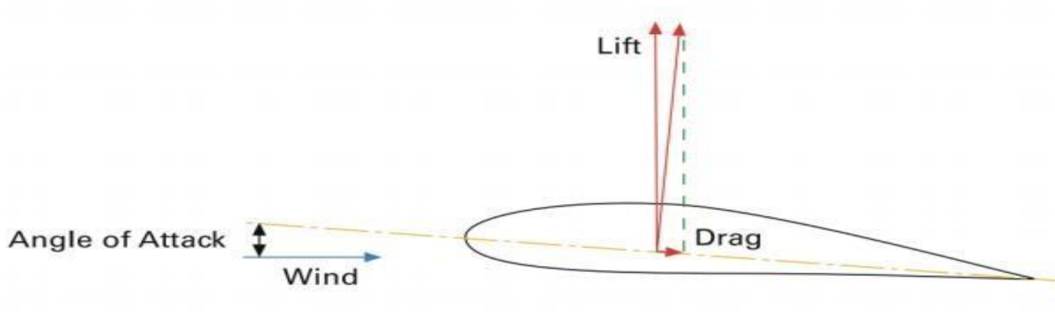

b. Lift and drag force on the blade

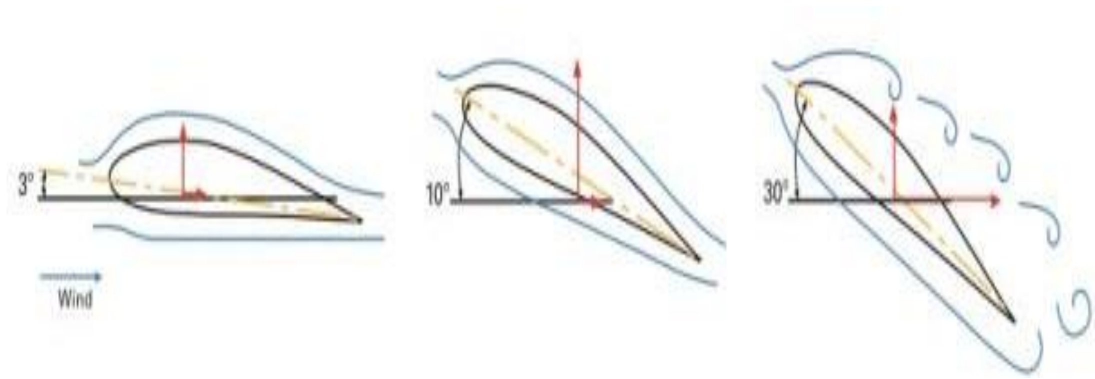

C. Blade at low medium and high angles of attack

Figure 3.4: Diagram of blade angle of wind turbine (Jansen et al, 1996).

The blade angle illustrates how the wind velocity affects the wind turbine blades, as seen in Figure 3.4. The blade angle, or β, is the angle that develops between the wind velocity vector and the blade's orientation. The wind turbine will extract the most energy from the wind when the blade is entirely affected by the wind velocity. When the wind speed is less than the system's required wind speed, the blade angle is frequently lowered to zero degrees in order to ensure optimal energy collecting efficiency. If the wind speed surpasses the specified figure and the blade angle stays at zero degrees, the system's power capture will be greater than its rated power. As a result, the generator and power equipment run at greater than rated output, which could be damaging to the system if it persists for a long time. This indicates that a control system is necessary for the wind turbine to be able to modify the blade angle in response to varying wind conditions.

The mechanical torque of a wind turbine is expressed as:

$$T_m = \frac{P_m}{\omega r} = \frac{1}{2}\rho\pi r^3 {V_W}^2 \frac{Cp}{\lambda} \tag{3.13}$$

In this case, Tm represents the mechanical torque produced by the wind turbine, while ωr denotes its rotor speed.

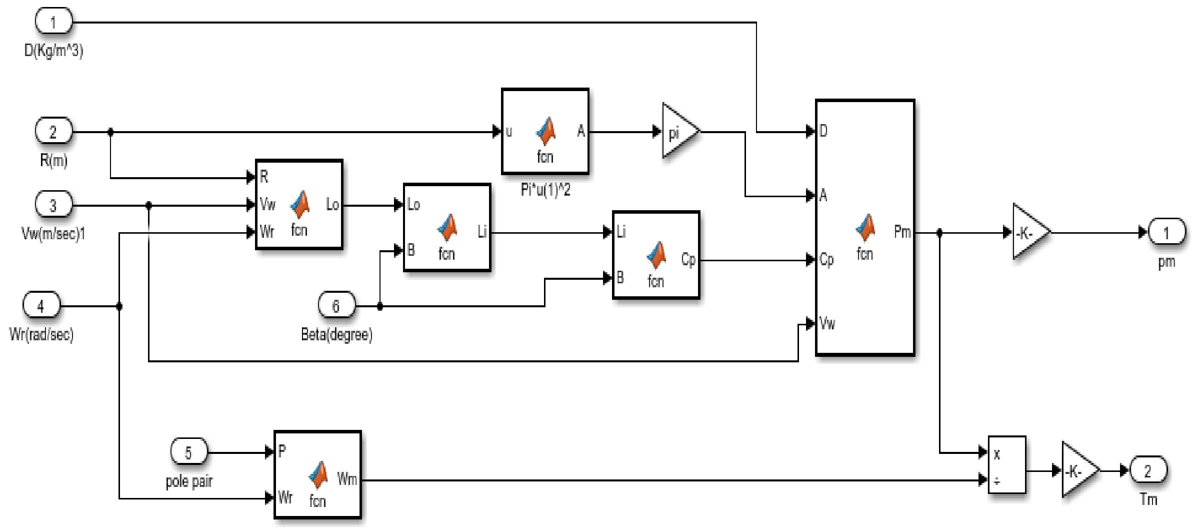

Figure 3.5: Simulink model to obtain mechanical torque and power

The correlations between wind speed, rotor speed, and the aerodynamic parameters of the turbine, such as the power coefficient (Cp), have been simulated in order to construct a Simulink model that computes mechanical torque and power from a wind turbine, as shown in figure 3.5 above.

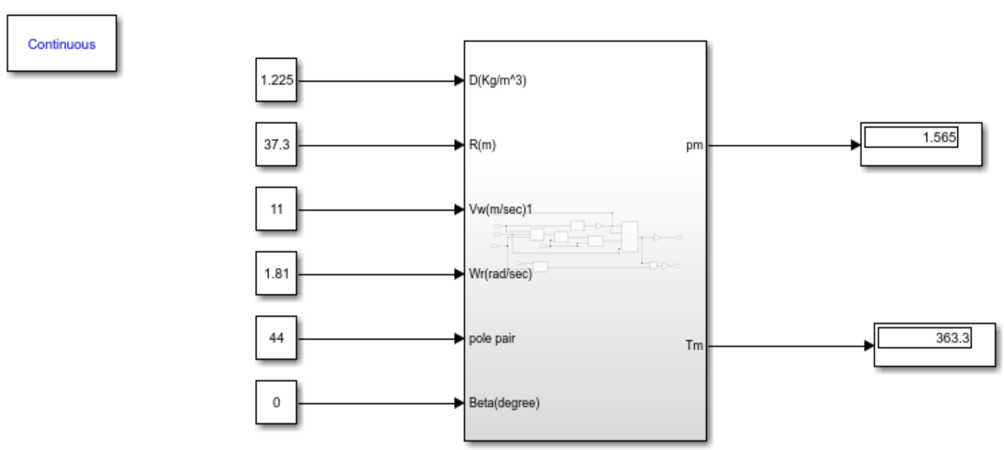

Figure 3.6: Overall wind turbine model

To develop an overall Simulink wind turbine model, numerous sub-models representing the various components and dynamics of the wind turbine system must be combined. Typical components include the wind speed input, aerodynamic rotor dynamics, control systems, generator, and drive train.

3.4. Modeling of drive trains

The mechanical parts of a wind turbine system's drive train consist of a gearbox with generator, a hub with blades, a rotor shaft (which can be quite lengthy in systems that use asynchronous generators to convert wind energy into electricity), and a pitching mechanism for the blades. To make calculations easier while preserving a respectable level of accuracy for transitory processes, lower mass models are being researched. This work anticipated that the system generator with multiple poles would not have a gearbox. A low-speed permanent magnet synchronous generator needs to be attached to the wind turbine in this situation.Based on this approximation, the one-lumped mass model drive train for the system analysis is selected; equation (3.14) (Coney, 2017) provides this information:

$$\frac{dwm}{dt} = \frac{1}{J_{eq}}(T_m - T_e - B_{wm}) \qquad (3.14)$$

The equivalent inertia of a wind energy system is the sum of the inertias of the generator and turbine. The rotational inertia Jeq in kg/m2 of a generator can be calculated using the following formula:

$J_{eq} = J_g + \frac{J_w}{ng^2}$, the gear ratio; ng for the current work is one as no gearbox has been considered.

Table 3.2 : Drive Train Parameters (Adama wind farm-1).

Parameters	***symbol***	***Value and units***
Damping coefficients	B	0.0197
Equivalent Inertia	J_{eq}	$0.003 kg/m^2$

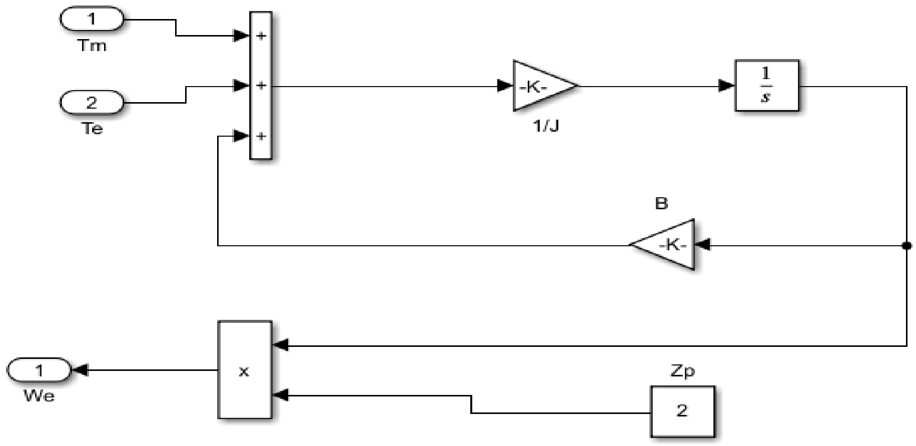

Figure 3.7: Simulink model of drive train

The drive train is in charge of transferring mechanical power from the rotor to the generator as depicted in figure 3.7 above. An accurate simulation of the wind turbine's drive train component is necessary to assess the stability and overall performance of the machine. The generator's electrical angular speed (rad/sec) can be explained as follows:

$$\omega e = \frac{zp}{2}\,\omega_g \tag{3.15}$$

3.5. Modeling of PMSG

A thorough mathematical model of PMSG is necessary for the development of machine control algorithms as well as the examination of the steady state and dynamic characteristics of wind energy conversion systems.

3.5.1. Modeling of a PMSG in the natural abc three phase stationary reference frame

A three-phase, Fourty four-pole PMSG cross-section is shown in Figure 3.8 below. Time-varying three-phase AC currents flowing through the stator's a, b, and c phase windings produce MMFs (fa, fb, and fc). These MMFs are oriented along the fixed abc axis. The rotor's d-axis is the center of symmetry for the flux generated by the permanent magnet. This suggests that the rotor, PMSG, and dq-axes have equivalent angular speed differences.

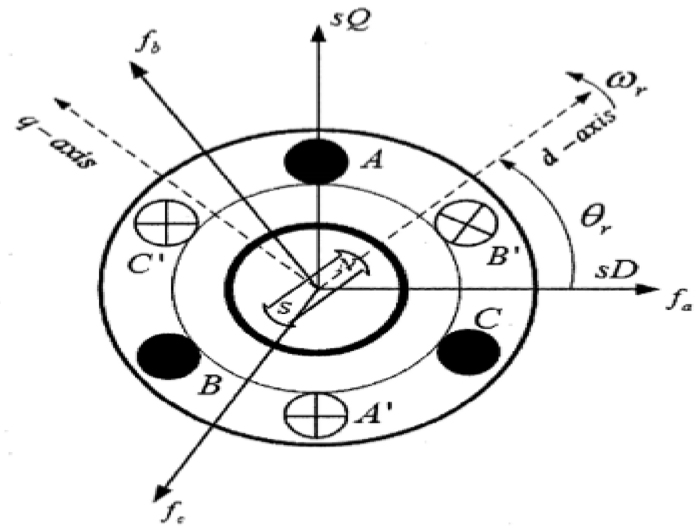

Figure 3.8: Cross-section view of the PMSG (Becerra et al, 2017).

One can calculate the phase flux connections induced by the PMSG and stator currents using the following equations (3.16), which relate the phase currents to the PMSG terminal voltages in state space (Acarnley, 2017).

$$\begin{aligned} V_{as} &= R_s i_{as} + \frac{d}{dt}\lambda_{as} \\ V_{bs} &= R_s i_{bs} + \frac{d}{dt}\lambda_{bs} \\ V_{cs} &= R_s i_{cs} + \frac{d}{dt}\lambda_{cs} \end{aligned} \tag{3.16}$$

Vas, Vbs, and Vcs stand for the instantaneous three-phase stator voltages, and ias, ibs, and icss stand for the instantaneous three-phase stator currents. Here, the instantaneous flux connections formed by the PMSG and the three phase AC currents are denoted by the symbols bs, cs, and λas, λbs, and λcs, respectively. These connections can be enlarged and approximated using equations (3.17) (Kong et al, 2018).

$$\begin{bmatrix} \lambda_{as} \\ \lambda_{bs} \\ \lambda_{cs} \end{bmatrix} = \begin{bmatrix} L_{aa} & L_{ab} & L_{ac} \\ L_{ba} & L_{bb} & L_{bc} \\ L_{ca} & L_{cb} & L_{cc} \end{bmatrix} . \begin{bmatrix} i_{as} \\ i_{bs} \\ i_{cs} \end{bmatrix} + \begin{bmatrix} \lambda_r \cos(\theta) \\ \lambda_r \cos(\theta - \frac{2\pi}{3}) \\ \lambda_r \cos(\theta + \frac{2\pi}{3}) \end{bmatrix} \tag{3.17}$$

Specifically, the numbers Laa, Lbb, and Lcc reflect the self-inductances of the a, b, and c three-phases. Lab, Lac, Lba, Lbc, Lca, and Lcb denote the mutual inductances between these phases, whereas λr indicates the rotor flux linkage generated by the permanent magnet synchronous generator. A function dependent on θ exists for all self- and mutual-inductances. The result is that all inductances are parameters that fluctuate with time.

3.7. Modeling of the PMSG in the dq-axes rotating reference frame

The PM synchronous machine is often evaluated in a dq-reference frame that rotates synchronously with the rotor, where the d-axis is orthogonal to the d-axis and aligned with the magnet axis. This frame is known as the popular machine model. The stator voltages, stator currents, and flux connections that make up the phase quantities of three-phase systems, such as PMSGs, are time-varying quantities. Any kind of electrical system may be broadly represented using the space phasor theory. Irrespective of the kind of current, AC or DC machine, or number of phases, it may generate transformation equations. Magnetic flux, voltage, currents, and other machine quantities are expressed using complex space vectors. The space phasor theory is particularly important because it can accurately explain the machine's performance in both steady state and transient operation, and it can be applied to any instantaneous fluctuation in voltage and current. Since it is not restricted to analyzing just the steady-state regime of a balanced three-phase system, it offers a general and comparatively simple model of the poly-phase system for both transient and steady-state events (Chen, 2017). The machine has two stages because the complex space vectors may be expressed in this way using two orthogonal axes. The design is made simpler by using the two-phase machine model, which reduces the number of equations. A permanent magnet generator's stator and a synchronous generator's wound rotor are constructed similarly. An excited coil produces the same back electromagnetic field as a permanent magnet. Consequently, the mathematical model may be derived using a synchronous generator. With a PMSG, the only distinction is the field current and damper windings calculations, which may be removed. The machine's performance is simulated and understood through the use of comparable circuits. This transformation technique makes it easier to understand and evaluate system models. By using the stator voltage equations in the dq-modeling of the AC machines, it is easy to get and model the equivalent circuits of the PMSG. According to the equation Ψf = Lmif, the flux from the permanent magnet along the rotor's d axis should be represented by a continuous current source. Ultimately, the following diagram illustrates the dq-modeling equivalent circuit of a permanent magnet synchronous generator (Lepka and Stekl, 2019):

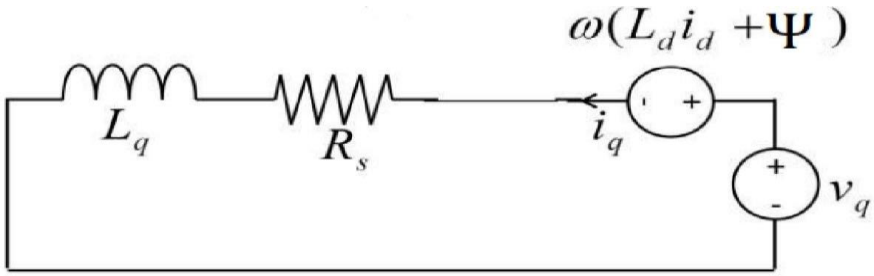

a. d-axis equivalent circuit

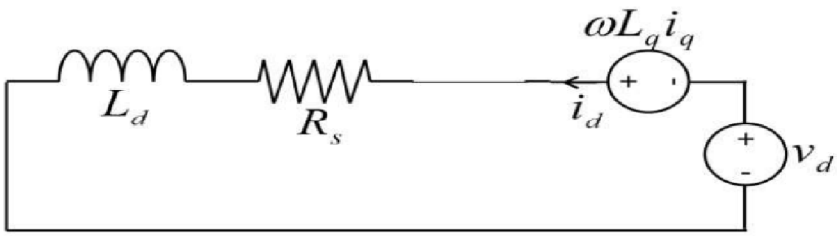

b. q-axis equivalent circuit

Figure 3.9: Equivalent circuits of the Permanent magnet synchronous generator (PMSG) in dqaxes (Chen, 2017).

The following state voltage equations for the PMSG are obtained by applying Kirchhoff's voltage law to the analogous circuits depicted in Figure 3.9 a and b.(Chen, 2017)

$$V_d = R_s i_d + L_d \frac{di_d}{dt} - \omega e \psi_q$$
$$V_q = R_s i_q + L_q \frac{di_q}{dt} - \omega e \psi_d \qquad (3.18)$$

Flux Linkages are given by:

$$\psi_q = L_q I_q$$
$$\psi_d = L_d I_d + \psi_f \qquad (3.19)$$

Substituting equations in (3.18) into (3.19) we can rewrite:

$$V_{q=} R_s i_q + L_q \frac{di_q}{dt} + \omega e(L_d i_d + \psi)$$
$$V_{d=} R_s i_d + L_d \frac{di_d}{dt} - \omega e L_q i_q \qquad (3.20)$$

To finish the PMSG mathematical model, the electromagnetic torque equation that is generated is computed as follows:

$$Te = 3(\frac{zp}{2})[\psi iq + (Ld - Lq) i_d i_q] \qquad (3.21)$$

The system parameters are arranged in appendix in table format.

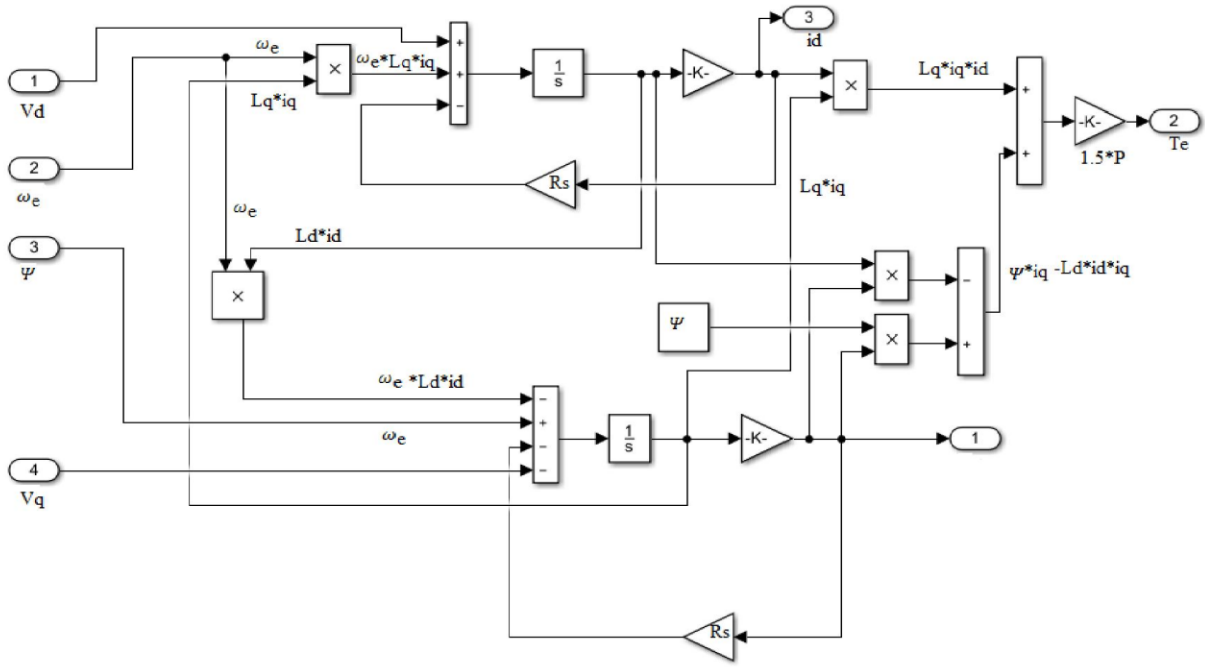

Figure 3.10: Simulink model of PMSG in dq-axis

The dq-axis approach reduces analysis and control complexity by transforming three-phase alternating current values into two direct current variables, as seen in Figure 3.10 above. This redesign was inspired by the Park makeoverThe modeling equation for understanding and analyzing the behavior of a permanent magnet synchronous generator has been constructed in a rotating reference frame (dq). The term "dq-transformation" refers to a coordinate transformation that converts a three phase stationary coordinate system into a dq-rotational coordinate system. There are two ways to finish this transition:

- Clarke transformation: converting the abc system to the αβ system.
- Park transformation: converting the αβ system to the dq system).

3.7.1. Clarke transformation

The complex current can be calculated using the following formula, where ia, ib, and ic stand for the instantaneous currents in each of the three phases:

$$\overline{is} = ia + \alpha ib + \alpha^2 ic \tag{3.22}$$

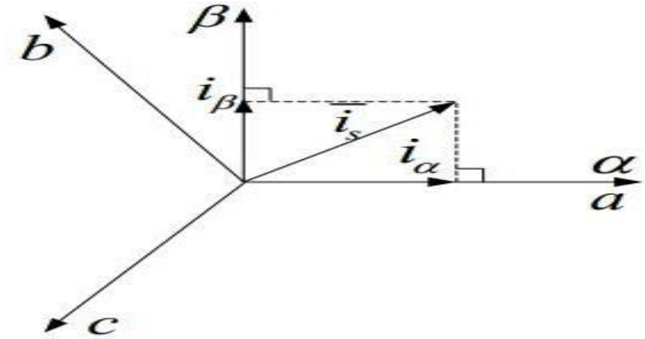

Figure 3.11: Clarke transformation(Boldea (2020)

Where $\alpha = e^{\frac{2\pi}{3}}$ and $\alpha^2 = e^{\frac{-2\pi}{3}}$, are spatial operators. Figure 3.11 depicts the Clarke transformation, where the α and a axes are in the same direction. The complex current $\overline{is}$ is projected on two orthogonal axes (α, β). These two axes are static in the three-phase stationary coordinate system.

3.7.2. Park transformation

In the Park transformation, the d axis corresponds to the grid voltage position. Park transforma tion is a projection of $\overline{is}$ onto rotating orthogonal axes (dq).

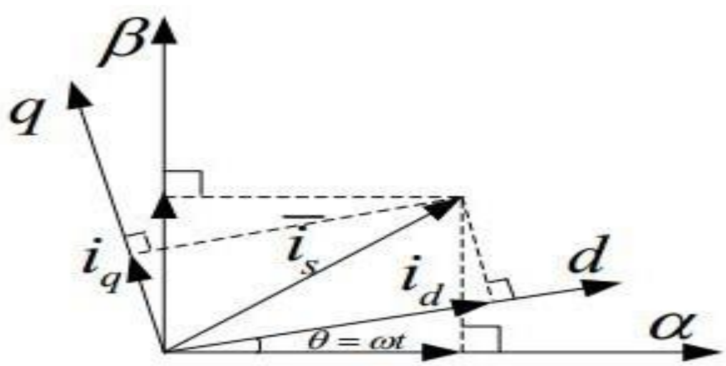

Figure 3.12: Park transformationBoldea (2020)

Figure 3.12 illustrates the Park transformation, which uses a rotating dq coordinates system with θ = ωt representing grid voltage position. You may create a matrix by combining these two transformations.

$$\begin{bmatrix} V_d \\ V_q \\ V_o \end{bmatrix} = \sqrt{\frac{2}{3}} \begin{bmatrix} \cos(\omega t) & \cos(\omega t - \frac{2\pi}{3}) & \cos(\omega t + \frac{2\pi}{3}) \\ -\sin(\omega t) & -\sin(\omega t - \frac{2\pi}{3}) & -\sin(\omega t + \frac{2\pi}{3}) \\ \frac{\sqrt{2}}{2} & \frac{\sqrt{2}}{2} & \frac{\sqrt{2}}{2} \end{bmatrix} \begin{bmatrix} V_a \\ V_b \\ V_o \end{bmatrix}$$

$$\begin{bmatrix} i_d \\ i_q \\ i_o \end{bmatrix} = \sqrt{\frac{2}{3}} \begin{bmatrix} \cos(\omega t) & \cos(\omega t - \frac{2\pi}{3}) & \cos(\omega t + \frac{2\pi}{3}) \\ -\sin(\omega t) & -\sin(\omega t - \frac{2\pi}{3}) & -\sin(\omega t + \frac{2\pi}{3}) \\ \frac{\sqrt{2}}{2} & \frac{\sqrt{2}}{2} & \frac{\sqrt{2}}{2} \end{bmatrix} \begin{bmatrix} i_a \\ i_b \\ i_o \end{bmatrix} \quad (3.23)$$

The inverse transformation from the d, q system to the a, b, and c systems is represented as follows.

$$\begin{bmatrix} V_a \\ V_b \\ V_o \end{bmatrix} = \sqrt{\frac{2}{3}} \begin{bmatrix} \cos(\omega t) & -\sin(\omega t) & \frac{\sqrt{2}}{2} \\ \cos(\omega t - \frac{2\pi}{3}) & -\sin(\omega t - \frac{2\pi}{3}) & \frac{\sqrt{2}}{2} \\ \cos(\omega t + \frac{2\pi}{3}) & -\sin(\omega t + \frac{2\pi}{3}) & \frac{\sqrt{2}}{2} \end{bmatrix} \begin{bmatrix} V_d \\ V_q \\ V_o \end{bmatrix}$$

$$\begin{bmatrix} i_a \\ i_b \\ i_o \end{bmatrix} = \sqrt{\frac{2}{3}} \begin{bmatrix} \cos(\omega t) & -\sin(\omega t) & \frac{\sqrt{2}}{2} \\ \cos(\omega t - \frac{2\pi}{3}) & -\sin(\omega t - \frac{2\pi}{3}) & \frac{\sqrt{2}}{2} \\ \cos(\omega t + \frac{2\pi}{3}) & -\sin(\omega t + \frac{2\pi}{3}) & \frac{\sqrt{2}}{2} \end{bmatrix} \begin{bmatrix} i_d \\ i_q \\ i_o \end{bmatrix} \quad (3.24)$$

Space Phasors for Generator Variables.

Equations (3.17) can be expressed as follows if the three-phase generator quantities are Xa, Xb, and Xc:

$$\begin{aligned} X_{a} &= X\cos(\omega t) \\ X_{b} &= X\cos(\omega t - \tfrac{2\pi}{3}) \\ X_{c} &= X\cos(\omega t - \tfrac{4\pi}{3}) \end{aligned} \quad (3.25)$$

In a three-phase system, the Space Phasor is calculated by adding the vector sums of the three phases. i.e

$$X = \frac{2}{3}(xa + xbe^{\frac{j2\pi}{3}} + xce^{\frac{j4\pi}{3}}) \tag{3.26}$$

Where, $e^{\frac{j2}{3}} = \cos(\frac{2\pi}{3}) + j\sin(\frac{2\pi}{3})$

X is called the space phasor or complex space vector.

The space phasor in a stationary two-phase system is described as follows:

$$X = X_d + jX_q \tag{3.27}$$

There is no zero sequence component for three-phase balanced system variables. An other method for figuring out the zero-sequence component is given as follows:

$$X = \frac{1}{3}(X_a + X_b + X_c) \tag{3.28}$$

It is necessary for the two-phase system's space phasor to match the three-phase system's. Therefore,

$$X_d = \mathrm{Re}\left[X\right] = \mathrm{Re}\left[\frac{2}{3}(X_a + \alpha X_b + \alpha^2 X_c)\right] = \frac{2}{3}(X_a - \frac{1}{2}X_b - \frac{1}{2}X_c)$$

$$X_q = \mathrm{Im}\left[X\right] = \mathrm{Im}\left[\frac{2}{3}(X_a + \alpha X_b + \alpha^2 X_c)\right] = \frac{1}{\sqrt{3}}(X_b - X_c) \tag{3.29}$$

$$\begin{bmatrix} X_d \\ X_q \\ X_o \end{bmatrix} = \begin{bmatrix} \frac{2}{3} & -\frac{1}{3} & -\frac{1}{3} \\ 0 & \frac{1}{\sqrt{3}} & -\frac{1}{\sqrt{3}} \\ \frac{1}{3} & \frac{1}{3} & \frac{1}{3} \end{bmatrix} \begin{bmatrix} X_a \\ X_b \\ X_o \end{bmatrix},$$

Under balanced conditions, the zero sequence component can calculated as:

$X_o = (X_a + X_b + X_c) = 0$

Assuming the balanced conditions, the abc-dq transformation:

$$T_{abc}{}^{-1} = \begin{bmatrix} 1 & 0 & 1 \\ -\frac{1}{2} & \frac{\sqrt{3}}{2} & 1 \\ -\frac{1}{2} & -\frac{\sqrt{3}}{2} & 1 \end{bmatrix} \tag{3.30}$$

Where, $$T_{abc} = \begin{bmatrix} \frac{2}{3} & -\frac{1}{3} & -\frac{1}{3} \\ 0 & \frac{1}{\sqrt{3}} & -\frac{1}{\sqrt{3}} \\ \frac{1}{3} & \frac{1}{3} & \frac{1}{3} \end{bmatrix}$$

The inverse transform (dq-abc transformation) is given by:

$$X_{abc} = T_{abc}{}^{-1} X_{dq} \tag{3.31}$$

Where, $$T_{abc}{}^{-1} = \begin{bmatrix} 1 & 0 & 1 \\ -\frac{1}{2} & \frac{\sqrt{3}}{2} & 1 \\ -\frac{1}{2} & -\frac{\sqrt{3}}{2} & 1 \end{bmatrix}$$

$$X_a = X_d + X_o$$

$$X_b = -\frac{1}{2} X_d + \frac{\sqrt{3}}{2} X_q + X_o$$

$$X_c = -\frac{1}{2} X_d - \frac{\sqrt{3}}{2} X_q + X_o \tag{3.32}$$

$$
\begin{aligned}
i_a &= i_\alpha + i_o \\
i_b &= -\frac{1}{2} i_\alpha + \frac{\sqrt{3}}{2} i_\beta + i_o \\
i_c &= -\frac{1}{2} i_\alpha - \frac{\sqrt{3}}{2} i_\beta + i_o
\end{aligned}
\tag{3.33}
$$

The coordinates of the dq-rotating reference frame, which are independent of time, can be obtained by translating the components of the stationary (αβ) reference frame. Boldea (2020) provides an equation for determining the current components in a dq-reference frame.

$$
\begin{aligned}
i_d &= i_\alpha \cos\theta + i_\beta \sin\theta \\
i_q &= -i_\alpha \sin\theta + i_\beta \cos\theta
\end{aligned}
\tag{3.34}
$$

In this case, id stands for both the component that produces torque and the flux. Because the phasor components in this reference frame are not time dependent, they can be easily manipulated. To determine the dq-coordinate system components, use the equations (3.24) for cos θ and sin θ, given the rotor position θ. Equation (3.35) provides a direct calculation for cos and sin θ [48].

$$
\begin{aligned}
\sin\theta &= \frac{\Psi_{r\beta}}{\Psi_{r\alpha}} \\
\cos &= \frac{\Psi_{r\alpha}}{\Psi_{r\beta}}
\end{aligned}
\tag{3.35}
$$

Based on the components id and iq from the dq-reference frame, the αβ- system coordinates can be obtained using equation (3.36) (Chinchilla et al, 2006).

$$
\begin{aligned}
i_\alpha &= i_d \cos\theta - i_q \sin\theta \\
i_\beta &= i_d \sin\theta + i_q \cos\theta
\end{aligned}
\tag{3.36}
$$

This model uses (equations 3.33 and 3.36) to convert from dq- to abc

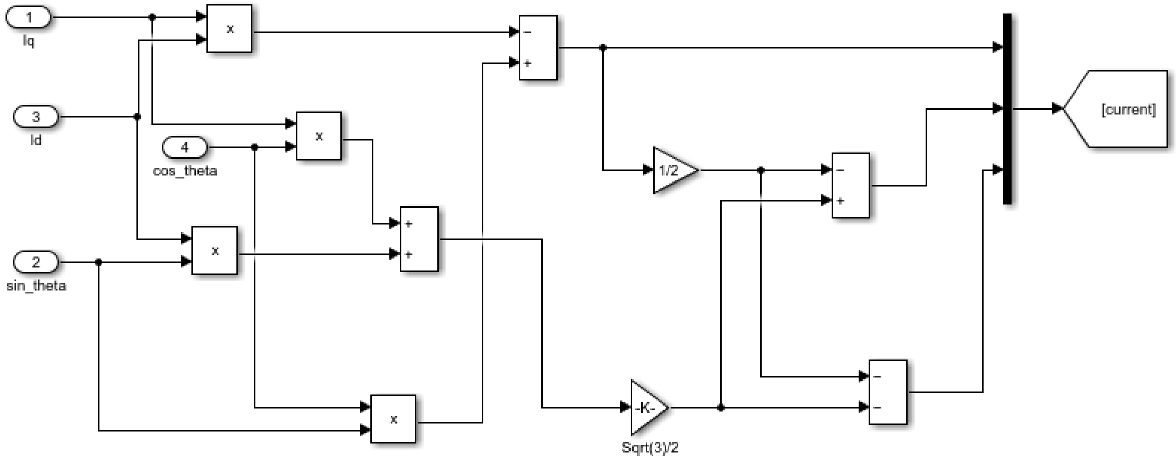

Figure 3.13: Simulink Model for three phase current by Clarke transformation

The figure 3.13 above depicts the Clarke transformation, also known as the αβ transformation, converts three-phase currents or voltages into two orthogonal components (α and β) in a stationary reference frame. This transformation is useful for simplifying three-phase system analysis and is frequently used as a precursor to subsequent transformations such as the Park transformation.

By using equation (3.37) the three phase voltages, can be determined as follows (Pena et al, 2016).

$$
\begin{aligned}
V_a &= V_\alpha + V_o \\
V_b &= -\frac{1}{2}V_\alpha + \frac{\sqrt{3}}{2}V_\beta + V_o \\
V_b &= -\frac{1}{2}V_\alpha - \frac{\sqrt{3}}{2}V_\beta + V_o
\end{aligned}
\tag{3.37}
$$

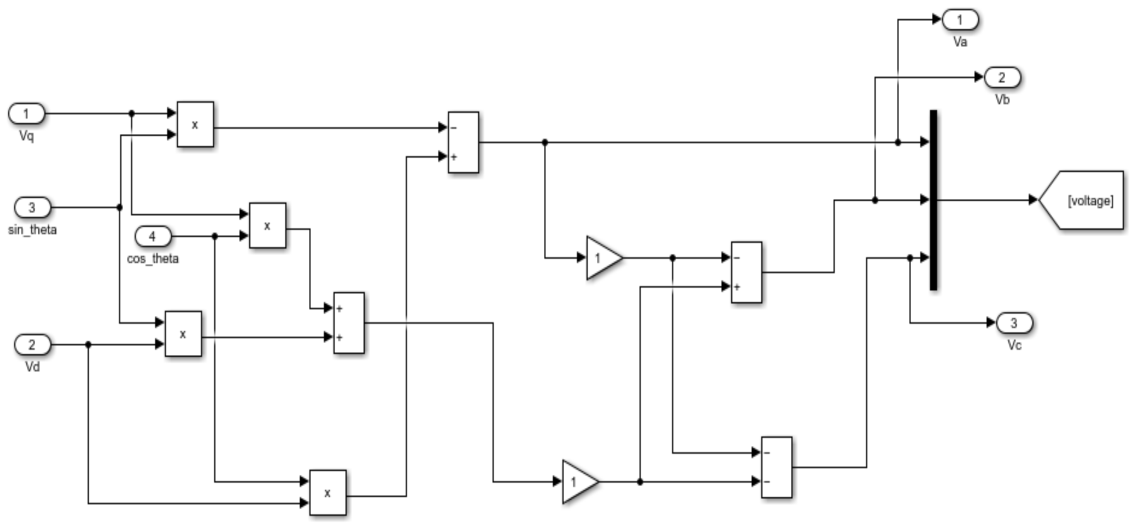

Figure 3.14: Simulink model for three phase voltage by Clarke transformation

Using a Simulink model that use the Clarke transformation to split three-phase voltages (va, vb, and vc) into two orthogonal components (α and β), Figure 3.14 above is used to control and study three-phase electrical systems, such as motor drives and power electronics.

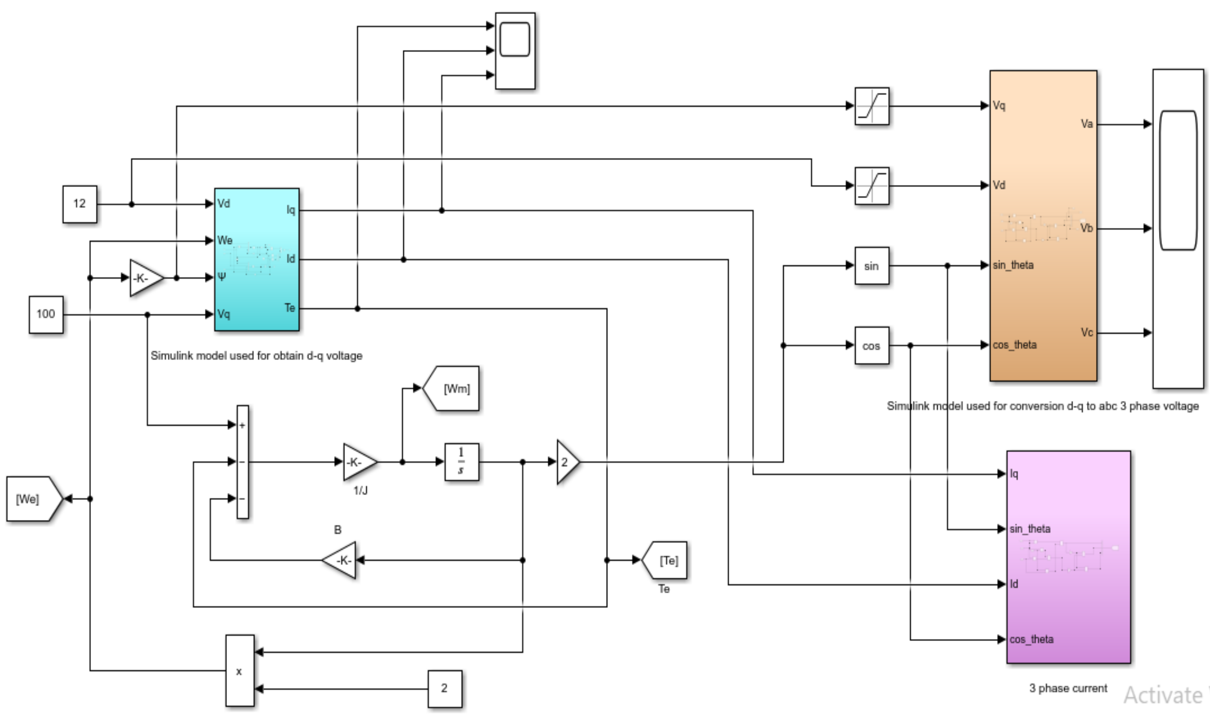

Figure 3.15: Simulink model of overall PMSG

A Permanent Magnet Synchronous Generator (PMSG) has several components, including electrical dynamics, mechanical dynamics, and control systems, as shown in the Simulink model in figure 3.15 above. In order to control and simplify the model, three-phase AC voltages and currents are frequently altered using Park and Clarke transformations into the dq-axis (rotating reference frame). I will discuss the main elements and their implementation in a PMSG Simulink model in this part. The main components of PMSG overall are Three-Phase Voltage and Current Generation, Park Transformation (αβ to dq), Electrical Dynamics in the dq Axis, Mechanical Dynamics Inverse Park Transformation (dq to αβ), and Inverse Clarke Transformation (αβ to abc).

The three-phase output AC power in this study is converted into a DC voltage at the PMSG terminals using a diode rectifier. Thus, all of the data that was utilized to simulate the PMSG came from Adama Wind Farm-1 and was included in the appendix.

3.8. Uncontrolled diode rectifier

A three phase diode rectifier's rectified (output dc voltage) (Vrec) is found using the following formula:

$$V_{O=}V_{rec} = \frac{3\sqrt{2}}{\Pi} V_{llrms} \tag{3.38}$$

Where, V_{llrms} represents the line-to-line voltage delivered to the rectifier as a root mean square.

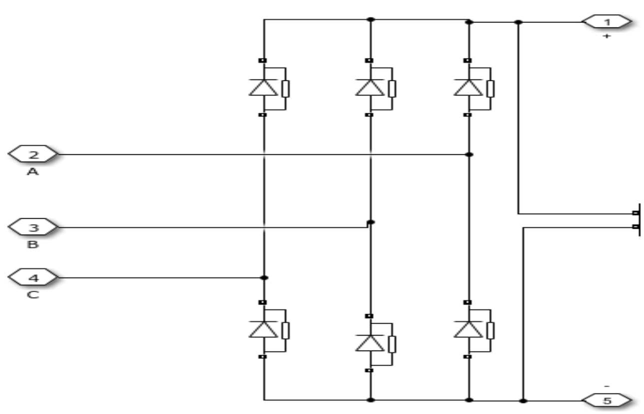

Figure 3.16: diode rectifier operating in three phases.

A three-phase diode rectifier is usually made using a bridge arrangement with six diodes, as seen in figure 3.16 above. The rectifier produces a pulsating DC output by converting the three-phase alternating current inputs. It is commonly used in industrial applications including DC motor drives, battery charging, and power supply devices that need DC power from an AC source.

3.9. Modeling and control of Battery energy storage system (BESS)

A battery converts chemical energy into electrical energy. Since the battery's output voltage is influenced by both current and state of charge (SOC), which is a nonlinear function of time, it is thought of as a nonlinear voltage source. (2020 Peterspon). Two significant indicators of battery state of charge and terminal voltage are described by the next two parameters:

$$\begin{aligned} & V_o + R_b i_b - K \frac{Q}{Q + \int ibdt} + A \exp(B \int ibdt) \\ & soc = 100(1 + \frac{\int i_{bdt}}{Q}) \end{aligned} \tag{3.39}$$

Rechargeable energy source or the percentage of the battery's maximum possible charge is shown by the State of Charge (SOC). This encompasses the subsequent items: The battery's capacity is denoted by Q, its internal resistance is represented by Rb, its polarization voltage is K, its open circuit voltage is V0, and the exponential voltage and capacity are represented by A and B, respectively.

3.9.1. Battery current and voltage controller design

The energy storage system is composed of the battery, the control system, and the bidirectional DC/DC converter. Figure 3.17 shows the control system of a bidirectional converter, which can control power flow in both directions. When IGBT S w1 is turned on and IGBT S w2 is turned off, the converter acts as a boost circuit and charges the battery. By discharging the battery while IGBT S w2 is turned on and IGBT S w1 is turned off, it operates as a buck circuit. The goal of the control is to deliver a DC bus voltage that is of excellent quality and has good dynamics. This system compares the DC bus voltage Vdc to its reference voltage, Vref, and sends the difference to a PI controller in order to determine the battery current reference Iref, which acts as the inner loop's input signal. The difference between Iref and battery current Ibatt is then used to determine the signal for the PWM generator to turn on or off S w1 and S w2. The battery reference current is computed as follows:

$$I_{bref=} \frac{B_{bdref}}{\frac{B_{chref}}{V_b}} \qquad (3.40)$$

In this case, Vb represents the battery voltage, Ibref the battery reference current, Bdisref the battery discharge reference, and Bchref the battery charging reference.

Therefore, Transfer function= $I_{bref=} \frac{B_{bdref}}{\frac{B_{chref}}{V_{bs}}} = (\tau_1), \tau_1 = \frac{1}{V_{bs}}$

$$K_p = K; \quad K_I = \frac{K}{\tau_1}$$

$$L = \frac{V_{batt} * (V_{dc} - V_{batt})}{i_{batt} * f_s * V_{dc}} \qquad (3.41)$$

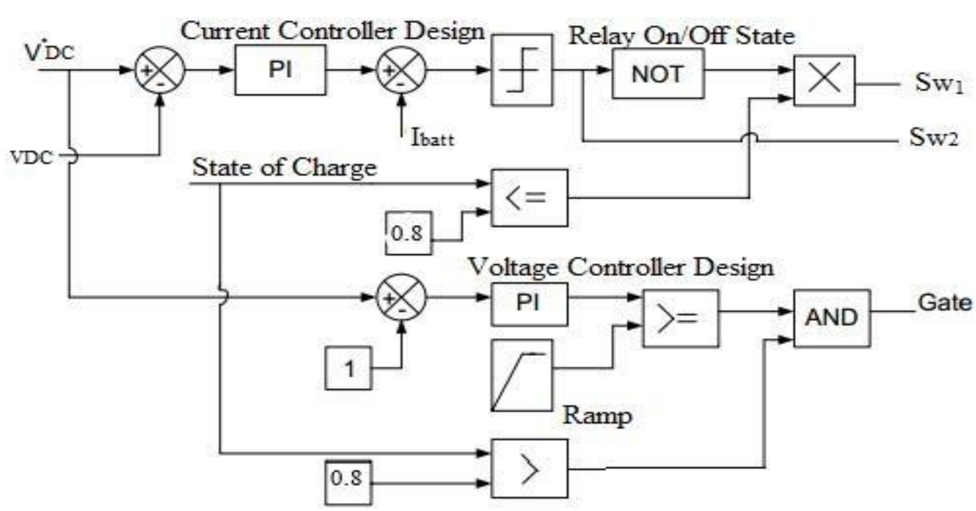

Figure 3.17: Control Strategy of battery charge and discharge (Petersspon, 2020)

The system control parameters are derived using equation (3.40) and reported in table 3.5.

Table 3.3 Battery Parameters

Parameters	*Value and units*
Rated Capacity(Q)	6.5Ah
Battery voltage(V_b)	400V
Sate of charge(SOC)	80%

Table 3.4 Battery control parameters

Control parameters	*Value*
K_{P1}	2sec
K_{i1}	120sec
K_{P1}	60sec
K_{i1}	550pu

The Battery control systems above are derived and calculated by using equation (3.40) above.

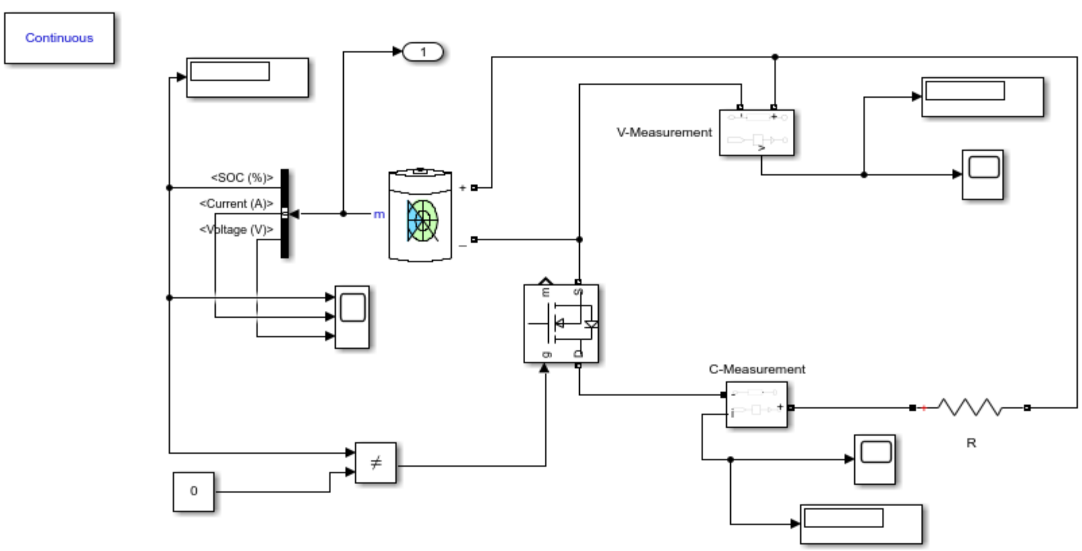

Figure 3.18: Overall Battery Simulink model

The battery model in figure 3.18 above is a Simulink representation that is used to mimic the behavior of real batteries in a range of settings, such as energy storage systems. Lithium-ion is modeled. Typically, the electrical characteristics, state of charge (SOC), and thermal dynamics are the main elements of a battery model.

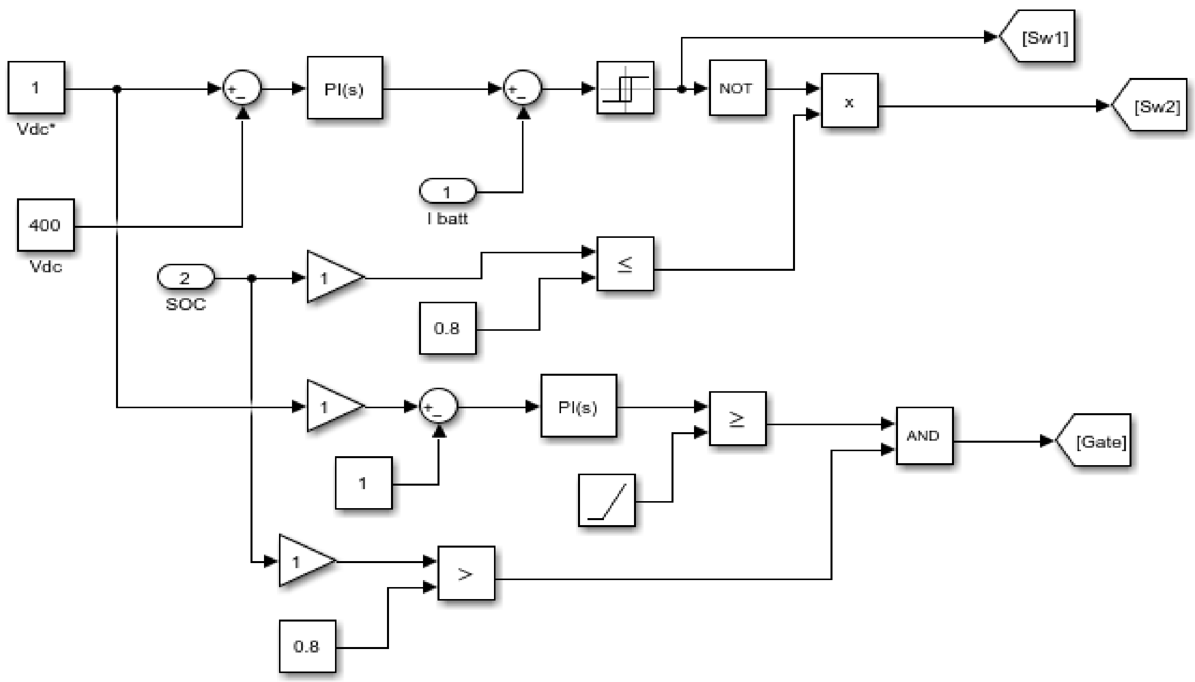

Figure 3.19: Battery controllers with a voltage and current Simulink model

In Simulink of figure 3.19 above, The voltage and current controllers for batteries are designed by designing control systems that can manage the battery's charging and discharging processes to maintain desired voltage and current levels. This often entails developing a feedback control loop using Proportional-Integral (PI) controllers.

3.10. DC To DC Converter

This electrical apparatus modifies the level of the DC voltage output by adjusting the input DC voltage. Three topologies are common to DC-DC converters. A boost converter was used in this thesis work.

3.10.1. Boost converter

The four components of the boost converter are the inductor, capacitor, diode, and electrical switch. The components of the boost converter are seen in the figure 3.20 below. The duration of the on and off switch determines the average output voltage. It continuously adjusts the ON and OFF times of the switch. The ratio of ON duty to switching time period is used to compute the switching duty cycle (D). During the switching phase, the converter operates in two modes: continuous conduction mode (CCM) and discontinuous conduction mode (DCM), depending on energy injection and absorption.(Mohan, Edouard Ned, and others, 2021).

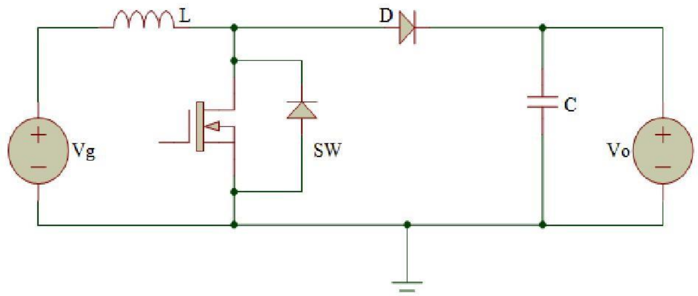

Figure3.20: Circuit diagram of boost converter time (Petersspon, 2021)

The figure 3.20 above illustrates how a DC to DC converter, sometimes referred to as a boost converter or step-up converter, increases the input voltage to raise the output voltage. It is widely utilized in power supplies, battery charging, and renewable energy systems. A boost converter is composed of an inductor, a capacitor, a diode, and a switch, usually a transistor.

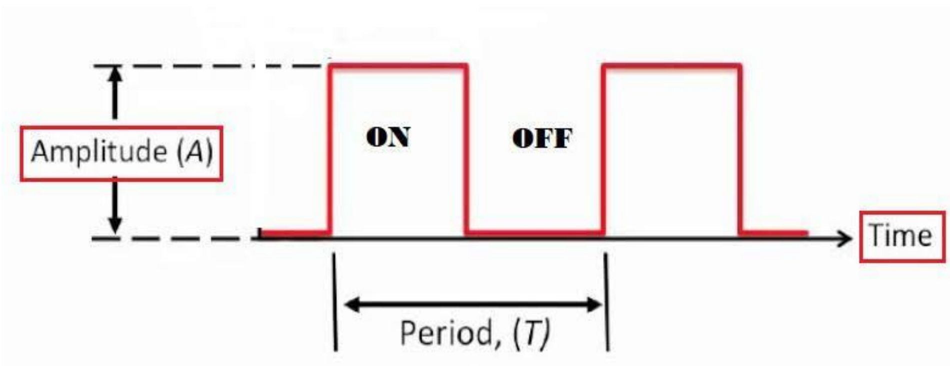

Figure 3.21: Waveform of PWM(Eduard Ned Mohan et al, 2021)

An algorithm for creating pulsating signals from messages is called pulse width modulation, or PWM as shown on figure 3.21 above . Power management for electrical equipment, LED dimming, and motor speed control are just a few of the many uses for it.

3.10.2. Steady state analysis of the boost converter

Under CCM, boost converter functions in two modes.

Mode 1: As seen in the picture, the switch Sw1 is activated at t=0. 3.22. The switch Sw and inductor L are both passed through by the increasing input current. In this mode, the load receives energy from the capacitor current that is stored in the inductor.

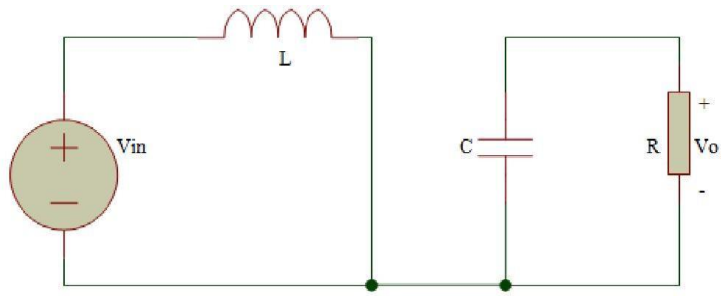

Figure 3.22: The ON State circuit diagram of the boost converter (Petersspon, 2021)

Turning on the switch causes the capacitor to discharge across the load and charges the inductor from the input voltage source Vin.

The duty cycle, $D = \frac{T_{on}}{T}$ where, $T = \frac{1}{f_s}$

Mode 2: Starts As soon as the switch is turned off, at t=DT. As seen in Figure 3.23, the channels that the current passing through the switch would now take are the load R, output capacitor C, diode D, and inductor L. Until the switch is turned back on during the subsequent cycle, the inductor current decreases. In this period, the input voltage and the energy stored in the inductor are transferred to the load.

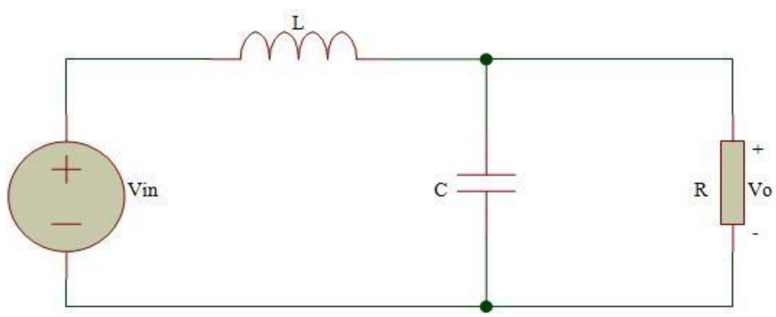

Figure 3.23: The OFF-State circuit diagram of the boost Converter(Petersspon,2021)

By multiplying the input voltage by the inductor voltage and turning off the switch, the load voltage is determined.

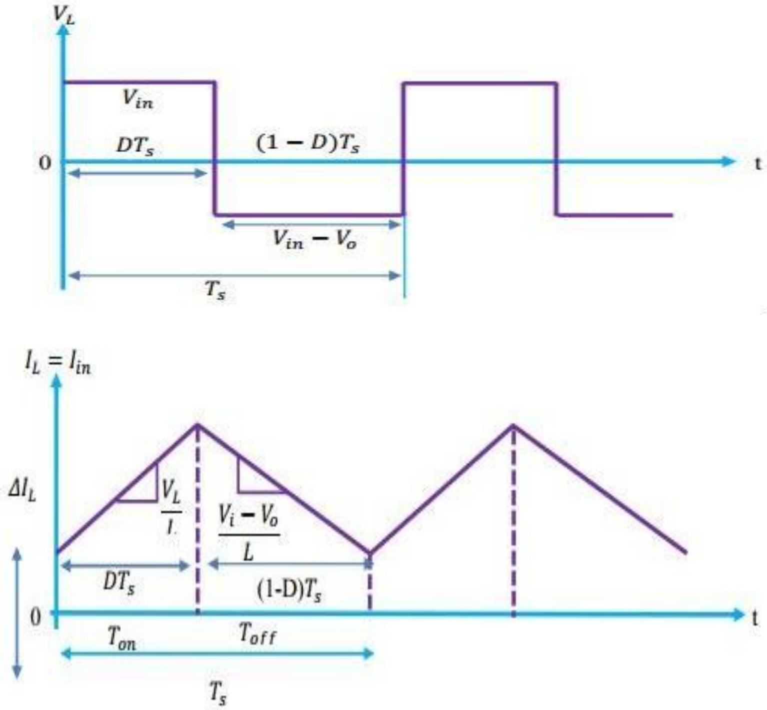

Figure 3.24: Inductor current waveform and voltage waveform(Petersspon, 2021)

The following equations are developed using the above-mentioned boost converter operating paradigm. Using the inductor voltage balance formula as a guide:

$$V_{in}(DT_s) + (V_{in} - V_o)(1 - D)T_s = 0$$
$$V_{in}(DT_s) - V_{in}(DT_s) - V_{in}(T_s) + V_o(DT_s) - V_oT_s = 0$$

$$V_o = \frac{V_{in}}{1 - D} \qquad (3.42)$$

Therefore; The duty cycle is: $D = 1 - \frac{V_{in}}{V_o}$

From the inductor current ripple analysis,

$$\triangle I_L = I_{\max} - \mathbf{I}_{\min}$$
$$\triangle I_L = \frac{V_{in}}{L} * (DT_S)$$
$$\triangle I_L = \frac{V_{in}}{L} * (D \frac{1}{fs})$$

$$L = \frac{DV_{in}}{\triangle I_L * fs * (\frac{V_o}{V_{in}})} \quad (3.43)$$

Where, $\triangle I_L = 0.243 * \frac{P_{out}}{V_{in}}$

For L> L_b , the boost converter runs in CCM where,

$$L_b = \frac{(1-D)^2 * D * R_{load}}{2fs} \quad (3.44)$$

The filter capacitor's minimum value that causes the voltage ripple () can be found by using the following formula:

$$C_{\min} = \frac{DV_o}{V_o * R_{load} * f_s} \quad (3.45)$$

The inductance needs to be built in such a way that the inductor current never stops flowing in order to operate the converter in continuous current mode, or CCM.

$$L_{\min} = \frac{(1-D)^2 * D * R_{load}}{2fs} \quad (3.46)$$

Where, $R = \frac{V_o}{I_o}$ is output resistance, and f is the switching frequency. In order to produce the appropriate output voltage ripple, the output capacitance is given by:-

$$C_{\min} = \frac{DV_o}{\triangle V_o * f_s} \quad (3.47)$$

$$\frac{\triangle V_o}{V_o} = 0.15$$

The International Electro-technical Commission (IEC) harmonics standard states that the acceptable range for CRF is 20% to 40%, which translates to:

1. Current Ripple Factor

$$\frac{\triangle I_l}{I_{out}} = 24.3$$

2. Voltage Ripple Factor

$$\frac{\triangle V}{V_o} = 15\%$$

3. Switching Frequency (fs)

f_s = 5Khz

Table 3.6 shows the system parameters computed using equations 3.43 and 3.47.

Table 3.5 Specifications for the DC to DC Boost Converter.

Parameters	***Symbol***	***Value and units***
voltage input	V_{in}	400V
Voltage output	V_{out}	800V
Power	P_{out}	1.5MW
Capacitor	C	7e-4F
Inductor	L	1706.6e-6H
Load resistance	R	1.76Ω
Duty of cycle	D	0.5
frequency switching	F_S	5KHz

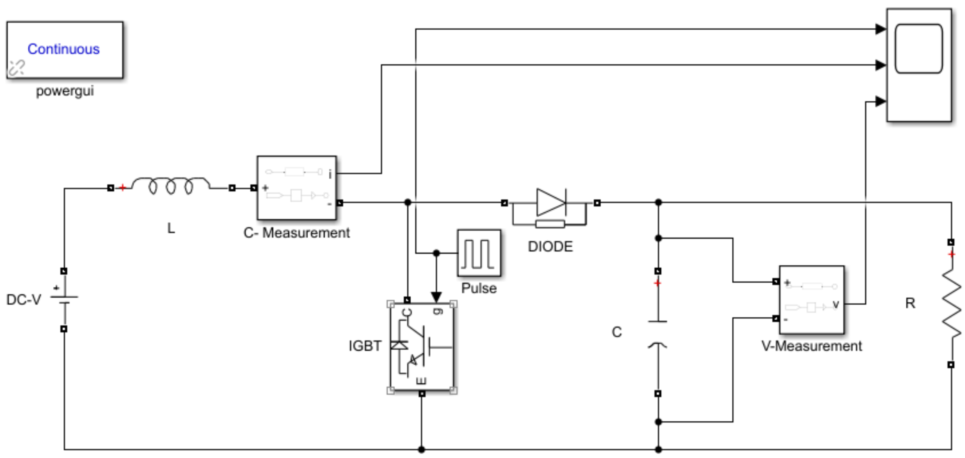

Figure 3.25: Simulink model DC to DC boost converter

3.11. Model of DC-Link

A similar circuit using the DC-link approach is shown in Figure 3.26 below. The machine side converter and the grid side are connected by the DC-link capacitor (Marko, 2011).

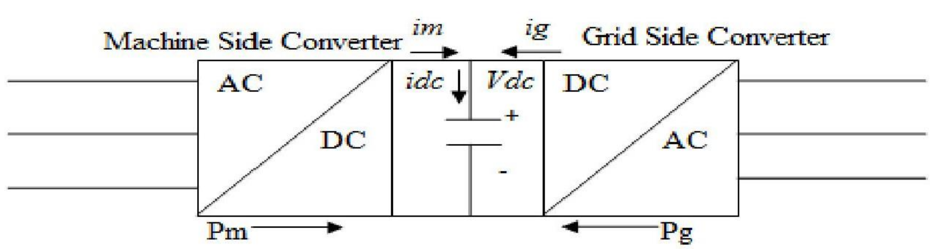

Figure 3.26: DC-link model(Marko, 2011)

The DC-link voltage (Vdc), capacitance (C), power flow (Pg) from the grid to the grid side converter, and power flow (Pm) from a renewable source to the machine side converter are illustrated in Figure 3.26. The energy of the capacitor is calculated using equation (3.48).

$$W_{dc} = \frac{1}{2} C V_{dc}^{\ 2} \tag{3.48}$$

The power flow from the machine side (Pm) and the grid side (Pg) together define the energy in the DC-link capacitor when energy losses are small. Equation (3.49) can be used to express the relationship.

$$\frac{dW_{dc}}{dt} = P_g + P_m \tag{3.49}$$

After removing the derivative portion, (3.47) becomes (3.48).

$$CV_{dc}\frac{dV_{dc}}{dt} = P_g + P_m \tag{3.50}$$

Where; $P_m = V_d i_d + V_q i_q$
$P_g = V_{dg} i_{dg} + V_{qg} i_{qg}$

According to equation (3.49), in order to maintain a constant DC-link voltage, −Pg = Pm is needed, which means that all of the machine side's power must be transferred to the grid side.

3.12. Grid side converter

Control signals for an IGBT's gate circuits are normally produced using a PWM signal generator. The simplest way to create a PWM signal is to take a frequency-alternating sawtooth or triangle waveform and combine it with a comparator. The output voltage waveforms are sinusoidal when contrasted to a triangle waveform when a sinusoidal control signal is used. Amplitude Vtri for the triangular waveform is maintained constant, let's say at 1 V. The PWM generator output is low when the triangle waveform value is smaller than the sinusoidal control signal value; otherwise it is high . The frequency of the triangle waveform determines the inverter switching frequency, whereas the primary output voltage waveform frequency equals the frequency of the sinusoidal control signal. The PWM algorithm defines two terms: amplitude modulation ratio and frequency modulation ratio. The following is an explanation of the amplitude modulation ratio (ma):

$$m_a = \frac{V_{control}}{V_{tri}} \tag{3.51}$$

Where, the sine control signal's amplitude is Vcontrol, and the triangular waveform's amplitude is Vtri. The following defines the frequency modulation ratio, or mf:

$$m_f = \frac{f_{tri}}{f_{control}} \tag{3.52}$$

Where, f control is the frequency of the sinusoidal control signal and fr is the frequency of the triangular waveform, commonly referred to as carrier frequency (Sachauder and Mehta, 2021).

3.12.1. Mathematical model of the grid side converter system model

The converter uses PWM and vector control techniques. Consider V_{dq} the d and q components of the converter output voltages in a dq rotating reference frame, and the DC-link voltage. If the amplitude of the triangle waveform in the PWM generator is 1 V, the d and q component signals are required to generate gate signals $V_{dnorm} = \frac{V_{d1,2}}{V_{dc}}$ And $V_{qnorm} = \frac{V_{Q1,2}V_{q1.2}}{V_{dc}}$ respectively.

Therefore, the amplitude modulation ratio of PWM generator is $ma = \sqrt{V_{dnorm}{}^{2} + V_{qnorm}{}^{2}}$ and It is possible to retrieve the converter output phase peak voltage.

As an output gain for control voltage, this is one way to think of the grid side converter. The analogous grid side converter circuit with grid filter in the dq axis reference frame is shown in Figure 3.27. In the analogous circuit, an inductor and a resistor make up the grid filter; resistance is denoted by Rf and inductance by Lf. Kirchhoff's voltage law is used to illustrate the relationships between the grid voltage and the converter output voltage in terms of current and grid filter parameters in the abc and dq axis reference frames, respectively, in (3.53) and (3.77).

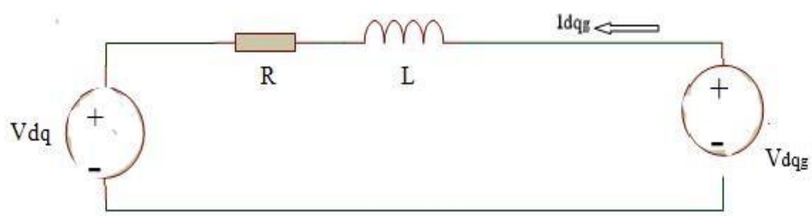

Figure 3.27: Grid side converter equivalent circuit in dq axes reference frame(Petersspon, 2021)

Applying d, q reference frame, (3.53) becomes (3.54),

$$\begin{bmatrix} V_{dg} \\ V_{qg} \end{bmatrix} = R_f \begin{bmatrix} I_{dg} \\ I_{qg} \end{bmatrix} + L_f \frac{d}{dt} \begin{bmatrix} I_{dg} \\ I_{qg} \end{bmatrix} + \omega s L_f \left[\begin{bmatrix} -i_q \\ i_d \end{bmatrix} \right] + \begin{bmatrix} V_d \\ V_q \end{bmatrix} \qquad (3.53)$$

$$V_{dgq} = R_f . I_{dqg} + \frac{di_{dqg}}{dt} + j\omega s L_f . i_{dqg} + V_{dq} \qquad (3.54)$$

Vdqg, idq, and Vdq, ωs represent the instantaneous space vectors of grid voltage, line current, converter output voltage, and grid voltage angular frequency, respectively.

3.13. STATCOM controller model

A PWM-based system that is connected to the grid is allegedly one component of the STATCOM idea.(Singh and Kadagala (2016). The voltage source PWM converter is connected to the grid by means of a transformer and grid filter, and it is shunt linked to a capacitor.

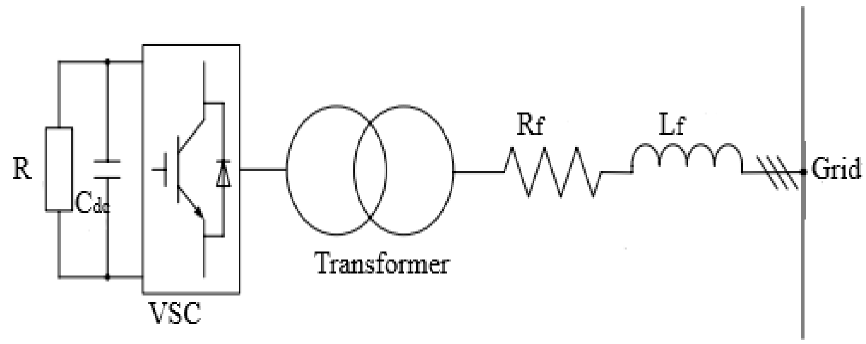

Figure 3.28: Configuration of STATCOM (Jung et al, 2017).

The circuit for the STATCOM system is shown in Figure 3.29. It has a supply voltage of V and a three-phase generating source. The equivalent impedance of the transmission line is (Rs + jLs). The load is linked at the point of common connection. As shown in Figure 3.29, a coupling transformer and filter with impedance (Rsh + jLsh) are used to link VSC to the PCC bus in addition. While the STATCOM dynamically absorbs or generates reactive power to adjust the bus voltage, the coupling transformer allows reactive power to flow from the inverter to the network. The operation of STATCOM can be examined using its mathematical model.

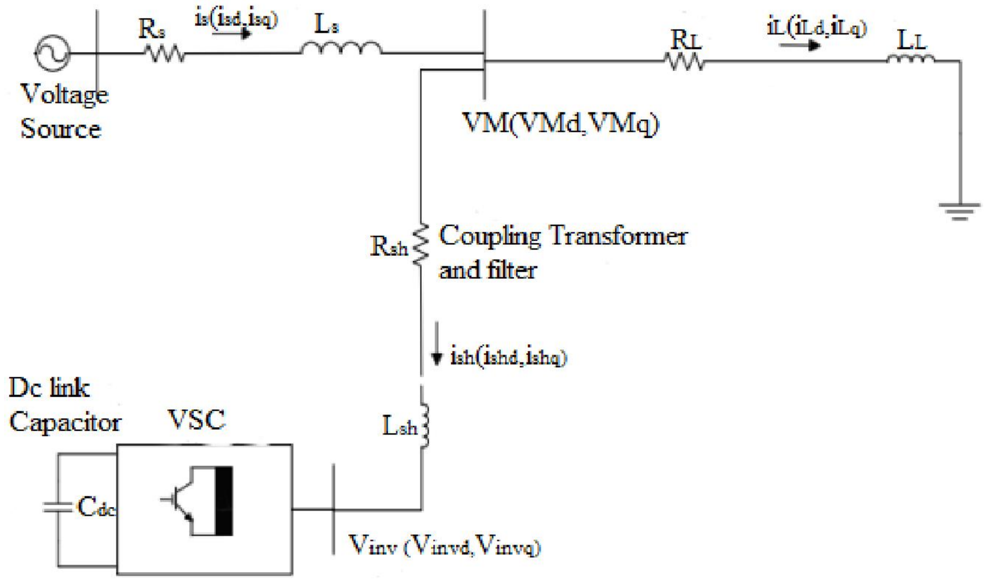

Figure 3.29: Single line circuit of a STATCOM (Kadagala ,2016).

3.13.1. Differential equations at the load source and shunt components:

Figure 3.30 displays the source side, load side, and shunt side KVL equations for every system component. The KVL equations for the source side are as follows:

$$\frac{di_{sd}}{dt} = \omega i_{sq} - \frac{R_s i_{sd}}{L_s} + (\frac{V_{sd} - V_{Md}}{L_s})$$

$$\frac{di_{sq}}{dt} = \omega i_{sd} - \frac{R_s i_{sq}}{L_s} + (\frac{V_{sq} - V_{Mq}}{L_s}) \tag{3.55}$$

Equations at load side:

$$\frac{di_{Ld}}{dt} = \omega i_{Lq} - \frac{R_s i_{Ld}}{L_L} + (\frac{V_{sd} - V_{Md}}{L_L})$$

$$\frac{di_{Lq}}{dt} = \omega i_{Ld} - \frac{R_s i_{Lq}}{L_L} + (\frac{V_{sq} - V_{Mq}}{L_L}) \tag{3.56}$$

Equations at shunt side:

$$\frac{di_{shd}}{dt} = \omega i_{shq} - \frac{R_{sh} i_{shd}}{L_{sh}} + (\frac{V_{shd} - V_{Md}}{L_{sh}})$$

$$\frac{di_{shq}}{dt} = \omega i_{shd} - \frac{R_{sh} i_{shq}}{L_{L}} + (\frac{V_{shq} - V_{Mq}}{L_{sh}}) \quad (3.57)$$

- **State space representation of STATCOM**

Using the power balancing equation on both the inverter and the DC side:

$$P_{dc} = P_{ac} \quad (3.58)$$

The values of grid side power in terms of current and the values of dc side power in terms of (Vdc, idc) are substituted:

$$V_{dc} i_{dc} = \frac{3}{2}(V_{gd} i_{shd} + V_{gq} i_{shq}) \quad (3.59)$$

The expression for current flowing through a capacitor is as follows:

$$i_{dc} = C_{dc} \frac{dV_{dc}}{dt} \quad (3.60)$$

From equation (3.58 and 3.59) equations (3.56) becomes,

$$\frac{dV_{dc}}{dt} = \frac{3}{2C_{dc}V_{dc}}(V_{gd} i_{shd} + V_{gq} i_{shq})$$

$$\frac{di_{shd}}{dt} = \frac{1}{L_{sh}}(V_{Md} - V_{gd} - R_{sh} i_{shd} + \omega i_{shq})$$

$$\frac{di_{shq}}{dt} = \frac{1}{L_{sh}}(V_{Mq} - V_{gq} - R_{sh} i_{shq} + \omega i_{shd}) \quad (3.61)$$

Therefore, $d_d = \frac{V_{gd}}{V_{dc}}$ And $d_q = \frac{V_{gq}}{V_{dc}}$

$$d_o = \frac{1}{2} + \frac{V_{gd}}{V_{dc}} \quad (3.62)$$

Hence, (3.61) can be written as:

$$\frac{dV_{dc}}{dt} = \frac{3}{2C_{dc}}(d_d i_{shd} + d_q i_{shq}) \quad (3.63)$$

As a result, the state space model of a STATCOM has the following expression:

$$\begin{bmatrix} \frac{dishd}{dt} \\ \frac{dishq}{dt} \\ \frac{dvdc}{dt} \end{bmatrix} = \begin{bmatrix} \frac{-Rsh}{Lsh} & \omega & \frac{-dd}{Lsh} \\ -\omega & \frac{-Rsh}{Lsh} & \frac{-dq}{Lsh} \\ \frac{3}{2Cdc}dd & \frac{3}{2Cdc}dq & 0 \end{bmatrix} \begin{bmatrix} i_{shd} \\ i_{shd} \\ V_{dc} \end{bmatrix} + \begin{bmatrix} \frac{1}{Lsh} & 0 \\ 0 & \frac{1}{Lsh} \\ 0 & 0 \end{bmatrix} \begin{bmatrix} V_{Md} \\ V_{Mq} \\ 0 \end{bmatrix} \quad (3.64)$$

$\dot{X}$ = [A]X + [B]U (3.65)

Table 3.6 STATCOM Parameters (Singh and Kadagala (2016)

Parameters	***Symbol***	***Value and units***
Angular Frequency	ωs	314rad/s
Grid Terminal Voltage	V	575V
DC Link Capacitor	C_{dc}	12000 μ F
Capacitor Voltage	V_{dc}	800V
Shunt Transformer	R_{sh} L_{sh}	0.002 Ω 0.06H
Transmission Line	R_{sh} L_{sh}	0.1433 Ω/km 3.32mH/km
Control Parameters (DC Voltage)	K_{P1} K_{i1}	7pu 100sec
Control Parameters (Current Controller)	K_{P2} = K_{P2} K_{i2} = K_{i2}	0.18pu 0.001sec
Control Parameters (AC Voltage Controllers)	K_{P3} K_{i3}	60pu 1400sec

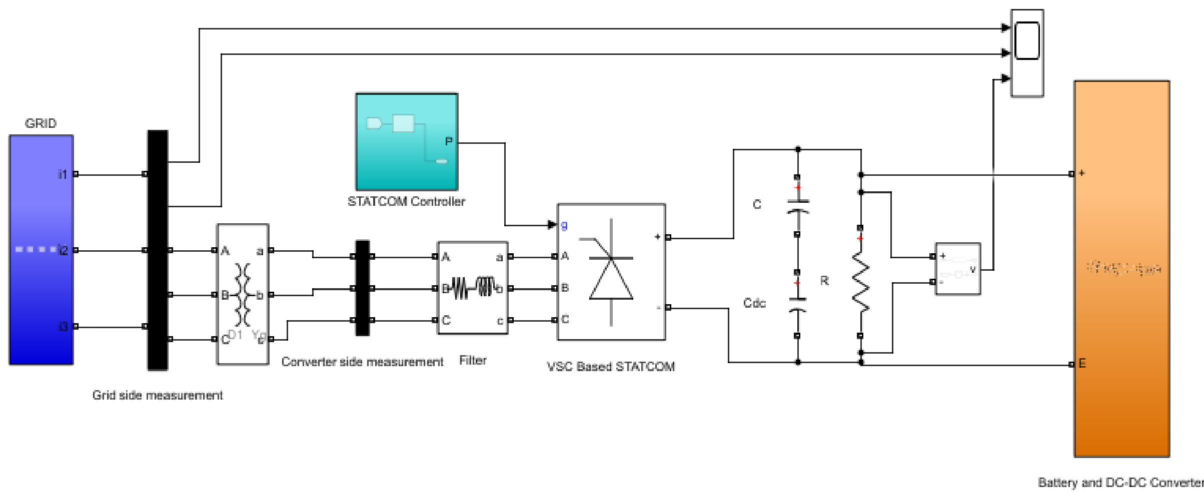

Figure 3.30: Overall Simulink model of STATCOM and its controller

3.13.2. Control Scheme

- **Design of DC-Link Voltage Controller:**

The primary responsibility of the dc-link voltage controller (PI) is to guarantee that 'Vdc' stays equal to 'Vdcref'. Real power is transferred from the AC system to the DC link in order to do this by changing ishdref. The relationship between DC voltage (Vdc) and DC current (idc) is given by equation (3.66).

$$V_{dc} = \frac{1}{C} \int i_{dc} dt$$

$$\text{Transfer Function} = \frac{V_{dc}}{I_{dc}} \tag{3.66}$$

∴ The transfer function in the Laplace domain is= 1/Cs

$$K_p = \frac{C}{T_S}; \quad K_i = \frac{K_p}{T_S}$$

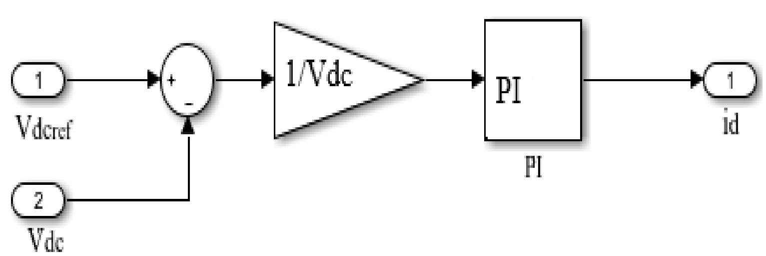

Figure 3.31: Simulink model for a DC voltage regulator

• **Reactive power (Q_g) controller:**

The 'Qg' is maintained at its reference value 'Qgref' by this controller. Thus, using the tuned controller parameters given in equation (3.67), the controller determines the reference quadrature axis current 'ishqref'. The current controller receives "ishqref" after that, where k is a particular time instant.

$$i_{shqref(k)} = i_{shqref}(k-1) + K_P[Q_{g(k)} - Q_g(k-1)] + K_i[Q_{g(k)}] \tag{3.67}$$

Where; $Q_{g(k)} = [Q_{g(k)} - Q_g(k-1)]$ (3.68)

In the equation (3.63) above, the reactive power Qg is provided by (3.64).

$$Q_g = \frac{3(V_{gq} i_{shd} - V_{gd} i_{shq})}{2} \tag{3.69}$$

• **Current controller design:**

It is easy to analyze a single input, single output (SISO) system. As a result, the system must be converted from its multiple input, multiple output (MIMO) configuration to a SISO configuration. The system and STATCOM instantaneous voltages are independent, but the active and reactive currents, ishd and ishq, are connected via a coupling term. To build the controller, the active and reactive shunt currents must be divided. The ishd differential equation formula is written as (3.69).

$$\frac{di_{shd}}{dt} = \frac{1}{L_{sh}}(V_{Md} - V_{invd} - R_{sh} i_{shd}) + \frac{1}{L_{sh}}(\omega L_{sh} i_{shq}) \tag{3.70}$$

It is assumed that values that are not subject to regulation remain constant.

$$K_1 = \frac{1}{L_{sh}}(V_{Md} - V_{invd} - \omega L_{sh} i_{shq})$$

Similarly, the q component is analyzed as:

$$\frac{di_{shq}}{dt} = \frac{1}{L_{sh}}(V_{Mq} - V_{invq} - R_{sh} i_{shq} + \omega L_{sh} i_{shq}) \tag{3.71}$$

$$K_2 = \frac{1}{L_{sh}}(V_{Mq} - V_{invq} - \omega L_{sh} i_{shd})$$

$$\begin{bmatrix} \frac{di_{shd}}{dt} \\ \frac{di_{shq}}{dt} \end{bmatrix} = \begin{bmatrix} \frac{-R_{sh}}{L_{sh}} & 0 \\ 0 & \frac{-R_{sh}}{L_{sh}} \end{bmatrix} \begin{bmatrix} i_{shd} \\ i_{shq} \end{bmatrix} + \frac{1}{L_{sh}} \begin{bmatrix} K_1 \\ K_2 \end{bmatrix} \tag{3.72}$$

Comparing (3.63) and (3.64),

$$\text{Transfer Function} = C(sI - A)^{-1}B + D = \frac{1}{R_{sh} + SL_{sh}}$$

The PI controller's transfer function is provided by:

$$\text{Transfer Function} = (1 + \frac{1}{s\tau_1})$$

$$K_P = \frac{L_{sh}}{T_s}; K_i = \frac{K_p}{\tau_1}; \tau_1 = \frac{L_{sh}}{R_{sh}}$$

The calculated closed loop transfer function demonstrates that the circuit parameters Rsh and Lsh determine KP and Ki values.

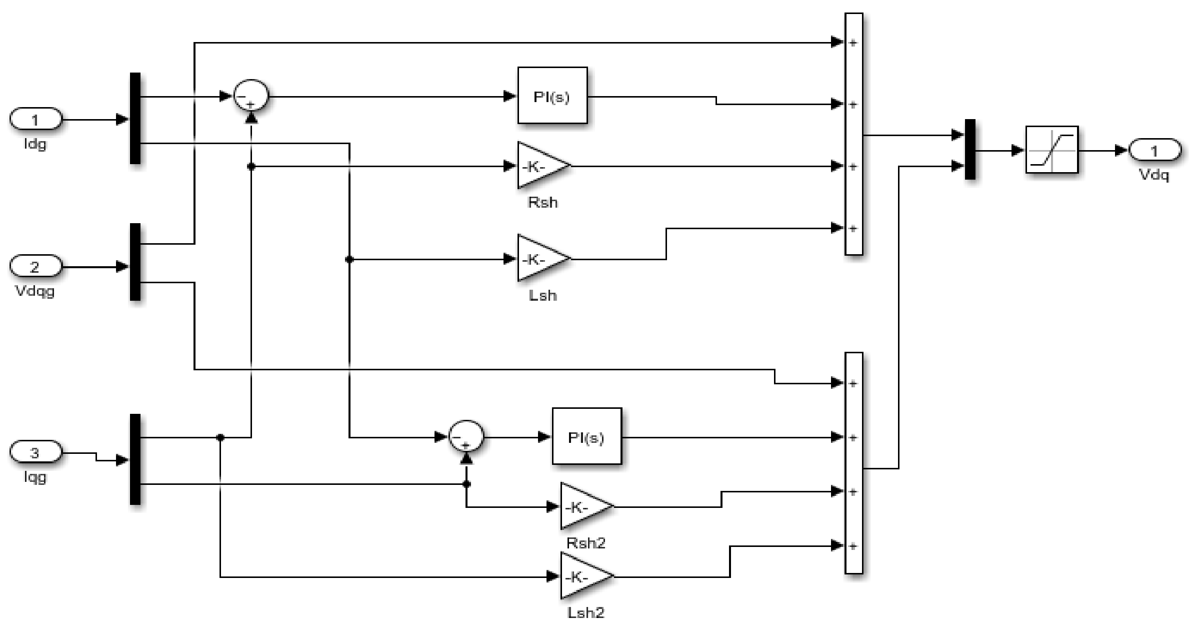

Figure 3.32: Simulink model of current controller

3.14. Calculation of active and reactive power

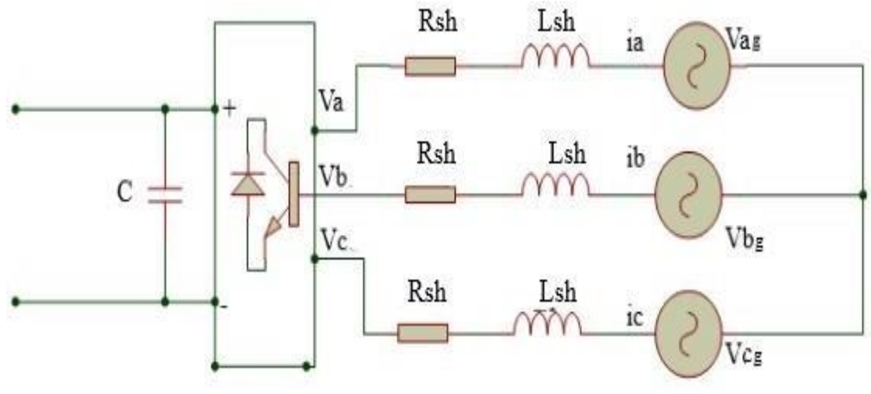

Figure 3.33: STATCOM-integrated grid-side converter (Kadagala 2016)

The grid side converter system seen in figure 3.33 is examined. The three-phase output voltages are represented by Vag, Vbg, and Vcg. The three-phase AC source Va, Vb, and Vc, which represents the grid, is on the right, while the Dc-link capacitor C is on the left. A resistor and an inductor make up the grid filter; resistance is represented by Rsh and inductance by Lsh. Equation 3.74 shows the voltage balance throughout the grid filter.

$$\begin{bmatrix} V_{ag} \\ V_{bg} \\ V_{cg} \end{bmatrix} = R_{sh} \begin{bmatrix} i_{ag} \\ i_{bg} \\ i_{cg} \end{bmatrix} + L_{sh} \frac{d}{dt} \begin{bmatrix} i_{ag} \\ i_{bg} \\ i_{cg} \end{bmatrix} + \begin{bmatrix} V_{a} \\ V_{b} \\ V_{c} \end{bmatrix} \tag{3.74}$$

It is possible to calculate the instantaneous active power transferred from the grid to the grid-side converter using equation (3.75).

$$P = V_a i_a + V_b i_b + V_c i_c = \mathrm{Re}(V_{dq} i_{dq}) = V_d i_d + V_q i_q = V_d i_d \tag{3.75}$$

Similarly, the instantaneous reactive power delivered by the grid-to-grid side converter can be found using equation (3.76).

$$q = \mathrm{Im}(V_{dq} i_{dq}) = V_q i_d + V_d i_q = -V_d i_q \tag{3.76}$$

3.15. Power grid model

To connect the PMSG wind turbine to the grid, a transmission line and a coupling transformer are needed. The coupling transformer, transmission line, and grid are shown in a single line schematic in Figure 3.34. where the transmission line reactance is represented by XL and the transformer reactance by XT. The corresponding resistances are disregarded. The grid voltage is represented by Vdqi. While ð denotes the angle of the grid voltage from VDQS, the filter's terminal voltage acts as a reference.

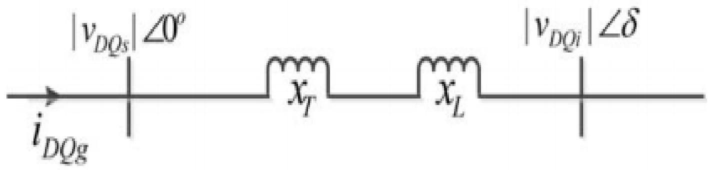

Figure 3.34: single line diagram of the grid, the transmission line and the transformer

The following formula can be used to represent the current going from the wind turbine to the grid:

$$i_{DQg} = \frac{\left|V_{Ds}\right|\sin 0 - \left|V_{DQi}\right|\sin\delta}{X_T + X_L} + j\frac{\left|V_{Ds}\right|\cos 0 - \left|V_{DQi}\right|\cos\delta}{X_T + X_L} \tag{3.77}$$

For unity power factor, the current and terminal voltage of the filter VDQs are in phase; thus, the real and imaginary parts of the current can be represented as:

$$i_{Dg} = \frac{-\left|V_{DQi}\right|\sin\delta}{X_T + X_L}$$

$$i_{Qg} = j\frac{\left|V_{Ds}\right| - \left|V_{DQi}\right|\cos\delta}{X_T + X_L} \tag{3.78}$$

3.16. Transformer modeling

The purpose of a transformer is to alter the voltage of an alternating current supply. It is constructed with two coils, referred to as the primary and secondary coils, encircling a laminated soft iron core consisting of insulated sheets of soft iron to minimize heat loss. When an alternating current is applied to the primary coil's terminals, an alternating magnetic flux is produced inside the core. The secondary coil generates an electromagnetic field as a result. The induced emf in secondary coils is related to the number of turns in both coils as well as the emf of the primary coil.

$$\frac{E_s}{E_p} = \frac{N_s}{N_p} \tag{3.79}$$

Where;

$$\frac{E_s}{E_p} = \frac{\text{Secondry e. m. f}}{\text{primary e. m. f}} \tag{3.80}$$

$$\frac{N_s}{N_p} = \frac{\text{number of turns in secondary coil}}{\text{number of turns in primary coil}} \tag{3.81}$$

When there is a difference between the number of turns in the primary coil (Np) and the secondary coil (Ns), the transformer generates a higher emf at the secondary coil than the main coil, indicating a step up. In power plants, this transformer is utilized to increase the emf prior to feeding it into the transmission lines (Andreas Peterson, 2020). A step-down transformer has fewer turns in its secondary (Ns) than in its primary (Np). If (Ns>np), the transformer's secondary coil's e.m.f. will be higher than the transformer's main coil's.

- Voltage transformation ratio (K)

Equations ((3.76) and ((3.77) yield the constant K, which is known as the voltage transformation ratio.

$$\frac{E_2}{E_1} = \frac{N_2}{N_1} = K \tag{3.82}$$

- A transformer is referred to as a step-up transformer if N2>N1 and K > 1.
- A transformer is referred to as a step-down transformer if N2<N1 and K<1.

Remember that input VA equals output VA for an ideal transformer.

$$V_1 I_1 = V_2 I_2 = \frac{I_2}{I_1} = \frac{V_1}{V_2} = \frac{1}{K} \tag{3.83}$$

Consequently, the voltage transformation ratio and currents have an inverse relationship.

$$\frac{I_1}{I_2} = \frac{V_2}{V_1} = K \tag{3.84}$$

In the grid evolution depicted in the figure below, a 120 KV, 2,500 MVA programmable voltage source serves as the generating station's representation using MATLAB/SIMULINK. After that, a star-delta transformer operating at 120 KV/21 KV is used in the grid to step down the output voltage. A medium transmission line has a voltage of between 20 and 100 kV, and its overhead length ranges from 50 to 150 km. Two dispersed transmission lines, each measuring 75 kilometers, serve as a representation of the transmission line. The transmission line is expressed as equivalent impedance and as system characteristics in equations (3.55).

The system parameters shown in Table 3.8 are taken from Adama wind farm-1

Table 3.7 Grid parameters

Parameters	***Symbol***	***Value and units***
Resistance	R	0.1456 Ω/km
Inductance	L	3.36mH/km
Capacitance	C	11.5nF/km
Voltage	V	21kV
Short Circuit Capacity	Z	2500MVA

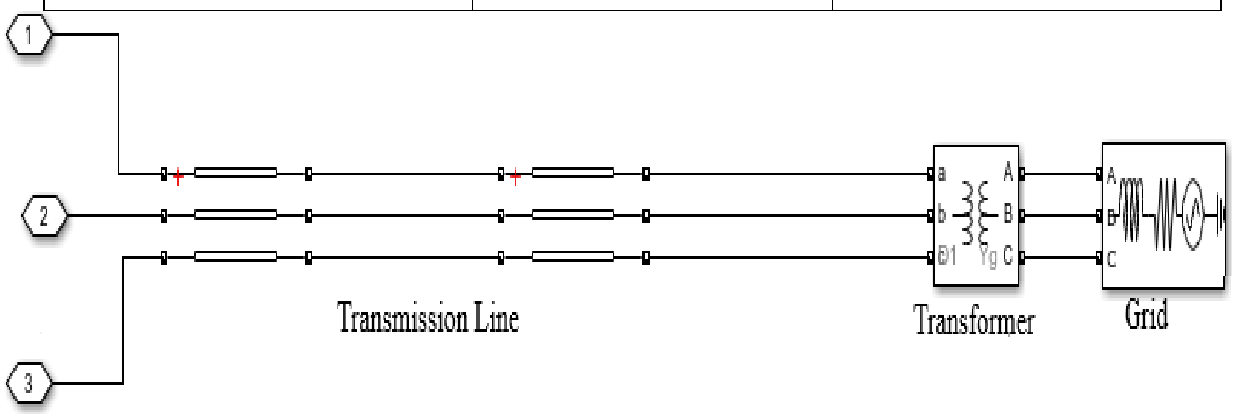

Figure 3.35: Simulink model of grid model

4. RESULTS AND DISCUSSIONS

Figure 4.1 depicts the suggested layout for a grid-connected PMSG-based variable speed wind turbine with BESS and STATCOM. To improve the system's dynamic performance, the VSC is connected to the STATCOM via BESS. The STATCOM is composed of an IGBT PWM converter, a three-phase coupling transformer filter, and a DC link battery. The STATCOM adjusts the voltage at the load terminal by exchanging reactive power with the system and real power with the DC bus. Direct current and quadrature current components can be used to control both active and reactive power. To set the d-axis current reference and keep the DC bus voltage constant, the STATCOM control method makes use of a DC link voltage controller. The voltage controller modifies the q-axis current reference (iq* = 0) to influence the reactive power of the grid. The first PI controller in the second control path sets the q-axis current reference iq* and keeps the voltage at the point of common coupling (PCC) at the specified level. The other two PI controllers monitor the reference currents (Id∗, Iq∗) and combine the outputs with cross-coupling correction terms to generate command voltages. The voltages Vds and Vqs are ultimately transformed into the frame of reference ABC.

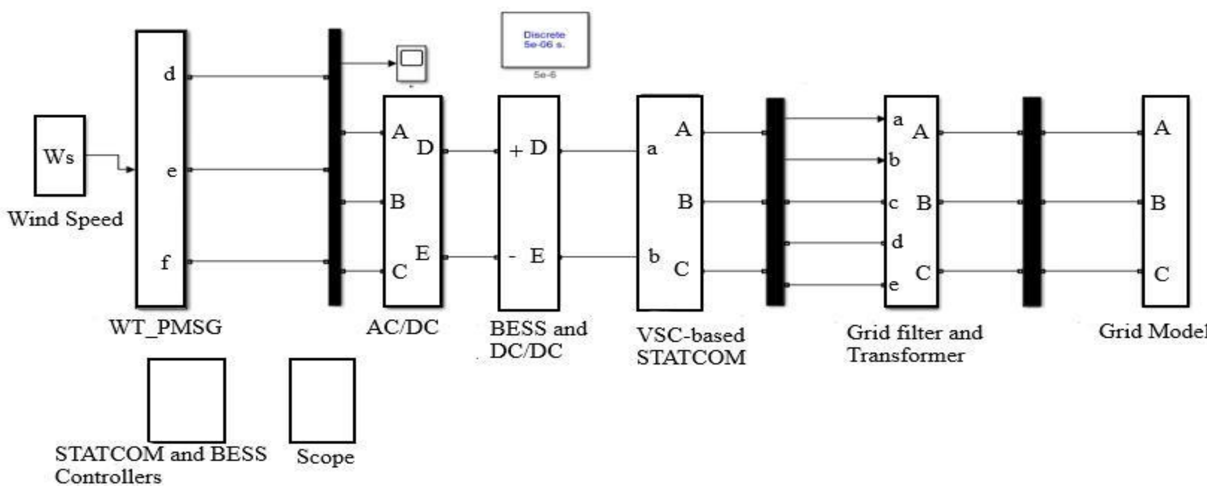

Figure 4.1: Overall PMSG wind turbine connected to grid with STATCOM and BESS model

4.1: Response of a Wind Turbine Using PMSG at Stepped Wind Speed

The wind turbine's rotor was initially set to 1460.7 RPM, and a rated wind speed of 12 m/s was employed in order to comply with the PMSG research. The energy conversion mechanism for wind turbines that produces electricity is examined in this research. A wind turbine model has been developed in MATLAB and Simulink to provide mechanical torque to the generating system. The mechanical torque required to produce electricity is a product of predictions made about the wind turbine's rotor aerodynamics. The electrical component of the wind turbine system is made up of a generating unit, which transforms wind energy into electrical power. A permanent magnet synchronous generator (PMSG) was used in this study's modeling. The mechanical torque (Tm) of the wind turbine's drive train is used to determine the rotor rotational speed (rad/sec). The amount of mechanical and aerodynamic torque that a permanent magnet synchronous generator (PMSG) gets is the same when it operates without a gearbox. The electrical rotation speed is used as an input by the simulation model to calculate the d and q component currents, as shown in Figure 4.2. The rotor's mechanical rotation speed is multiplied by the number of pole pairs (Zp) to determine its electrical rotation speed.

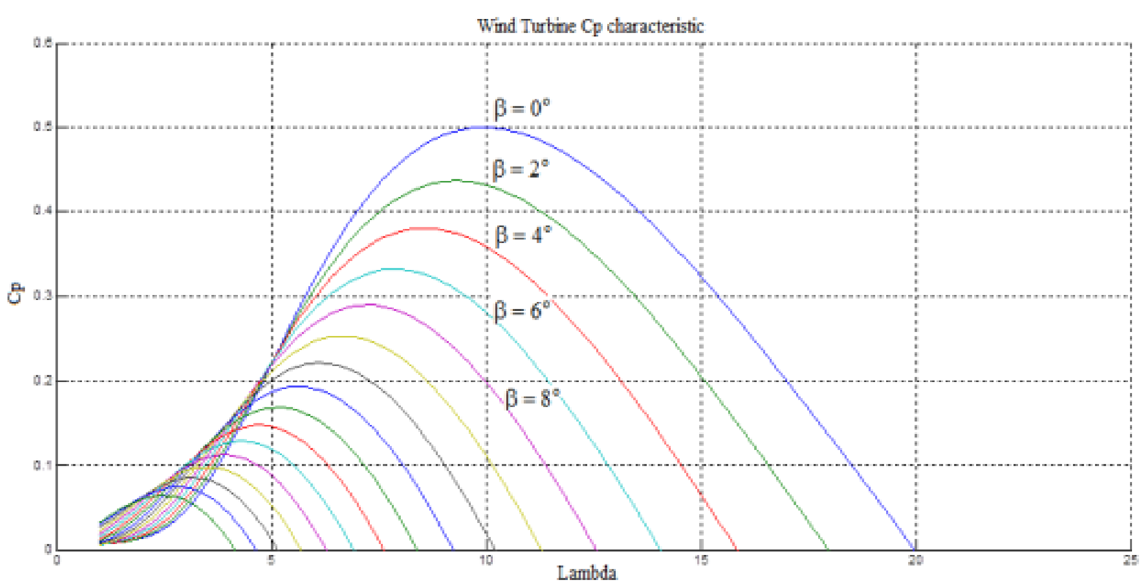

Figure 4.2: Power Coefficient vs. lambda

The angle that forms between the blade's orientation and the wind velocity vector is known as the blade angle. The wind turbine reaches its peak power output when the wind speed (β) completely affects the blades. When the wind speed is less than the system's rated speed, the blade angle is frequently set to zero degrees to enhance energy capture efficiency.

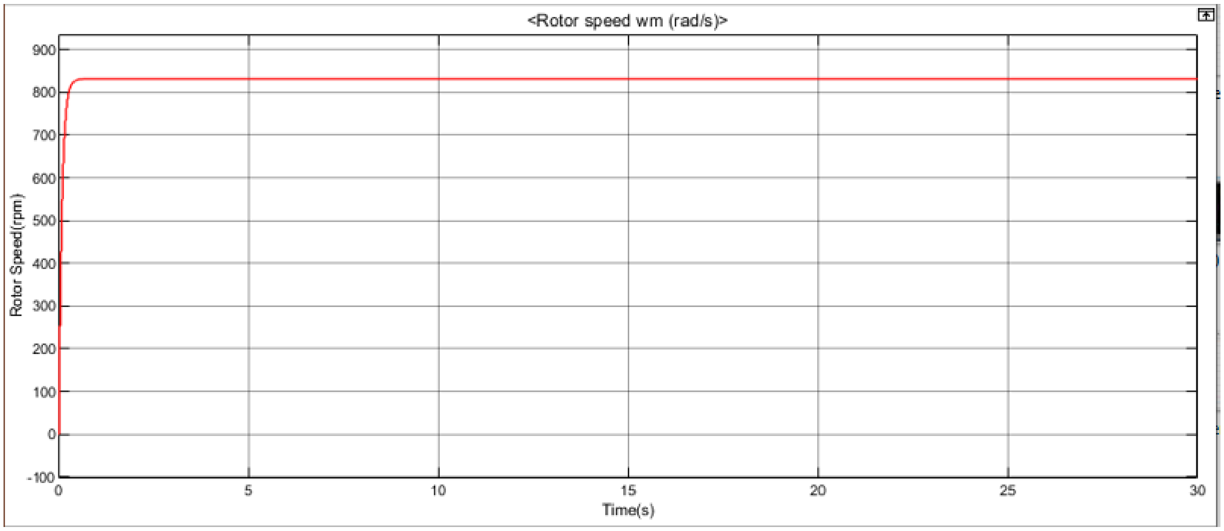

Figure 4.3 : The response of rotational speed for step wind speed

The figure above 4.3, shows that the rotor speed response sheds light on the dynamic behavior of the turbine and the efficiency of the control system during abrupt changes in step wind speed. The dynamics of the rotor speed reaction to incremental changes in wind speed influencing control schemes employed to maximize the response.

The three-phase system model's abc current is calculated utilizing the supplied dq-current components. Figure 4.4 shows that the three-phase current achieves steady state after approximately 0.5 seconds.

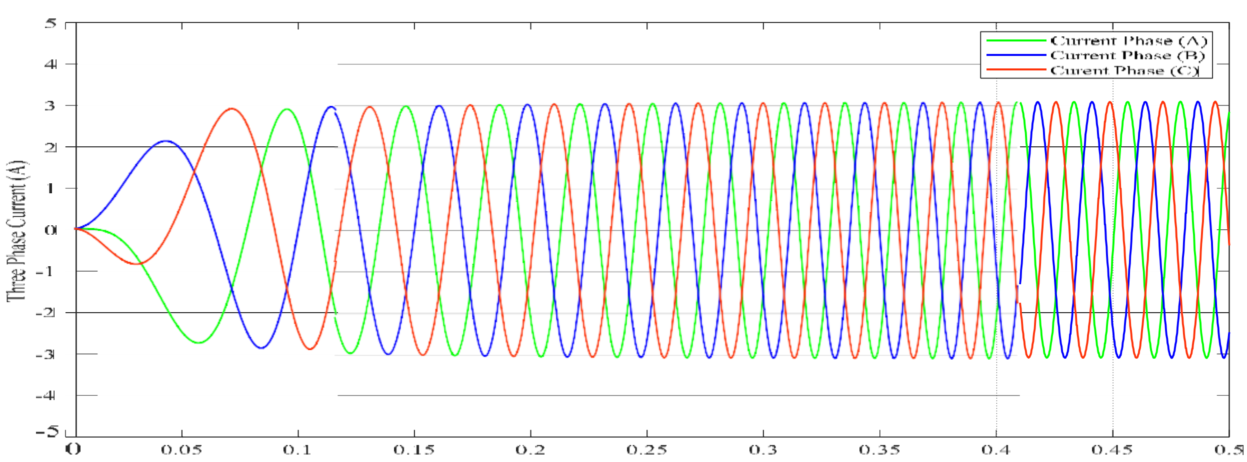

Figure 4.4 The response of three-phase currents for step wind speed

As shown on the figure 4.4 above, Abrupt fluctuations in wind speed cause a variation in the mechanical power input to the PMSG. An alteration in mechanical power results in an equivalent alteration in the electrical power output. As a direct result of the power output, the three-phase currents will likewise alter to suit the new operating circumstances.

The electromagnetic torque is then calculated using the current components listed above.

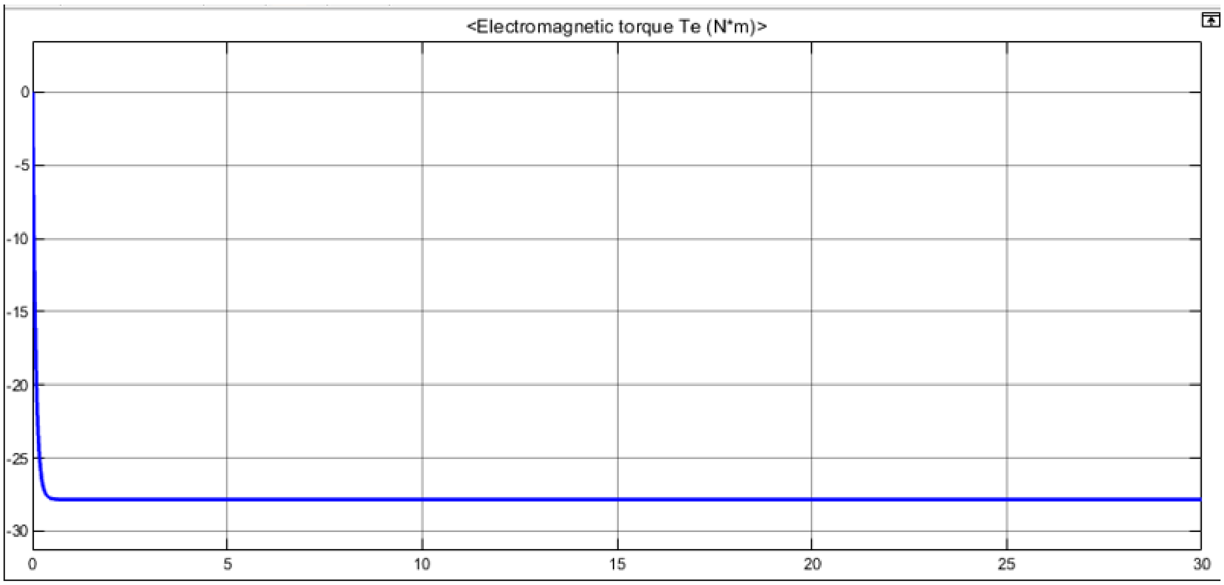

Figure 4.5: The response of the electromagnetic torque for step wind speed

The figure 4.5 above shows Step variations in wind speed cause a proportional shift in the turbine rotor's aerodynamic torque. This alteration affects the electromagnetic torque as it travels through the drivetrain to the PMSG. The mechanical power available from the wind is increased with each step increase in wind speed, and this inturn affects the mechanical torque on the rotor.

On the figure 4.6 below, a rectifier is used to correct the AC voltage output. An elementary diode bridge rectifier is the one that is used. Once more, control and increase are applied to the rectified voltage. Wind-generated alternating current (AC) is sent into an unregulated rectifier. Rectifying alternating current (AC) results in the creation of direct current (DC). Step-up or boost converters are a specific type of DC to DC power converter that generate an output voltage (800V) that is higher than the input voltage.

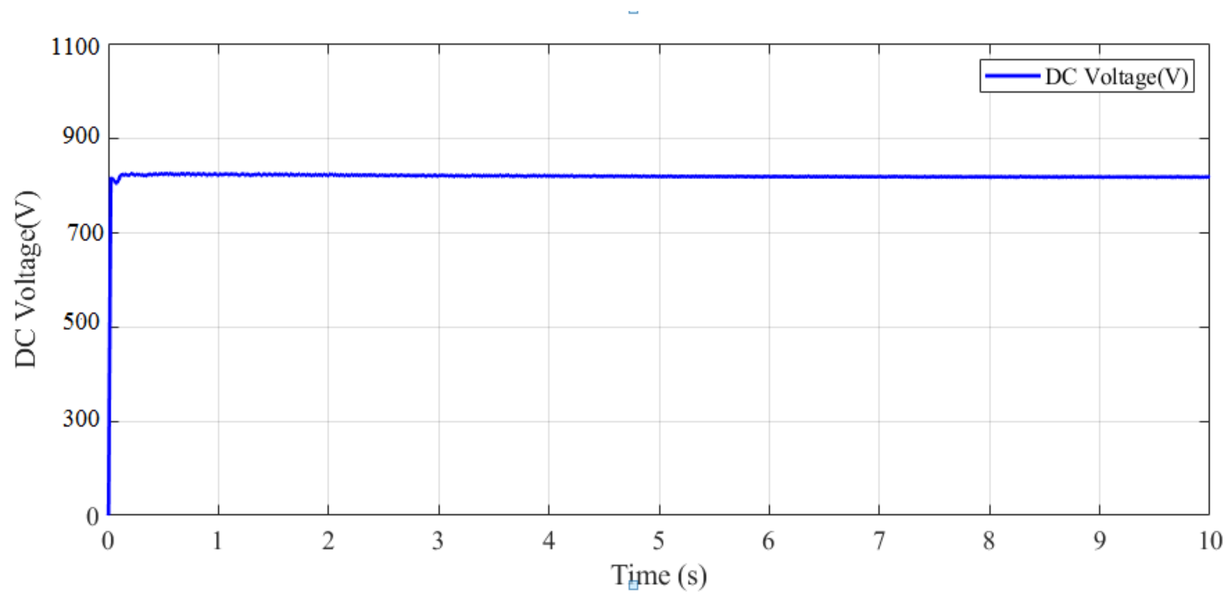

Figure 4.6: Output voltage across DC load response for step wind speed.

As shown in Figure 4.7, When power fluctuations occurs and low Energy production in the system, the BESS can be used to provide Active power to level the power fluctuations by charging operation. As the current is negative during charging, the battery's state of charge (SOC) gradually increases. At 80% SOC, the battery voltage is approximately 400V, exceeding the nominal value. This is due to the fact that as the battery's state of charge increases, so does its voltage.

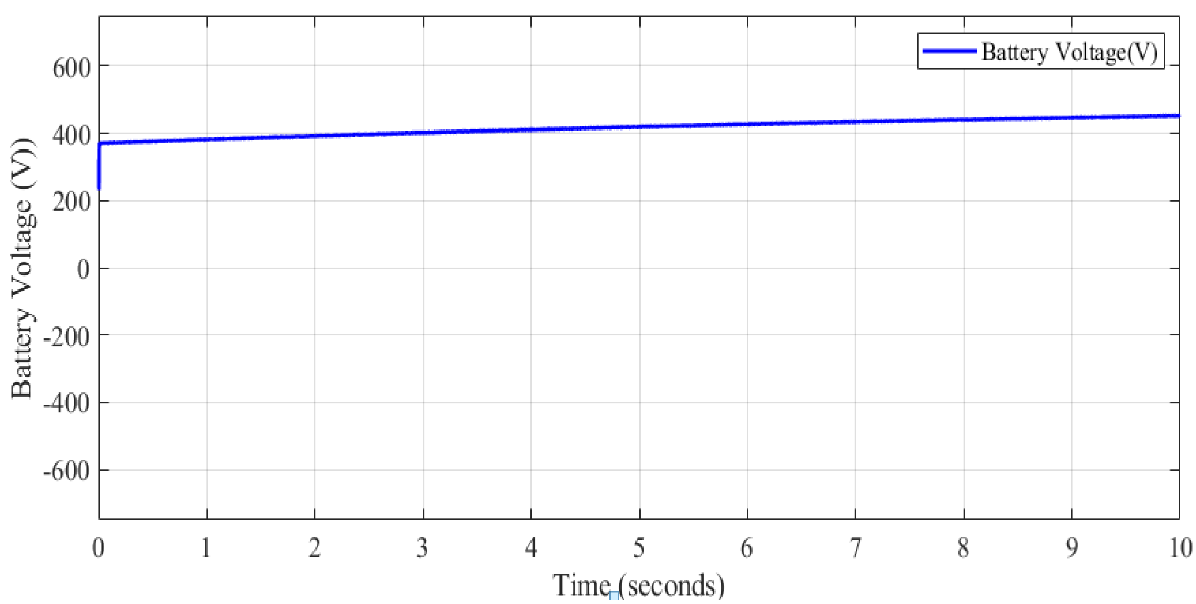

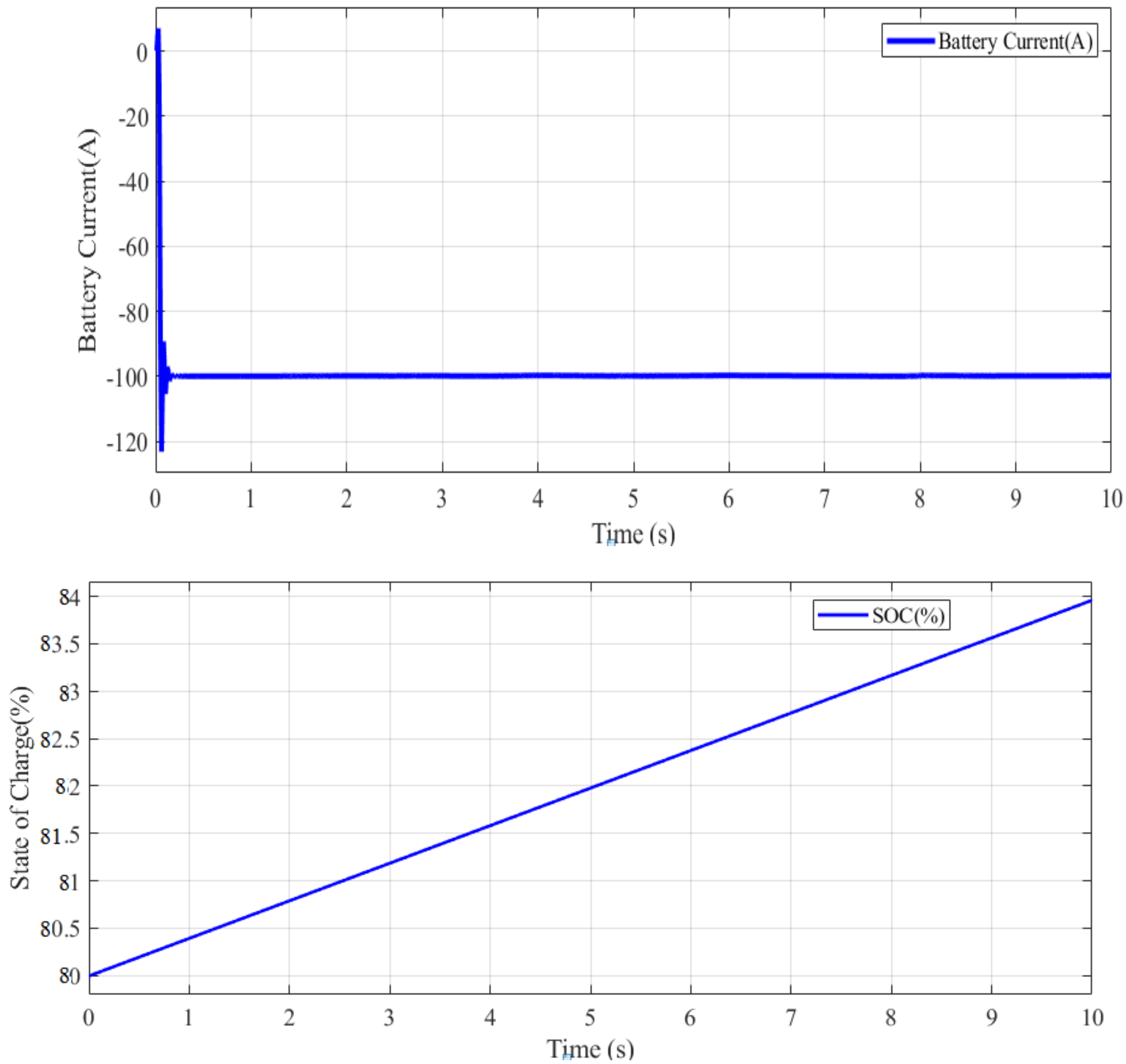

Figure 4.7: Charging characteristics of battery

As shown in Figure 4.8, When power fluctuations occurs and There is high Energy production in the system, the BESS can be used to store surplus Active power to level the power fluctuations by discharging operation. Also the Figure illustrates how the battery state of charge decreases and current increases when a three-phase fault with a resistance of 0.001 Ω is applied between the 5 and 5.1 second mark. The battery supplies power for the AC load. In terms of dynamic performance, or DC link voltage, Figure 4.9 compares the traditional method, STATCOM, and STATCOM with BESS. Table 4.1.a shows that the system utilizing BESS in addition to STATCOM outperformed the systems utilizing STATCOM only in terms of dynamic performance.

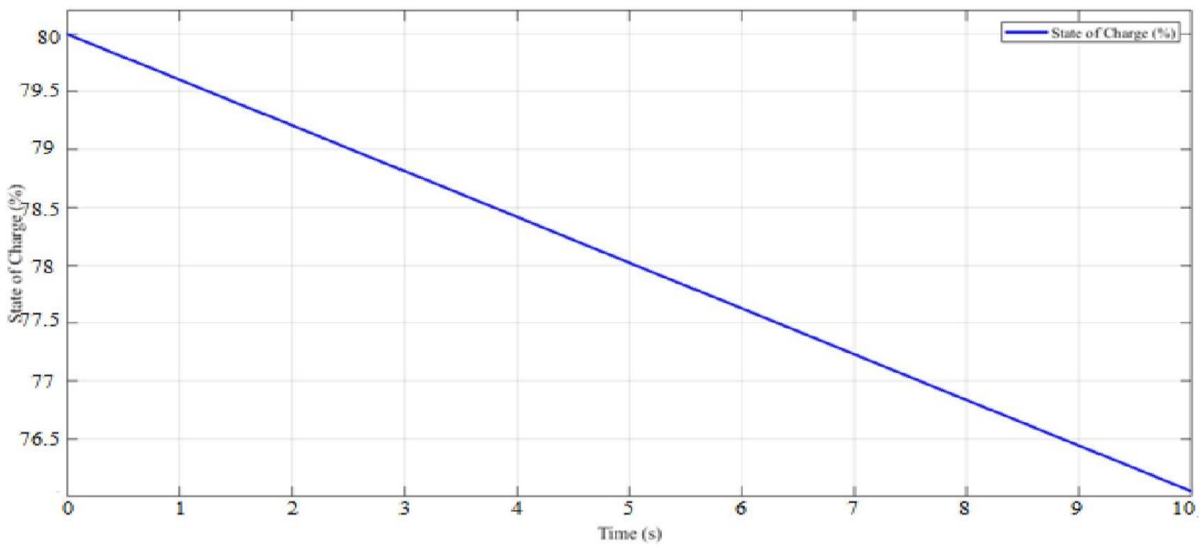

Figure 4.8: Discharging characteristics of battery

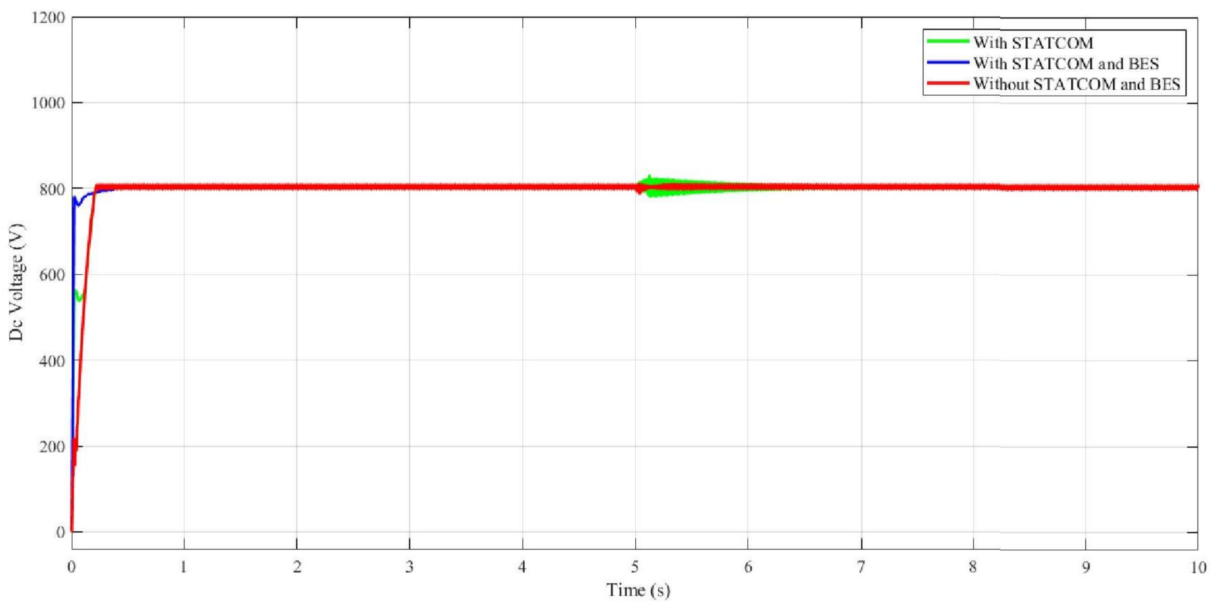

Figure 4.9: DC-Link voltage response for step wind speed.

When transferring energy between the AC-DC or DC-AC conversion processes, a DC link is utilized as an intermediate step. Usually, the DC link is made up of resistors or more sophisticated power electronics components to manage voltage and current levels, as well as capacitors to smooth out voltage ripples and inductors to filter current harmonics.

It is evident that a PWM inverter converts the DC source from the boost converter to AC power. Square pulses are generated by the PMW generator. It is linked to RL filters, whose output is pure sine waves rather than the generated square waves. Figures (4.11) and (4.12) show the voltage and current output characteristics of the AC load. The AC load has a phase-to-phase voltage of 800V and a current of 260A.

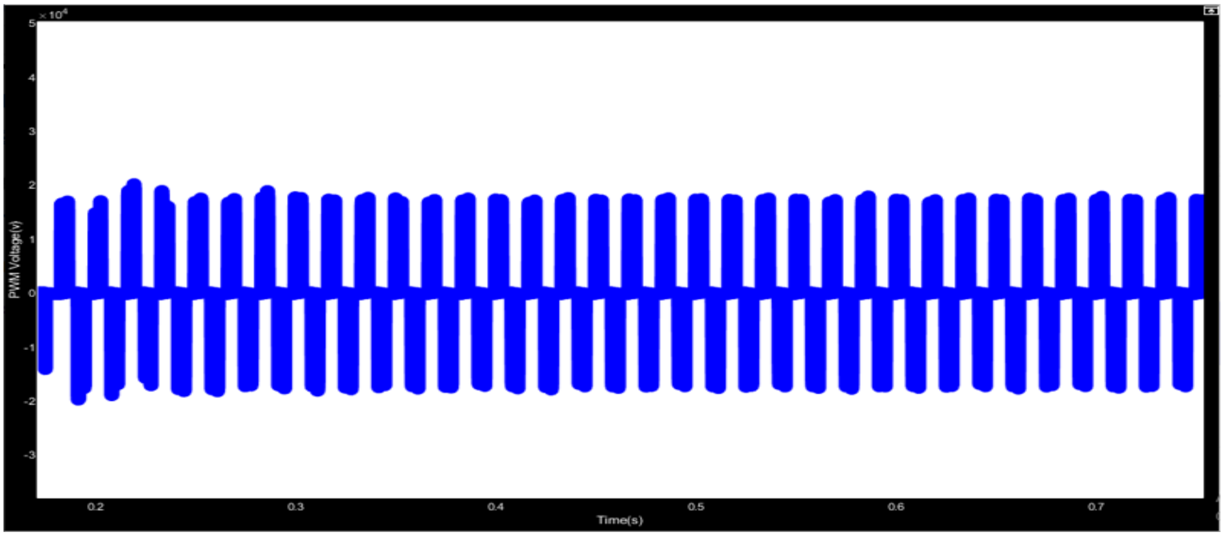

Figure 4.10: PWM inverter voltages response for step wind speed

From figure 4.10 above, Rotor speed in a wind turbine varies when there is an abrupt shift in wind speed, or step change. The mechanical power supplied to the generator is impacted by this change in rotor speed, and this effects the generator's output of electrical power. For steady voltage and frequency to be maintained, the generator which is normally connected to the grid via a PWM inverter must adjust to these fluctuations.

A PWM inverter converts the DC voltage from the DC link into AC voltage with a controlled frequency and amplitude suitable for grid connection or load requirements. PWM inverters use high-frequency switching of semiconductor devices (like IGBTs or MOSFETs) to synthesize a sinusoidal AC output from the DC input.

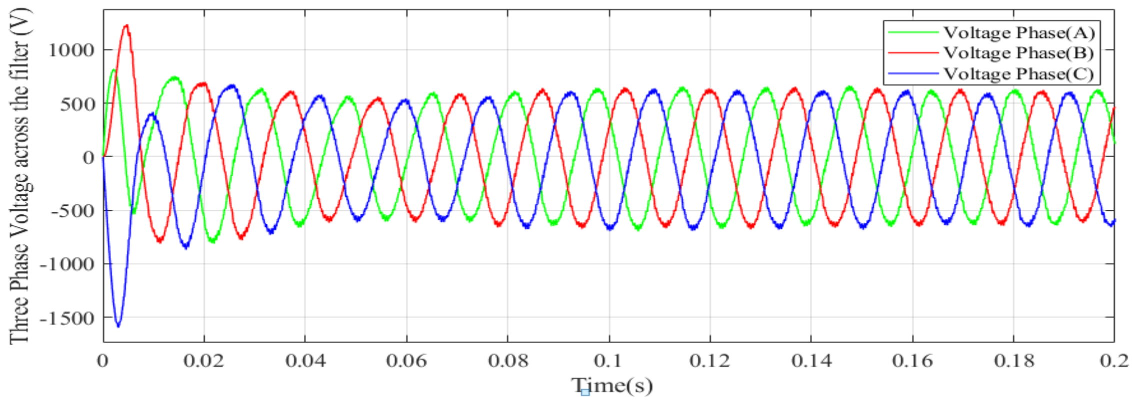

Figure 4.11: output of three phase voltage response across the filter for step wind speed

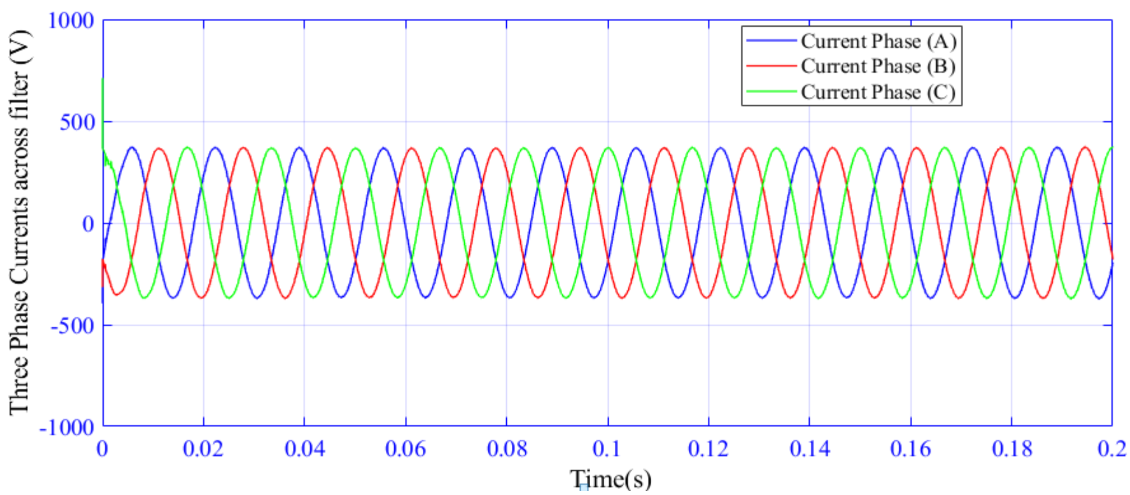

Figure 4.12: output of three phase current response across the filter for step wind speed

Three-phase AC voltage is produced from DC electricity using an inverter called the VSC. Harmonics are filtered and output is amplified by the transformer. The VSC must be managed by the controller.

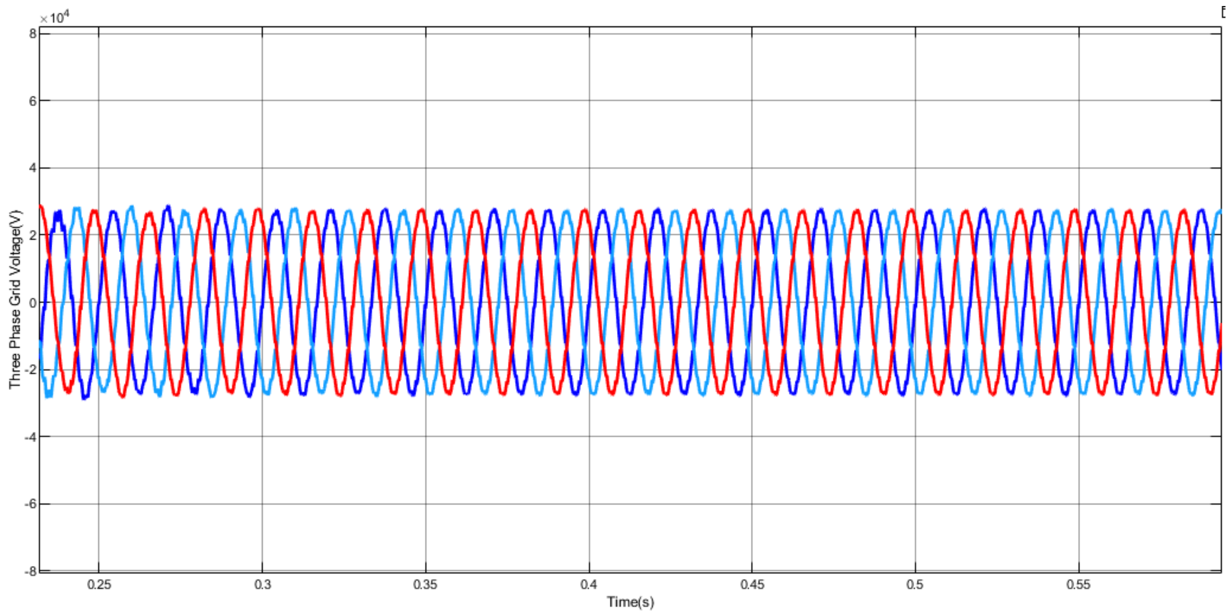

Figure 4.13: Three -phase output voltage response across the grid for step wind speed

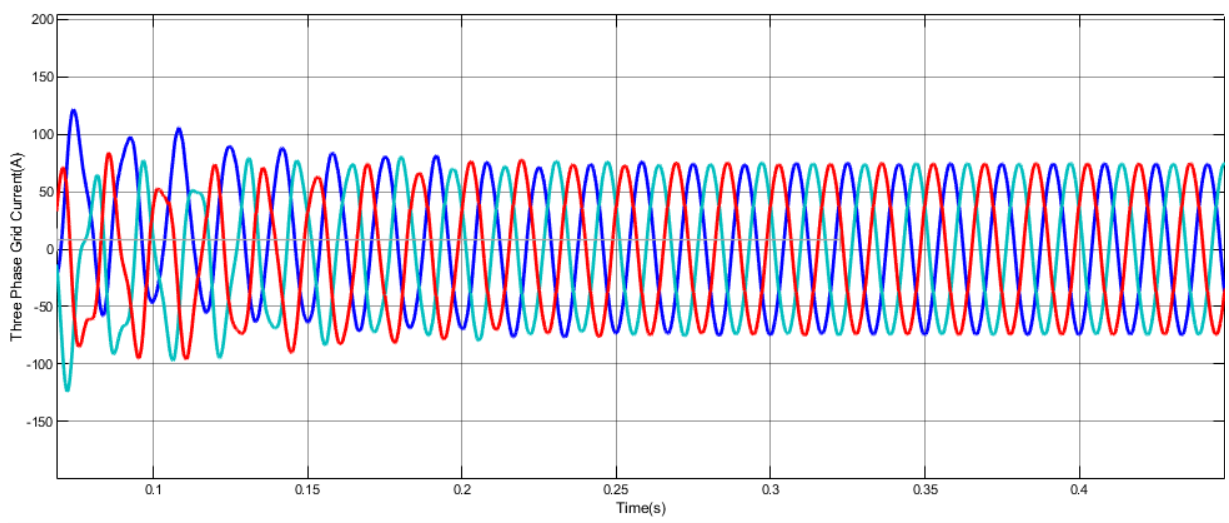

Figure 4.14: Three -phase output current response across the grid for step wind speed

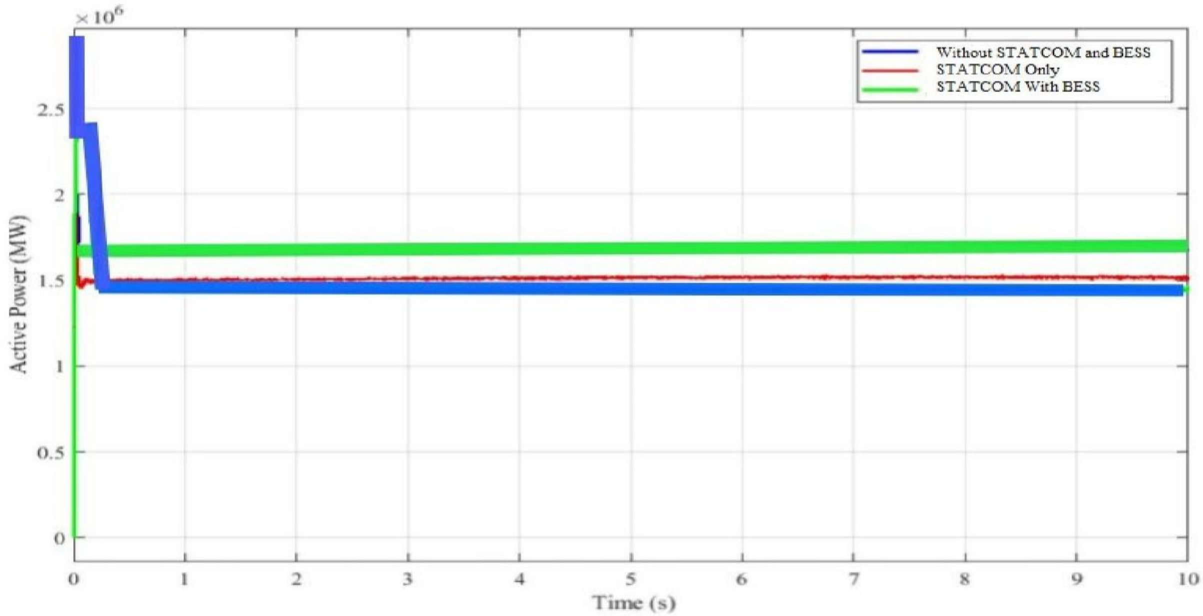

Figure 4.15: Active power in response to step wind speed

A number of important elements affect the active power response in a power system, especially when it comes to renewable energy sources like wind turbines. In order to maintain stability and efficiency, these variables control how fast and efficiently the system can adapt to variations in generation or demand. Those affecting factors are: Wind Speed Variability, Turbine Inertia and Mechanical Dynamics, Generator Characteristics, Power Electronics and Inverter Dynamics, Energy Storage Systems and Grid Conditions and Interconnection.

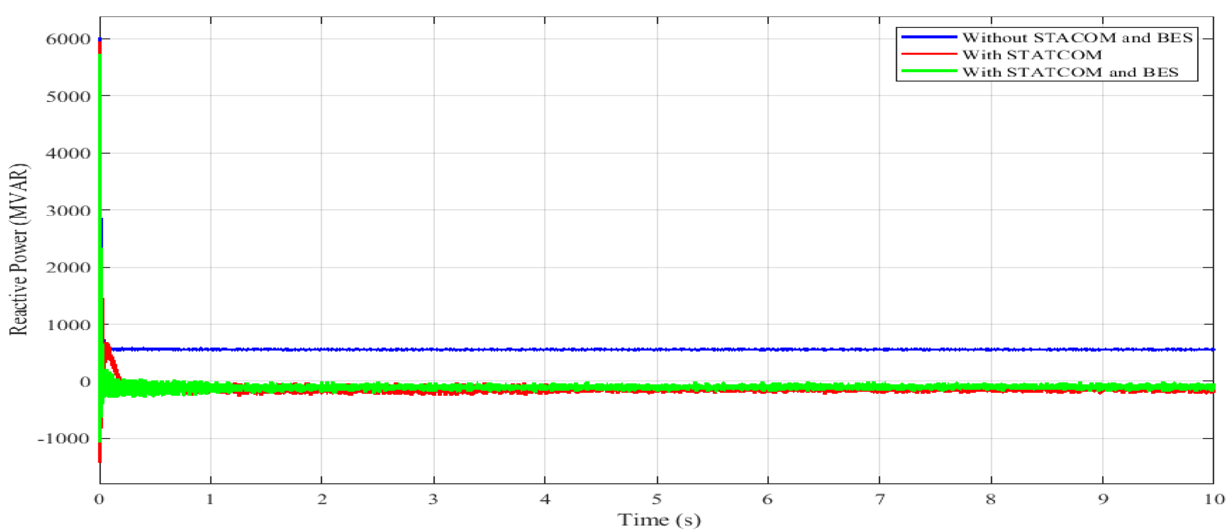

Figure 4.16: Reactive power in response to step wind speed

The integration of a BESS and STATCOM compensator allows for the separate absorption and injection of real and reactive power into the grid. The overloaded transmission line can be relieved by combining FACTS and BESS if significant power transfer changes occur on the transmission line. The STATCOM's reactive power injection capability allows for quick voltage adjustment. But without active power capabilities, it cannot totally eliminate rotor oscillations. Connecting a BESS to the STATCOM instantly lowers the voltage and rotor oscillations. Capacitive or inductive compensation requires the controller to inject or absorb a very small amount of active power into or out of the AC system via BESS. Integrating active and reactive correction into a single power system is the aim of employing STATCOM and BESS. When the grid receives more active electricity, the systems' ability to produce reactive power can be constrained.

Table 4.1 : Comparisons of dynamic performance of a PMSG-based wind turbine subjected tostep wind speed using STATCOM and STATCOM with BESS.

		ωe	**T_e**	**V_{dc}**	**P**	**Q**
Overshoot (%)	WSWB	0	0.23367	0.1787	0.96	0.87
	STATCOM ONLY	0	0.23367	0.016898	0.54	0.554
	SWB	0	0.23367	0.08	0.39	0.12
Settling time(s)	WSWB	1.33	3.92	6.58	2.0436	6.2653
	STATCOM only	1.33	3.92	6.5	1.0806	1.6169
	SWB	1.33	3.92	1.700	1.00	1.5926
Rise time(s)	WSWB	7.48	3.43	5.0745	2.1314	4.00944
	STATCOM only	7.48	3.43	4.9798	1.2279	1.58209
	SWB	7.48	3.43	3.459	1.1	1.5

From Table 4.1 above, we can conclude that, Power electronic devices like STATCOM and STATCOM with BESS can have a major impact on the dynamic performance of a wind turbine based on a Permanent Magnet Synchronous Generator (PMSG) during a step change in wind speed. These devices can affect overshoot, settling time, and rise time.

Voltage Overshoot: By offering reactive power support, the STATCOM will assist in reducing voltage overshoot when exposed to a step increase in wind speed.

Reactive Power Overshoot: The STATCOM responds rapidly to variations in reactive power consumption, but because it solely manages reactive power, there may be a greater voltage overshoot than in a system that supports active power.

Voltage Settling Time: Because the STATCOM cannot directly control active power imbalanc es, it may take longer to settle voltage variations than a system with active power support. However, it can swiftly stabilize voltage fluctuations by regulating reactive power.

Voltage Rise Time: Following a step change in wind speed, STATCOM's quick reactive power adjustment response results in a comparatively short rise time for voltage stabilization. It might not, however, operate as quickly as a system that has more active power assistance.

Rise Time of Frequency: BESS's ability to control active power also enhances frequency response, which shortens the rise time needed to stabilize both voltage and frequency.

Generally speaking, we can conclude about overshoot, Settling time, Rise time as follows:

Overshoot: Because active power from the BESS and reactive power from the STATCOM are instantly available, the STATCOM with BESS arrangement greatly minimizes overshoot in both voltage and frequency.

Settling Time: The installation of BESS significantly reduces the settling time because it can quickly supply or absorb active power to balance the power system.

Rise Time: With the STATCOM and BESS arrangement, the rise time is shortened because the BESS can react to power imbalances faster than the STATCOM can, hence enhancing its reactive power support.

4.2. Response of a PMSG based Wind Turbine When Subjected to Stochastic Wind Speed Series

The average wind speed, ramp wind component, gust wind component, and fluctuation wind component are the four components of wind speed that are shown in Figure 4.1. The effects of STATCOM and STATCOM with BESS on the dynamic performance of a grid-connected PMSG based wind farm with a stochastic wind speed series were examined using time domain simulations, as shown in the following figure below.

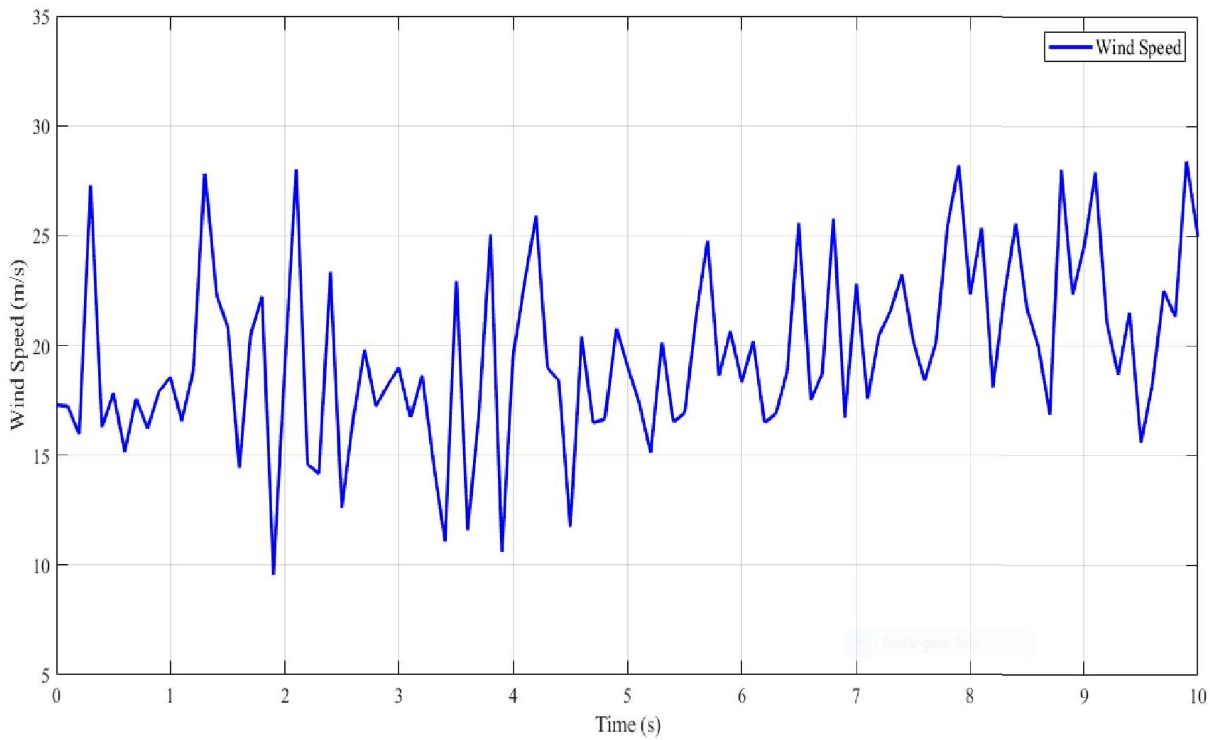

Figure 4.17: Wind speed response for stochastic wind speed series

The response of the PMSG's rotor speed and electromagnetic torque to the stochastic wind speed series is depicted in Figures 4.18 and 4.19. STATCOM and STATCOM with BESS are used to minimize electromagnetic torque (overshoot, settling time, and rising time) and rotor speed caused by stochastic wind speed. Furthermore, a comparison of the data in Table 4.2 shows that the grid-connected PMSG based wind farm's dynamic performance is improved by the STATCOM with BESS.

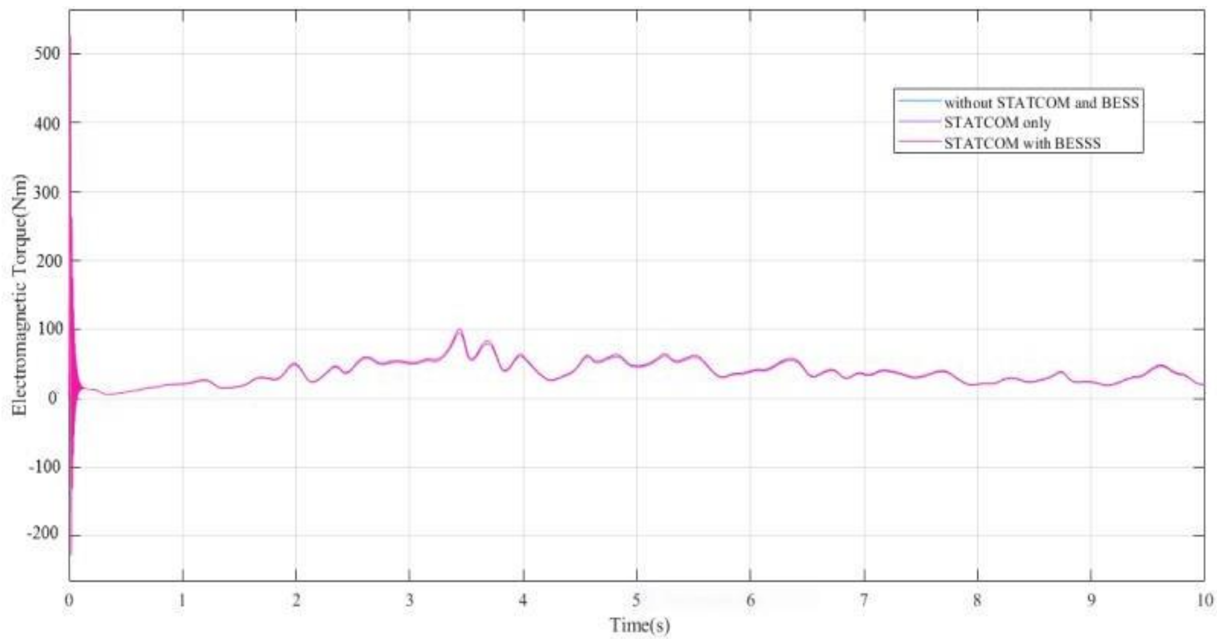

Figure 4.18: Electromagnetic torque response for stochastic wind speed series

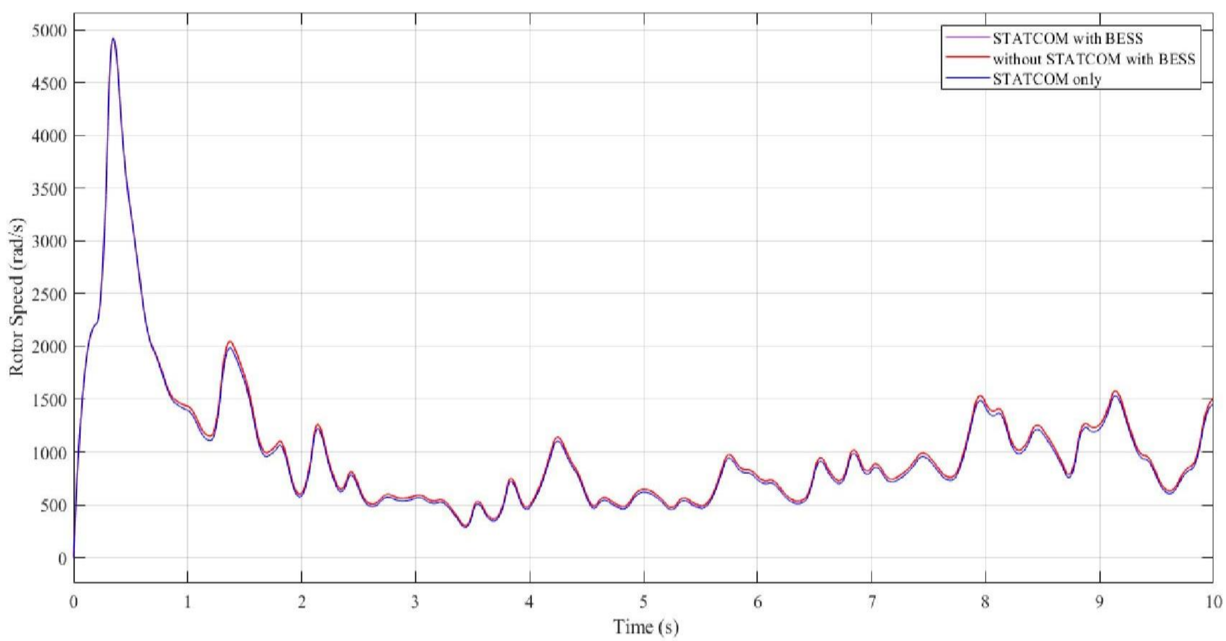

Figure 4.19: Rotor speed response for stochastic wind speed series

DC-link voltage responses with and without the STATCOM with BESS are compared in Figure 4.20.The results showed a reduction in fluctuations, overshoot, settling time, and rising time when using STATCOM and STATCOM with BESS. And study of the STATCOM using BESS reveals that it is superior to the STATCOM. Furthermore a comparison of the data in Table 4.2

shows that the grid connected PMSG based wind farm's dynamic performance is improved or enhanced by the STATCOM with BESS.

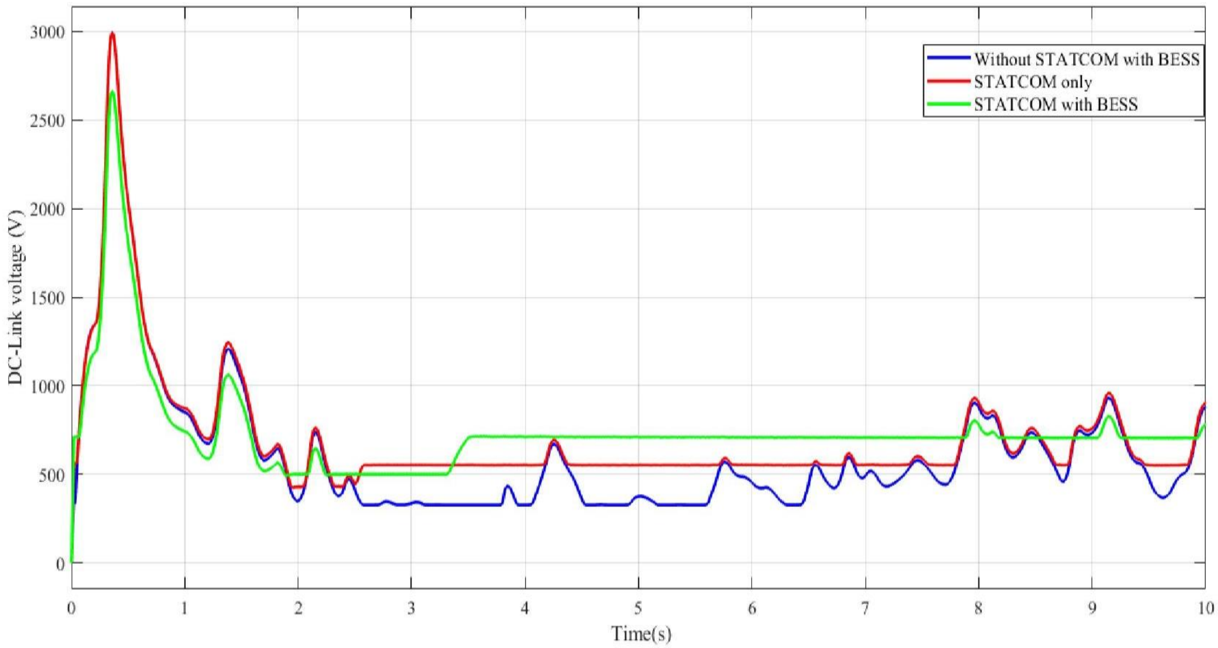

Figure 4.20: DC-Link voltage response for stochastic wind speed series

The active power responses to stochastic wind speed series of a grid-connected PMSG-based wind turbine are shown in Figure 4.21. The findings show that the almost average real power, settling time, rise time, overshoots, and variations of the PMSG-based wind turbine's active power caused by random wind speed were all considerably decreased by the STATCOM with BESS. Additionally, a comparison of the data in Table 4.2 demonstrates that the STATCOM with BESS enhances the dynamic performance of the grid-connected PMSG-based wind farm.

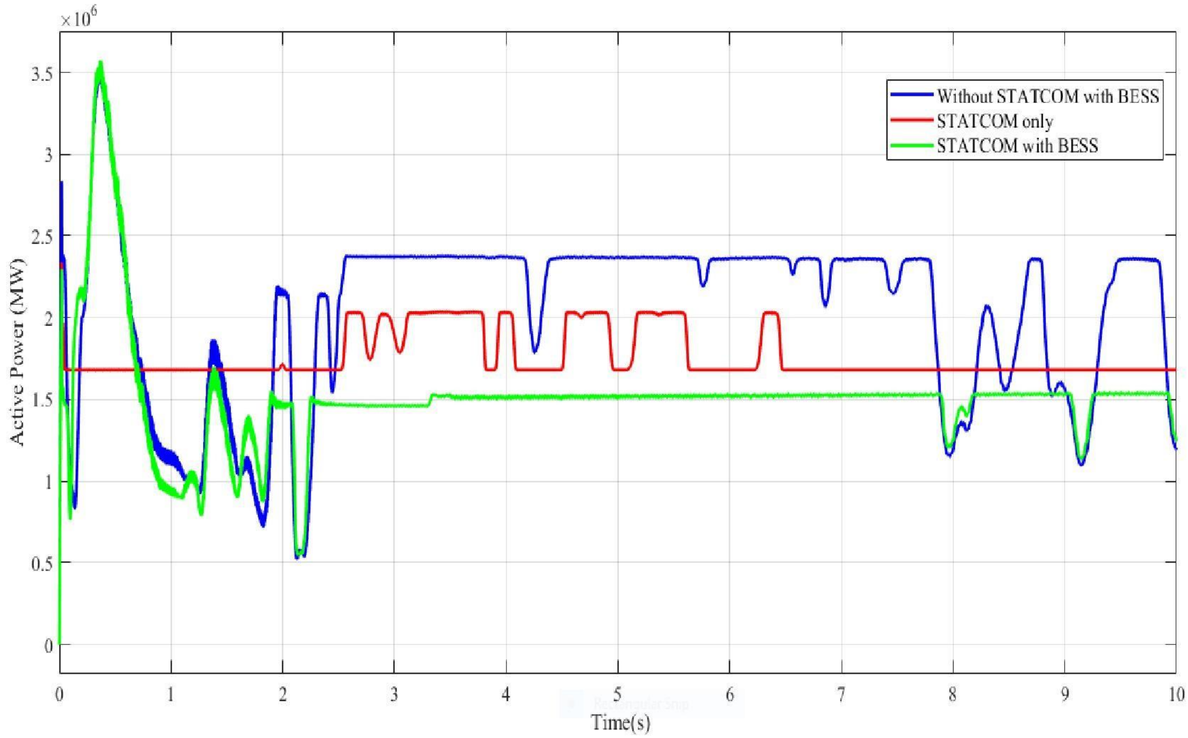

Figure 4.21: Active power response for stochastic wind speed series

The stochastic wind significantly affects the STATCOM control system because its goal is to keep reactive power at zero for a unity power factor. Consequently, Figure 4.22's results show that the stochastic wind speed series induced reactive power oscillations were reduced in the STATCOM and STATCOM with BESS, leading to less power variations. Furthermore, a comparison of the data in Table 4.2 shows that the STATCOM with BESS enhanced or improves the dynamic performance of the grid-connected PMSG-based wind farm.

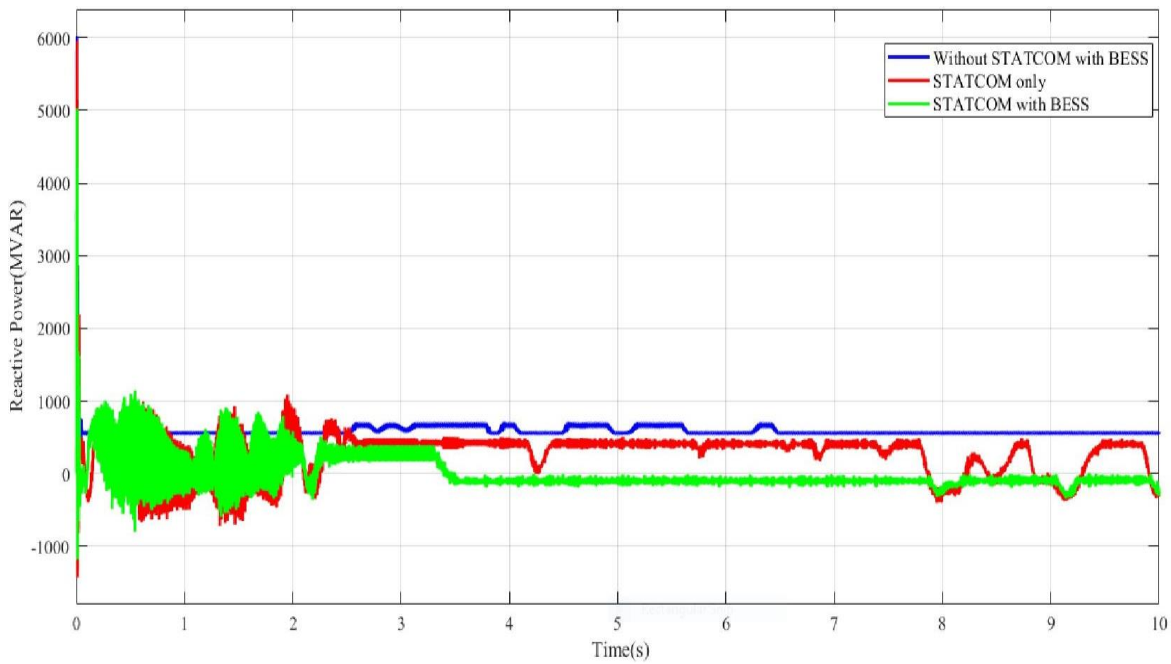

Figure 4.22: Reactive power response for stochastic wind speed series

Table 4.2: Comparisons of dynamic performance of a PMSG-based wind turbine subjected to stochastic wind speed

		ωe	**T_e**	**V_{dc}**	**P**	**Q**
Overshoot (%)	WSWB	0.2388	0.257	0.2397	0.39	0.95
	STATCOM only	0.2388	0.257	0.2394	0.19	0.44
	SWB	0.2388	0.257	0.239	0.18	0.38
Settling time(s)	WSWB	2.2	2.17	1.99	1.99	1.98
	STATCOM only	2.2	2.17	1.98	1.9	1.99
	SWB	2.2	2.17	1.9	1.29	1.28
Rise time(s)	WSWB	1.3	2.12	7.89	9.51	4.00
	STATCOM only	1.3	2.12	7.51	2.1	2.48
	SWB	1.3	2.12	7.50	1.18	2.01

5. CONCLUSIONS AND FUTURE WORK

This thesis provides a comprehensive technique for modeling and simulating wind energy conversion systems, which is one of the key research aims. Simulations suggest that using a STATCOM with BESS improves the dynamic performance of wind farms. The wind turbine was modeled using relevant aerodynamic equations that define the turbine's behavior in relation to wind speed and other characteristics such as blade radius, power coefficient, and air density, and the PMSG was calculated using the state space equation. BESS, STATCOM, and their control system were designed theoretically and through simulations.

5.1.Conclusions

The stochastic wind speed series and the integration of a PMSG-based wind farm into the grid both degrade dynamic performances, which can have positive or negative consequences on the dynamic stability of a power system. Given this, the research for this thesis has shown that a power system containing a PMSG-based wind farm is negatively impacted by stochastic wind speed series. Furthermore, the thesis suggests that dynamic performances can be enhanced by integrating BESS with STATCOM. The use of STATCOM in conjunction with BESS yielded positive outcomes in terms of enhanced reactive, active power, and DC-Link voltage performance. Reactive power's dynamic performance is a useful tool for maintaining voltage stability and power quality. As a result, it has been demonstrated that STATCOM combined with BESS may effectively improve the dynamic performance of a wind farm based on PMSG that is exposed to stochastic wind speed series.

5.2. Future Work

Further research can look at how the grid-connected PMSG-based wind farm performs dynamically when using intelligent power converter controllers like ANN and ANFIS in combination with the STATCOM compensator. Creating sophisticated control algorithms to anticipate future power needs and adjust to shifting wind conditions in order to maximize the efficiency of the BESS and STATCOM.

Also putting machine learning concepts into practice to enhance real-time decision-making and increase system efficiency and responsiveness can be done in the future. In order to ensure optimal use of stored energy and uphold grid stability, more advanced EMS designs can be developed to regulate the energy flow between the wind turbine, BESS, and grid.

6. REFERENCE

Abdelateef Mostafa, E. A. El-Hay, & M. M. ELkholy (2023). A detailed analysis, comparisons, and insights included in the most current advancements in soft computing-based wind energy conversion systems with grid integration. Engineering Archives: Computational Methods 30(3), 1439–1478.

Abu-Rub, M. Mariusz, and Kamal Al-Haddad. In 2014. *Power Electronics for Industrial, Transportation, and Renewable Energy Systems.* John Wiley & Sons Ltd, ISBN: 978-1-118-63403-5.

Ackermann, T.2012. *Wind Power in Power Systems*, John Wiley & Sons, 1120 pages, ISBN: 978-0-470-97416-2.

Andreas Petersson,2020. " Doubly-fed induction generator analysis, modeling, and control for wind turbines.," Ph.D. dissertation, Chalmers University of Technology, Goteborg, Sweden.

A.U. Lawan and Haider Abbas, 2021. "PMSG Wind Turbine Interfacing with Grid and The Dynamic Performance Improvement of MMC Inverter STATCOM Capability."

Ayele Nigussie Legesse, Dr Akshay Kumar Saha, and Dr Rudiren Pillay Carpanen, 2018." Modeling and analysis of effects on a power system's dynamic performances as well as mitigation under stochastic wind disturbances comprise PMSG-BASED WIND POWER INTEGRATION. Electrical Engineering Technology Journal, page 6.

Barua, A. (2017). Study of reactive power compensation using STATCOM (Doctoral dissertation, National Institute of Technology Rourkela).

B. Singh and V. S. Kadagala, , 2018 "Simulation of three-level 24-pulse voltage source converters-based static synchronous compensator for reactive power control," IET Power Electronics, vol. 7, no. 5, pp. 1148–1161.

C. Schauder and H. Mehta, Jul. 2018. "Control of sophisticated static VAR compensators using vector analysis," IEE Proceedings-C, vol. 140, no. 4, pp. 299-306.

E. Muljadi, C.P. Butterfield, Aug-Sept 2020. "Wind Farm Power System Model Development," World Renewable Energy Congress VIII, Colorado. Eduard Ned Mohan, Tore M. Undeland.

E. Hau, 2022." The basics, technologies, applications, and economics of wind turbines, 2nd edition. Berlin, Germany: Springer.

Eduard Ned Mohan, Tore M. Undeland, and William P. Robbins, 2021.” Power Electronics: Transistors, Utilization, and Architecture’’, 3rd Edition. Hoboken, NJ: John Wiley & Sons.

Ethiopian Electric Power.2020; The overall Energy Situation in Ethiopia. [May 25, 2020] Energypedia, http://www.eep.gov.et.

Irene Ndunge Muisyo ,Christopher Maina Muriithi, and Stanley Irungu Kamau Published 25 June 2022.” Optimizing STATCOM Controller Performance for Grid-Connected Wind Power Generating Plants with Improved LVRT Capability.”

J. Lepka and P. Stekl, 2019 “3-Phase AC Induction Motor Vector Control Using a 56F80x, 56F8100 or 56F8300 Device, Design of Motor Control Application”, An application note, AN1930 Rev.2, 2/2019, Freescale Semiconductor Inc.

Kumar, P. M., & Barua, A. (2019). Study of reactive power compensation using STATCOM (Doctoral dissertation).

Kundur P., Neal J.B., and Mark G.L,2022. “Stability and Control of the entire Power System”, Aslam P. Memon, (2022), “Utilizing Artificial Neural Networks for Electrical Alternator Excitation Systems Applications”, M. Phil, Thesis, Department of Electrical Engineering, Mehran University of Engineering and Technology, Jamshoro, Sindh, Pakistan, 2022, Supervised by A. Rashid sheikh & M. A. Unar.

L. Whei-Min and H. Chih-Ming, 2019. “A creative technique for regulating the variable speed wind turbine generation system and determining the greatest power point.,” vol. 35, no. 6, pp. 2440–2447.

Lekshim and Vishnu J, 2021. “Enhancement of Intermittent Stability in Wind Integrated System Based on PMSG with FOD Controlled FACTS Device.” International Conference on Computer Technologies, Power, and Circuits [ICCPCT], 2021.

M.M. Chowdhury and M. E. Haque, 2019. “A Direct-Drive Grid-connected Wind Energy System the STATCOM with super-capacitor energy storage.”

M. Haque, M. Negnevitsky and K. Muttaqi, 2019. “An innovative method of controlling a wind turbine with a permanent magnet synchronous generator that operates at different speeds,” IEEE Industrial Applications Transactions, vol. 46, pp. 331 – 339.

M. Chinchilla, S. Arnaltes, J.C. Burgos, March 2020. “Grid-connected variable-speed wind energy systems are managed using permanent magnet generators.”, Journal of Energy Conversion published by IEEE., 130–135.

Mezigebu Getinet Yenealem ,Livingstone M. H. Ngoo,Dereje Shiferaw, and Peterson Hinga Published 25 August 2020.”Management of Voltage Profile and Power Loss Minimization in a Grid-Connected Microgrid System Using Fuzzy-Based STATCOM Controller.”

Raouf, A., Tawfiq, K. B., Eldin, E. T., Youssef, H., & El-Kholy, E. E. (2023). Wind Energy Conversion Systems Based on a Synchronous Generator: Comparative Review of Control Methods and Performance. *Energies*, *16*(5), 2147.

Rolan, A. Luna, G. Vazquez, D. Aguilar and G. Azevedo, 2020. “modeling of a permanent magnet synchronous generator in a variable speed wind turbine.” in IEEE International Symposium on Industrial Electronics, Seoul.

Rui Zhu , An-lei Zhao, Guang-chao Wang, Xin Xia, and Yaopan Yang, Published 28 August 2020. “A Model for Improving Energy Storage Performance in Grid-Connected Wind-Solar Hybrid Energy Storage Systems.”

S. Morimoto, T. Nakamura, and Y. Takeda, , Jan 30 2018. "Power maximization control of variable speed wind generation system using permanent magnet synchronous generator," Electrical Engineering in Japan, vol. 150, pp. 11-19.

T. Sun, Z. Chen, F. Blaabjerg, “Voltage recovery of grid-connected wind turbines with DFIG after a short-circuit fault,” 2017 IEEE 35th Annual Power Electronics Specialists Conference, vol. 3, pp. 2015 -2017, 20-25 June 2017.

V. Akhmatov, 2021, Analysis of dynamic behaviour of electric power systems with large.

William P. Robbins, 2019.”Power Electronics: Converters, Applications, and Design, 3rd Edition. Hoboken, NJ: John Wiley & Sons Inc.

Y. Wang, V. Silva and M. Lopez-Botet-Zulueta, 2018. “Effect of high variable renewable energy penetration on frequency dynamics in the interconnected system of continental Europe.” IET Renewable Power Generation, vol. 10, no. 1, pp. 10 – 16.

APPENDIX-1

1. Wind Turbine data from Adama wind farm-1

WTG Version	***Parameters(1.5/77)***
Nominal power of wind turbines (MW)	1.5
The Quantity of wind turbines	34
Inertia constant of wind turbines (H(s))	4.32
Diameter of the rotor (m)	77
Rotor radius (m) of a wind turbine	37.7
Height of the Tower(m)	65
Air density	1.225kg/m^3
Cut-in wind speed	3m/s
Rated wind speed	11m/s
Optimal speed ratio (λ_{opt})	6.14
Maximum Power coefficient ($C_{p,max}$)	0.45
Cut-out wind speed	22m/s
Swept area	4649m^2
Number of blades	3
Power control	Collective pitch control/rotor speed control

2. Generator data (PMSG) from Adama wind farm-1

Generator Type	***PMSG,1.5MW,620V,12.7Hz,multipole (non-salient pole)***
Rated Mechanical Power	1.5MW
Rated Apparent Power	1.6MVA
Generator inertia	35000(J/kg.m^2))
Rated Power Factor	0.97
Speed Range	9-17.3rpm
Rated speed	17.3
Shaft stiffness (pu)	0.3
Number of Pole Pairs	44
Rated Rotor Flux Linkage	1.48
Stator Winding Resistance	0.006Ω
d-axis Synchronous Inductance	0.395mA
q-axis Synchronous Inductance	0.395mA
Rated current	680A
Static friction	0.01
Viscous damping	1.5

3. Overall MATLAB simulink model

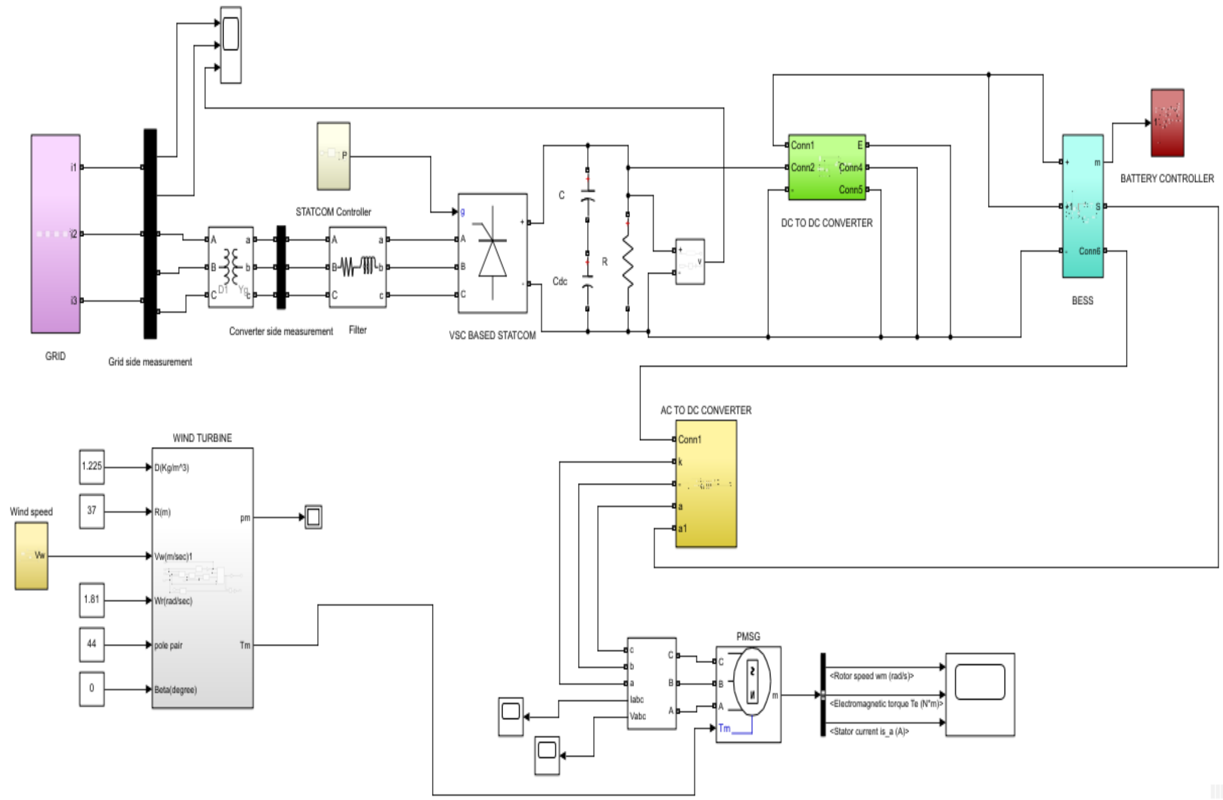

4. Simulink model to obtain mechanical torque and power

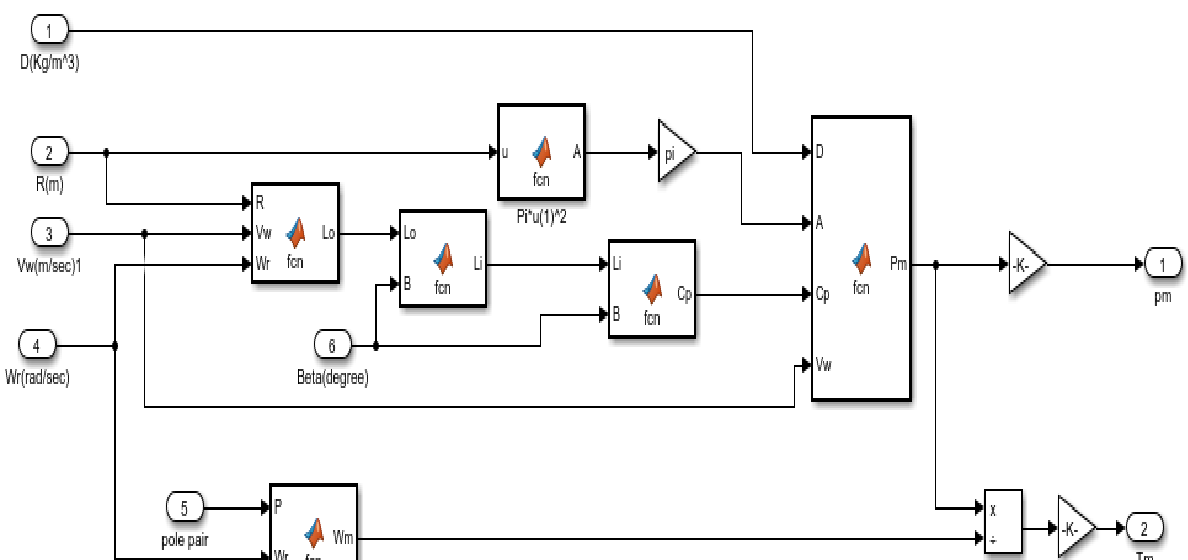

5. Simulink model of stochastic wind speed

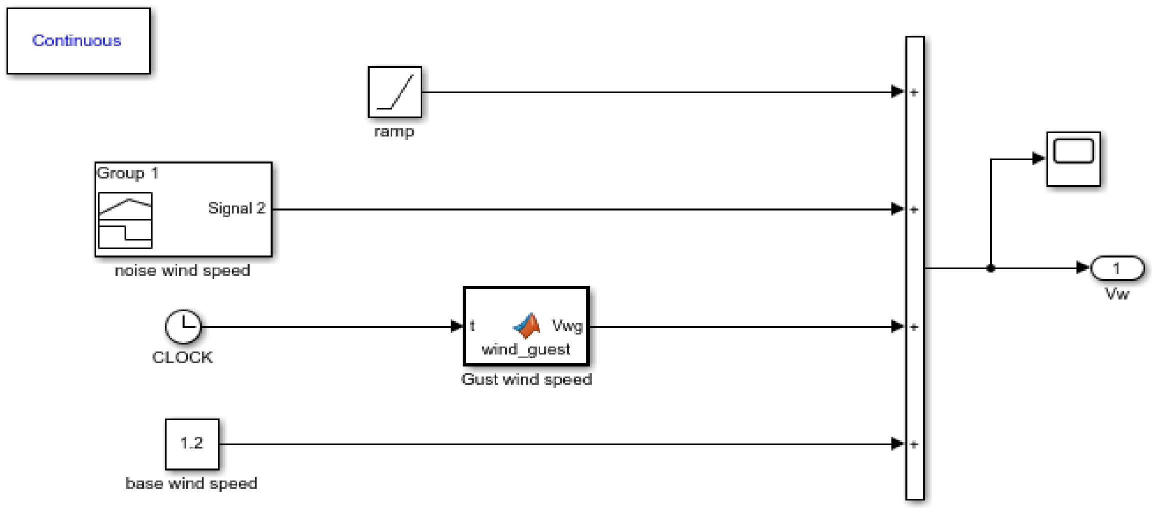

6. Simulink model of overall PMSG

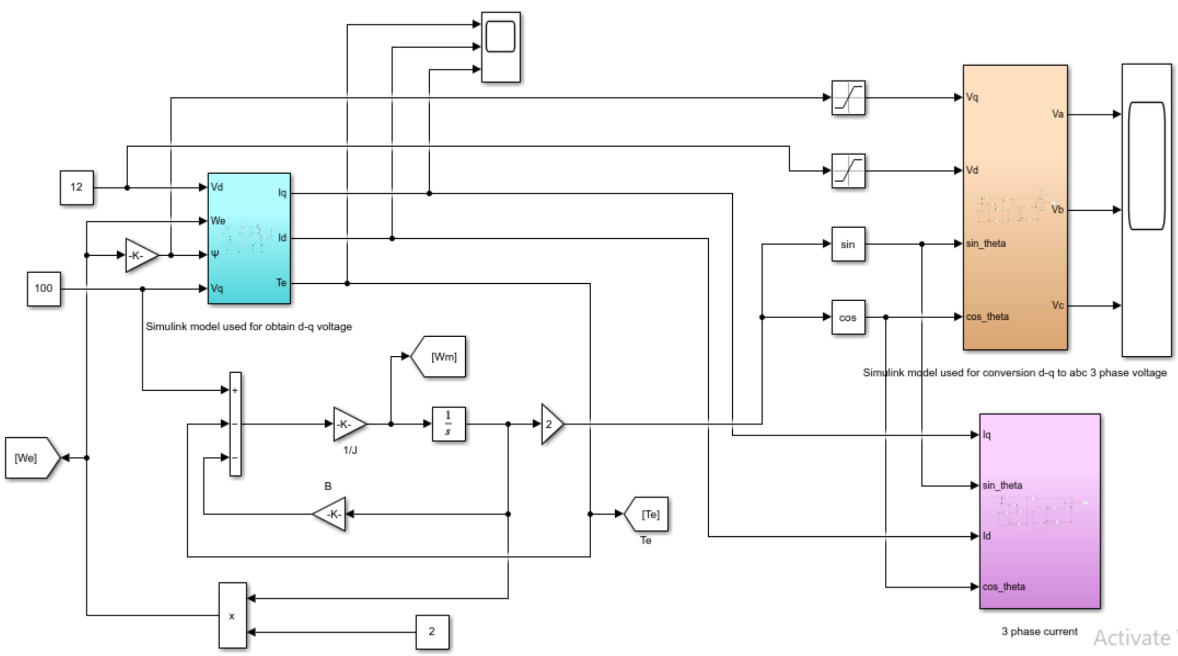

7. Simulink model of Power coefficient(Cp) of the rotor

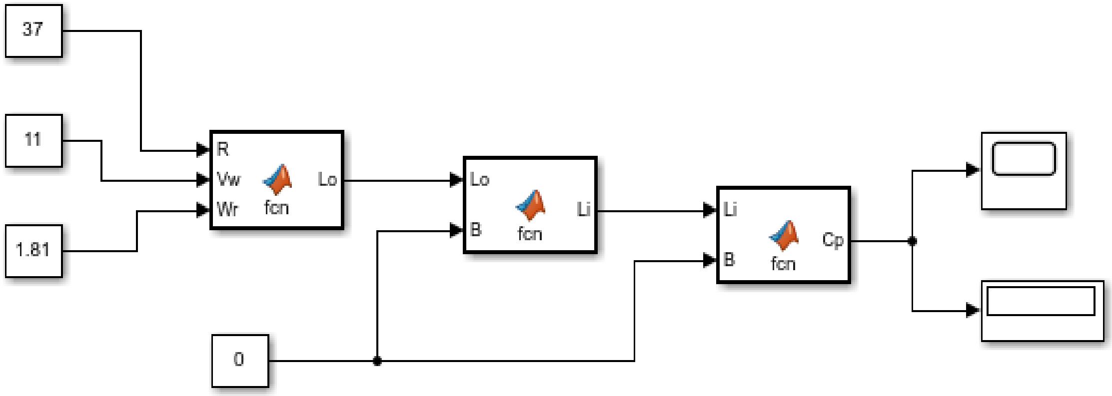

8. MATLAB code for Power coefficient(Cp) of the rotor

```
Cp = fcn(Li,B)
C1=0.654;
C2=116;
C3=0.4;
C4=5;
C5=21;
C6=0.0068;
Cp=C1*(C2*Li-C3*B-C4)*exp(-C5*Li)+(C6*Li);
```

9. MATLAB code for Gust wind speed

```
Vwg = wind_guest(t)
Tg=6;
T1g=2;
maxg=8;
if t<=T1g
    Vwg=0;
elseif t>T1g && t<T1g+Tg
        Vwg=(maxg/2)*(1-cos(2*pi*((t-T1g)/Tg)));
else t>T1g+Tg
        Vwg=0;
end
```